

UNCLASSIFIED

AD NUMBER

ADB009670

LIMITATION CHANGES

TO:

Approved for public release; distribution is unlimited.

FROM:

Distribution authorized to U.S. Gov't. agencies only; Test and Evaluation; JAN 1975. Other requests shall be referred to Air Force Aeronautical Systems Division, Wright-Patterson AFB, OH 45433.

AUTHORITY

asd, usaf ltr, 4 may 1977

THIS PAGE IS UNCLASSIFIED

THIS REPORT HAS BEEN DELIMITED
AND CLEARED FOR PUBLIC RELEASE
UNDER DOD DIRECTIVE 5200.20 AND
NO RESTRICTIONS ARE IMPOSED UPON
ITS USE AND DISCLOSURE,

DISTRIBUTION STATEMENT A

APPROVED FOR PUBLIC RELEASE;
DISTRIBUTION UNLIMITED,

ASD/XR-TR-75-1



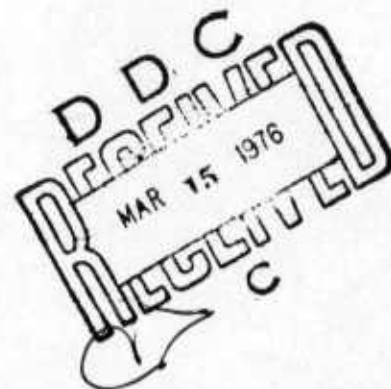
ADB009670

ASDIR-II

VOLUME III

REFERENCE DOCUMENTATION

JANUARY 1975



Distribution limited to U.S. Government agencies only; report contains test and evaluation information; January 1975. Other requests for this document must be referred to ASD/XRH, Wright-Patterson AFB, OH 45433.

DEPUTY FOR DEVELOPMENT PLANNING
AERONAUTICAL SYSTEMS DIVISION
WRIGHT-PATTERSON AIR FORCE BASE, OHIO 45433

NOTICES

When Government drawings, specifications, or other data are used for any purpose other than in connection with a definitely related Government procurement operation, the United States Government thereby incurs no responsibility nor any obligation whatsoever; and the fact that the Government may have formulated, furnished, or in any way supplied the said drawings, specifications, or other data is not to be regarded by implication or otherwise as in any manner licensing the holder or any other person or corporation, or conveying any rights or permission to manufacture, use, or sell any patented invention that may in any way be related thereto.

This technical report has been reviewed and is approved for publication.

James H. Hall
JAMES H. HALL
COLONEL, USAF
 Deputy for Development Planning

ACCESSION for	
RTIS	Write Section <input type="checkbox"/>
DCC	Diff Section <input checked="" type="checkbox"/>
UNCLASSIFIED	<input type="checkbox"/>
JUSTIFICATION	
BY	
DISSEMINATION/AVAILABILITY CODES	
Dist.	MAIL, BOX, or SPECIAL
B	

REPORT DOCUMENTATION PAGE		READ INSTRUCTIONS BEFORE COMPLETING FORM
1. REPORT NUMBER	2. GOVT ACCESSION NO.	3. RECIPIENT'S CATALOG NUMBER
14 ASD/XR-TR-75-1, Volume III		
4. TITLE (and Subtitle)	5. TYPE OF REPORT & PERIOD COVERED	6. PERFORMING ORG. REPORT NUMBER
6 ASDIR-II, Volume III, REFERENCE DOCUMENTATION.	Final rpt. July 72 - Dec 74	
7. AUTHOR(s)	8. CONTRACT OR GRANT NUMBER(s)	
10 Charles W. Stone, 1st Lt., USAF Stanley E. Tate	N/A	
9. PERFORMING ORGANIZATION NAME AND ADDRESS	10. PROGRAM ELEMENT, PROJECT, TASK AREA & WORK UNIT NUMBERS	
Deputy for Development Planning ASD/XRH Air Force Systems Command - USAF Wright-Patterson AFB, Ohio 45433	(12) 140 P.	
11. CONTROLLING OFFICE NAME AND ADDRESS	12. REPORT DATE	
Deputy for Development Planning ASD/XR Air Force Systems Command - USAF Wright-Patterson AFB, Ohio 45433	11 Jan 1975	
14. MONITORING AGENCY NAME & ADDRESS (if different from Controlling Office)	13. NUMBER OF PAGES	
	135	
	15. SECURITY CLASS. (of this report)	
	UNCLASSIFIED	
	15a. DECLASSIFICATION/DOWNGRADING SCHEDULE	
	N/A	
16. DISTRIBUTION STATEMENT (of this Report)		
Distribution limited to US Government agencies only; report contains test and evaluation information; January 1975. Other requests for this document must be referred to ASD/XRH, Wright-Patterson AFB, OH 45433.		
17. DISTRIBUTION STATEMENT (of the abstract entered in Block 20, if different from Report)		
18. SUPPLEMENTARY NOTES		
19. KEY WORDS (Continue on reverse side if necessary and identify by block number)		
Infrared Signature Infrared Detectability Infrared Signature Prediction Infrared Suppression Computer Modelling Infrared Analysis Infrared Survivability ASDIR		
20. ABSTRACT (Continue on reverse side if necessary and identify by block number)		
The Aeronautical Systems Division Infrared Signature Prediction Program (ASDIR) is a state-of-the-art functionally modularized computer code. Volume III is a compilation of the essential reference material.		

ASDIR-II
VOLUME III
REFERENCE DOCUMENTATION

TABLE OF CONTENTS

TABLE OF CONTENTS	i
ABSTRACT	ii
"AIRCRAFT ENGINE INFRARED SIGNATURE PREDICTION PROGRAM (SIGNIR), USERS MANUAL (U)" PARCELLS, R.F., BLASER, A.N., MOURITSEN, T.E., VOUGHT AERONAUTICS, R2-53390/1R-2947, 30 SEP 1971 -- EXTRACTS	1
"HOW TO USE FS + TAU5." LINDQUIST, G., UNIVERSITY OF MICHIGAN, MEMO, 28 JAN 1970	64
"ADDITIONS AND CHANGES TO FS." LINDQUIST, G., UNIVERSITY OF MICHIGAN, MEMO, 17 APRIL 1970	72
"HOW TO USE THE PROGRAM PLUMES." LINDQUIST, G., UNIVERSITY OF MICHIGAN, MEMO, 22 JULY 1970.	75
"IR RADIATION FROM ROCKET EXHAUST PLUMES IN SPACE", SIMMONS, F., AND LINDQUIST, G., UNIVERSITY OF MICHIGAN, R3211-1-F, OCT 1970 -- EXTRACTS	89
"A BAND MODEL FORMULATION FOR VERY NONUNIFORM PATHS" LINDQUIST, G., AND SIMMONS, F.S., UNIVERSITY OF MICHIGAN, PUBLISHED IN: J. QUANT. SPECTROSC. RADIAT. TRANSFER, VOL 12, PP. 807-820, PERGAMON PRESS 1972	104

ASDIR-II

VOLUME III

REFERENCE DOCUMENTATION

ABSTRACT

Contained in this volume are the documents, referenced in Volumes I and II of this report, which are essential to the understanding of key segments of ASDIR-II. In particular, these documents compliment the hot parts segment "SIGNIR" and the plume signature calculation "ALPLUM". All of the subject material is of such a nature that it is either not available through usual sources or it is sufficiently essential that immediate availability is necessary.

(Compilation of
supporting docs)

1.0 SIGNIR



**VOUGHT
AERONAUTICS**

P O BOX 5907 DALLAS TEXAS 75222

AIRCRAFT ENGINE INFRARED SIGNATURE PREDICTION
PROGRAM (SIGNIR), USER'S MANUAL (U)

Report 2-53390/1R-2947

30 September 1971

Submitted to: Naval Air Systems Command
Contract N00019-70-C-0393

By

R. F. Parcells
A. N. Blaser
T. E. Mouritsen

~~"In addition to security requirements which apply to
this document and must be met, each transmission sent
side the Department of Defense must have been approved
of Commander, Naval Air Systems Command, Department of
the Navy, Washington, D. C. 20360."~~

REPRODUCED WITH APPROVAL OF NAVAL AIR SYSTEMS
COMMAND.

TABLE OF CONTENTS FOR SIGNIR

1.0	SIGNIR.....	1
2.0	ABSTRACT.....	2
3.0	PROGRAM DESCRIPTION.....	3
3.1	GENERAL.....	3
3.2	COMPUTATIONAL PROCEDURE.....	4
3.3	ANALYTICAL METHODS INCORPORATED.....	8
3.3.1	Exhaust System Gas Flow.....	8
3.3.1.1	Compressible Fluid Flow.....	8
3.3.1.2	Surface Boundary Layer.....	10
3.3.2	Exhaust System Surface Cooling.....	21
3.3.2.1	Film Cooling.....	22
3.3.2.2	Convection-Film Cooling.....	27
3.3.2.3	Transpiration Cooling.....	33
3.3.3	Exhaust System Radiation.....	37
3.3.3.1	Geometric Radiation View Factor.....	38
3.3.3.2	External Geometric Radiation View Factors.....	39
3.3.3.3	Gray Body Interchange Factors.....	40
3.3.4	Exhaust System Heat Balance.....	44
3.3.5	Exhaust System Radiation Emission.....	46
3.3.5.1	Spectral Emission.....	46
3.4	SPECIAL COMPUTATION CONSIDERATIONS.....	50
3.4.1	Thrust Change Resulting from Suppressing Exhaust System....	51
3.4.2	Pressure Loss Parameters.....	57
3.4.3	Heat Transfer Parameters.....	58
4.0	REFERENCES FOR SIGNIR.....	61

VOUGHT AERONAUTICS COMPANY

2.0 ABSTRACT

The scientific computer program SIGNIR was written to provide predictions of the infrared emission from axisymmetric turbojet, turbofan and turboshaft engine exhaust system hot surfaces. This manual provides the program user with all information necessary to obtain predictions of the infrared signature of any selected exhaust system. The program conducts its own internal flow analysis and thermal balance to provide the system surface temperature distribution. Both surface radiation, including multiple surface reflections, and special surface cooling methods are employed by the program. The radiant intensity of the emitted energy, attenuated by the atmosphere, is provided for selected ranges and system off-axis angles for infrared wavelengths of from one to 15 microns at 0.05 micron increments. Also, selected infrared radiant intensity bandwidth summations may be requested which can include the detector response characteristics.

The physical exhaust system selected is translated into a mathematical program model by the user. All required internal program decisions are keyed from the model input data. This manual provides the user with a description of the program, the analytical techniques employed, the methods required to model the selected exhaust system, program input data requirements and output data available. The user will find that little knowledge is required of the program's internal operations to be capable of utilizing program SIGNIR for exhaust system signature predictions.

3.0 PROGRAM DESCRIPTION

The description of the infrared signature prediction program (SIGNIR) is provided by the following sections which cover a general description of the program, the program computational procedure and the analytical methods utilized in obtaining the solution. A section covering special data computation is provided to aid the program user.

3.1 GENERAL

The program SIGNIR is a digital computer program written for the purpose of providing predictions of the hot metal infrared emission from aircraft engine exhaust systems. The program is designed to be applicable to axi-symmetric turbojet, turbofan, or turboshaft engine exhaust systems. It predicts the spectral intensity of the radiant energy emitted from exhaust system hot metal in the wavelength band of from one to 15 microns. In general, the information required by the program is as follows:

- . Exhaust system physical characteristics.
- . Engine operating conditions.
- . Special surface cooling flow conditions.
- . Exhaust system surface properties.

The predictions provided by the program for the combination of a selected maximum of 30 engine off-axis angles, five detector ranges and three detector altitudes are:

- . Spectral radiant intensity
- . Selected radiant intensity bandwidth summation

Optional exhaust system information which can be requested from the program is:

- . Internal fluid flow properties.
- . Surface boundary layer data.
- . Internal and external geometric radiation view factors.
- . Surface temperature distribution.
- . Thrust information.

VOUGHT AERONAUTICS COMPANY

Program SIGNIR is made up of 71¹ subprograms. This program is written in Fortran IV for the IBM 360 system.² A program flow diagram, a program listing and a basic task description for each of the subroutines are provided in the Appendices. All necessary computer control information required to operate this program is discussed in section 7.³

3.2 COMPUTATIONAL PROCEDURE

The process of computing the intensity of the infrared energy emitted from aircraft exhaust system hot metal requires a knowledge of the metallic surfaces temperature, emissive properties and their relative physical positioning within the system. From this information, the radiant energy emitted and reflected from the exhaust system to a point in space can be determined. The computational procedure established by this program for the prediction of exhaust system hot metal infrared radiation is shown by major subjects in the general block diagram presented on figure 1.

The input data required by the program provides a physical model (nodal system) of the exhaust system configuration, the properties and conditions of the exhaust gases entering the system. The program undertakes a one-dimensional, isentropic, compressible flow analysis which generates the axial distribution of exhaust gas flow conditions and properties within the system. Where two gas streams at different temperatures flow within a single passage, compound flow considerations are utilized. The program adjusts the flow at the nozzle throat to balance with the ambient pressure or a choked condition dependent on the system's entrance flow data.

With the internal flow properties defined, a surface boundary layer analysis is conducted to obtain the coefficients of convection and friction along each surface within the system. This analysis is primarily dependent on the surface's axial static pressure distribution and the upstream boundary layer conditions. An area weighted average coefficient of convection for each of the model's surface nodes (isothermal regions established by the input data) is computed for the system thermal analysis. The axial force on each surface, internal to the system, is computed utilizing both the frictional and pressure-area forces.

¹Reduced by ASD

²Modified for ASD CDC 6600

³See ASDIR-II User's Manual

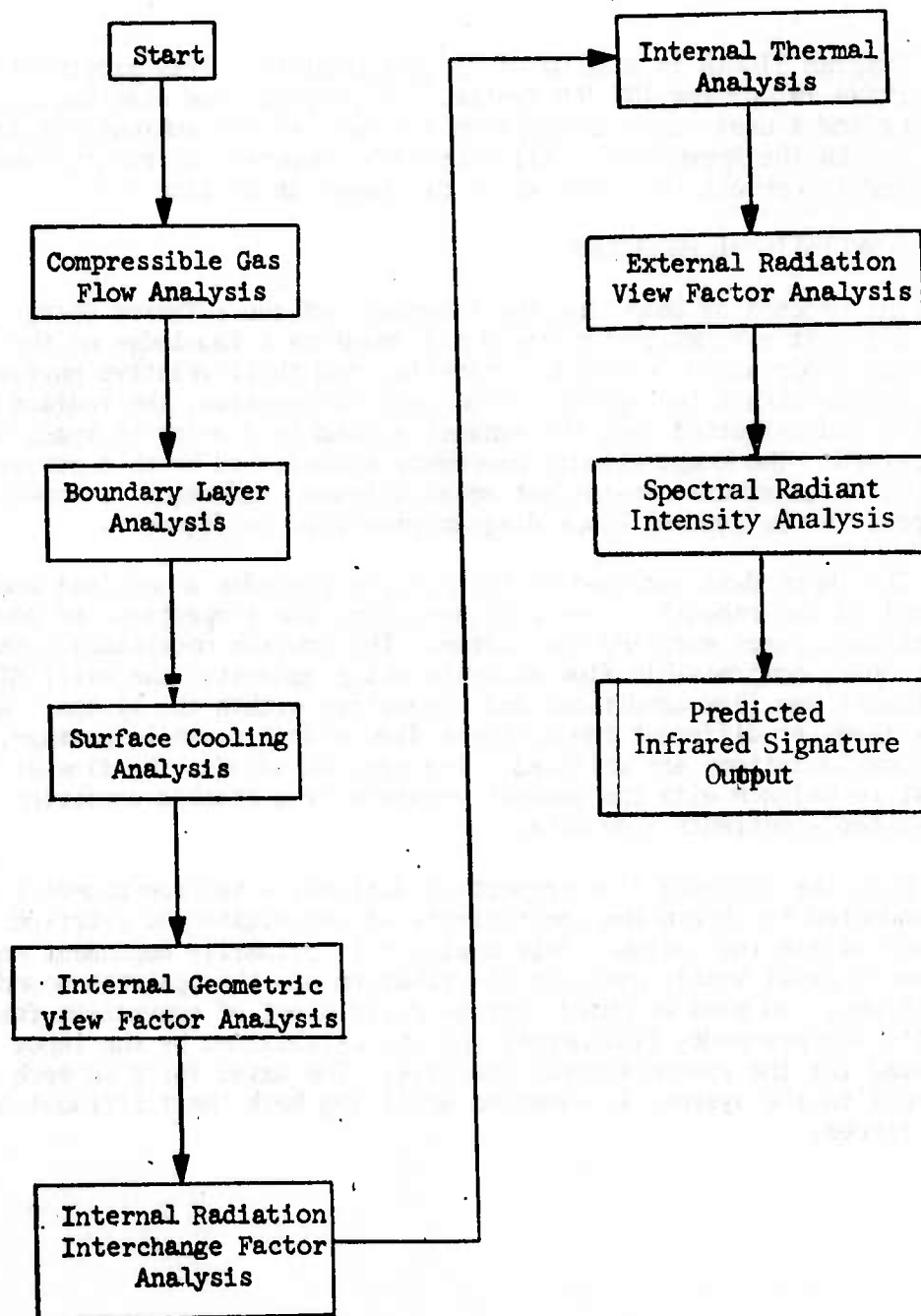


FIGURE 1: Program SIGNIR Analysis

VOUGHT AERONAUTICS COMPANY

The next step taken by the program is the calculation of the temperatures along any surfaces cooled by transpiration, film or convection-film cooling methods. The program accepts a fixed coolant flow rate or computes a system coolant flow balance when coolant source conditions are defined. The calculation for these cooling methods are dependent on the physical design of the wall itself and the conditions of the gas flow adjacent to it. The axial surface temperature distribution is an area weighted average across each of the nodes involved along the cooled surface.

The calculation of internal system geometric radiation view factors is the next step in the programs computational procedure. One of the more difficult factors in radiation calculations is determining the fraction of energy leaving one given surface that will be intercepted by another given surface, or a portion of that surface. Geometric view factors provide this description. This program computes view factors for each node taking advantage of the symmetry of the system and considering each node as a frustum of a right circular cone, a cylinder or a disk. View factors are computed for each node's view of all other nodes within the system including itself. The computation procedure accounts for shadowing when the view between two nodes is partially obscured by some intervening surface.

With the geometric radiation view factors computed and system surface emissivities available from input data, the overall radiation interchange factor (script F) is computed. This factor, used in the radiation calculations, accounts for the view between two surfaces, the non-black nature of these surfaces and the fact the multiple reflections between all surfaces are occurring. Two surfaces, which geometrically can not see each other, can interchange energy through energy reflection from other surfaces within the system. The computational procedure considers all surfaces to be diffused surfaces, i.e. the emitted and reflected energy departing a surface has the same distribution as that of a black body which follows Lambert's law of cosines.

At this point in the computational procedure, all essential information necessary to conduct a system internal heat balance has been acquired. The steady state thermal analysis considers energy radiation, convection and conduction. The conduction between nodes along the same surface is neglected since the thermal gradient along the walls are expected to be low. Radiation from the hot gas has also been neglected since this energy contribution to a surface is small when compared to the convection from the hot gas and or the radiation from exhaust system surfaces at near the same temperatures. The programs thermal analysis provides the temperature of each of the surface nodes within the exhaust system.

VOUGHT AERONAUTICS COMPANY

The next step accomplished by the program is the determination of the radiation interchange factors between a detector fixed in space and the nodes established for the exhaust system. The view factors are computed between the detector and those nodes which can be viewed by the detector. In turn, overall radiation interchange factors are computed which consider the multiple energy reflection which occur between nodes, the emissive properties of the surfaces and the geometric view factors as was done previously with the internal interchange factors.

With the overall interchange factors and system node temperatures, the radiant energy passing from the system hot metal to the detector is determined utilizing the Stefan-Boltzmann law. In turn, the energy distribution is computed considering the radiant energy to be distributed in accordance with Planck's law. This energy distribution is placed in the more common terms of spectral radiant intensity which eliminates any consideration of the area of energy collection by the detector.

3.3 ANALYTICAL METHODS INCORPORATED

The analytical method utilized by program SIGNIR is presented in this section under the general topics of exhaust system gas flow, surface cooling, radiation, internal heat balance and radiation emission. By presenting the analytical methods in this sequence, the progression of information is similar to that presented by the computational procedure of section 3.2.

3.3.1 Exhaust System Gas Flow

An internal gas flow analysis is conducted by SIGNIR under the control of RIMAIN. The primary effort is to determine the distribution of gas stream properties and the surface boundary layer convection coefficients. The following sections cover the analytical procedures utilized in computing the compressible flow and surface boundary layer.

3.3.1.1 Compressible Fluid Flow

The sub-program COFLOW establishes the flow properties within a compound stream based on a one-dimensional, isentropic flow analysis. The method employed is based on the analysis presented in reference 1 which assumes that the primary and secondary streams of a mixed turbofan exhaust system can be handled separately. Its theory has been found to agree well with experimental findings. COFLOW provides an array of compound-flow properties associated with flow areas for a given combination of flow rates. The fluid static pressure is chosen to be constant across adjacent streams. If a single stream configuration is employed, the same analytical procedure is employed utilizing only the single stream.

The nomenclature used within this section is as follows:

A	- flow area, ft. ²
C _F	- flow coefficient
g	- acceleration of gravity, ft./sec. ²
j	- an integer (corresponding to the subscript j)
k	- ratio of specific heats
\dot{m}	- mass flow rate, lb _m /sec.
M	- flow Mach number
n	- number of compound streams
P	- static pressure, lb _f /ft. ²
P _T	- total pressure, lb _f /ft. ²
ΔP	- increment in static pressure, lb _f /ft. ²
R	- gas constant, lb _f ft./lb _m ^{OR}
T	- static temperature, ° _R
T _T	- total temperature, ° _R
V	- flow velocity, ft./sec.
σ	- compound-flow indicator
ρ	- density, lb _m /ft. ³

VOUGHT AERONAUTICS COMPANY

subscripts:

- amb - ambient conditions
- ex - nozzle exit
- i - an integer, stream number
- j - an integer, relates physical conditions and flow properties at the same static pressure conditions

The sub-program COFLOW computes an array of fluid properties compatible with values of static pressure decremented from the total pressure provided to the ambient static pressure, i.e.

$$P_j = P_T - j \cdot \Delta P \quad (1)$$

The stream properties for a perfect gas are computed by the following isentropic flow relationships:

$$M_{i,j} = \sqrt{\frac{2}{(K_i - 1)} \left[(P_T / P_j)^{(K_i - 1)/K_i} - 1 \right]} \quad (2)$$

$$T_{i,j} = T_{T,i,j} \left[1 + \left(\frac{K_i - 1}{2} \right) M_{i,j}^2 \right]^{-1} \quad (3)$$

$$V_{i,j} = M_{i,j} \sqrt{K_i g R_i T_{i,j}} \quad (4)$$

$$\rho_{i,j} = P_j / R_i T_{i,j} \quad (5)$$

$$A_{i,j} = \dot{m}_i / (\rho_{i,j} V_{i,j}) \quad (6)$$

VOUGHT AERONAUTICS COMPANY

A compound flow indicator, β is used to determine if choking occurs at a static pressure value which is greater than ambient pressure (choked convergent nozzle). Compound-flow is subsonic when $\beta > 0$, sonic at $\beta = 0$ and supersonic when $\beta < 0$. The indicator is evaluated by the equation given in reference 1 as

$$\beta_j = \sum_{i=1}^n \frac{A_{i,j}}{K_i} \left(\frac{1}{\dot{m}_{i,j}} - 1 \right) \quad (7)$$

This shows that at the compound-choke condition, some streams can be supersonic while others are subsonic. For a single stream, $n = 1$, $\beta = 0$ when the stream mach number is one. The sub-program COFLOW is limited to two streams ($i = 2$). Once the array of stream properties are formed, the total flow area,

$$A_{Tj} = \sum_{i=1}^n A_{i,j} \quad (8)$$

at the nozzle exit is determined from the program at

$$\beta = 0, \text{ if } P > P_{amb} \quad (9)$$

or at

$$P = P_{amb} \text{ if } \beta > 0. \quad (10)$$

The total flow area of the array is adjusted by a flow coefficient

$$C_F = A_{T(ex)} / A_{ex} \quad (11)$$

which is an adjustment toward two-dimensional flow considerations.

3.3.1.2 Surface Boundary Layer

The conditions within the compressible turbulent boundary layer which exists along each of the exhaust system surfaces is computed by sub-program TURBLT. This is a segment of an existing

VOUGHT AERONAUTICS COMPANY

computer program written by A. H. Ybarra of Vought Aeronautics Company of LTV Aerospace Corporation. The analytical methods employed are basically those presented by reference 2 in which the boundary layer is expressed in terms of the momentum integral and moment-of-momentum integral, simplified by a Mager-type transformation and solved simultaneously. Ybarra incorporated an empirical modification to the moment-of-momentum equation which improved the methods agreement with test data.

The following is a list of nomenclature for symbols used within this section.

$b(x)$	- transformation parameter
C_f	- local skin friction coefficient, dimensionless
$c(x)$	- transformation parameter
C_p	- specific heat at constant pressure, $\text{Btu/lb}_m\text{-}^\circ\text{R}$
d	- exact differential
e	- exponential base, $e = 2.718281828$, dimensionless
F_1	- empirical factor
F_2	- empirical factor
H	- boundary layer shape factor, dimensionless (incompressible transformed denoted by subscript tr)
h	- enthalpy, Btu/lb_m
h_c	- convection heat transfer coefficient, $\text{Btu/hr.ft}^2\text{-}^\circ\text{R}$
M^c	- Mach number, dimensionless
m	- power law profile exponent, dimensionless
p	- pressure, lb_f/in^2
Pr	- Prandtl number, dimensionless
R	- Radius of symmetry, ft.
Re_θ	- Reynolds number based on momentum thickness, dimensionless
R_g	- gas constant, $\text{lb}_f\text{-ft./lb}_m\text{-}^\circ\text{R}$
r_g	- recovery factor, dimensionless
S	- enthalpy ratio factor, $S = (h_s/h_o) - 1.0$, dimensionless
T	- temperature, $^\circ\text{R}$
U'	- transformed velocity along surface, ft/sec.
u	- physical velocity along surface, ft/sec.
V	- transformed velocity normal to surface, ft/sec.
v	- physical velocity normal to surface, ft/sec.
X	- transformed coordinate along surface, ft.
x	- physical coordinate along surface, ft.
Y	- transformed coordinate normal to surface, ft.
y	- physical coordinate normal to surface, ft.

VOUGHT AERONAUTICS COMPANY

γ	- ratio of specific heats, dimensionless
Δ	- transformed boundary layer thickness, ft.
Δ^*	- transformed boundary layer displacement thickness, ft.
δ	- physical boundary layer velocity thickness, ft.
δ^*	- physical boundary layer displacement thickness, ft.
θ	- boundary layer momentum thickness, ft.
μ	- absolute viscosity, lb./sec-ft.
ν	- kinematic viscosity, ft ² /sec.
ρ	- density, lb./ft ³
τ	- shear stress, lb./ft-sec ²
ψ	- transformed velocity potential, l/sec.
ϕ	- velocity potential, l/sec.
∂	- partial derivative symbol

Subscripts

e	- local inviscid flow, at edge of boundary layer
i	- incompressible
o	- freestream stagnation conditions
ref	- at Eckert reference enthalpy conditions
s	- local stagnation conditions
T	- total conditions, unsubscripted indicates static conditions
tr	- transformed
w	- at the surface, wall
1	- current value, at end of current increment
2	- previous value, at start of current increment

For steady, compressible, turbulent flow the boundary layer equations, in which the flow variable appear as time-averaged quantities, are expressed by the continuity and momentum equations for axisymmetric system as

$$\frac{\partial(\rho u)}{\partial x} + \frac{\partial(\rho v)}{\partial y} + \frac{\rho u}{R} \frac{dR}{dx} = 0 \quad (12)$$

and

$$\rho u \frac{\partial u}{\partial x} + \rho v \frac{\partial u}{\partial y} = - \frac{dP}{dx} + \frac{\partial \tau}{\partial y} \quad (13)$$

These two partial differential equations, in their present form, can not be solved simultaneously. To simplify and reduce the difficulty of integration, a Mager-type transformation is performed which transforms the physical coordinates as

$$X = \int_0^x b(x) dx \quad (14)$$

and

$$Y = c(x) \int_0^y \frac{dy}{\rho} \quad (15)$$

where

$$b(x) = (T_{T0} / T_{ref}) (T_e / T_{T0})^{\frac{\gamma+1}{2(\gamma-1)}} \quad (16)$$

$$c(x) = (T_e / T_{T0})^{1/2} \quad (17)$$

The velocities can be replaced through the definition of a stream function, as

$$\begin{aligned} \frac{\partial \psi}{\partial y} &= \frac{\rho u}{\rho_0} \\ \frac{\partial \psi}{\partial x} &= - \frac{\rho v}{\rho_0} \end{aligned} \quad (18)$$

and the transformed velocities by the relations

$$\left. \begin{aligned} u &= \frac{\partial \psi}{\partial Y} \\ v &= - \frac{\partial \psi}{\partial X} \end{aligned} \right\} \quad (19)$$

Applying equations 14, 15 and 18 to the boundary layer equations 12 and 13 result in the following transformed continuity and momentum equation:

$$\frac{\partial U}{\partial X} + \frac{\partial V}{\partial Y} = 0 \quad (20)$$

$$U \frac{\partial U}{\partial X} + V \frac{\partial U}{\partial Y} = U_e \frac{\partial U_e}{\partial X} (1+S) + \nu_e \frac{\partial^2 U}{\partial Y^2} \quad (21)$$

where the enthalpy term is defined as

$$S = (h_s/h_o) - 1.0 \quad (22)$$

where h_s is the local stagnation enthalpy.

The boundary conditions applicable to the equations 20 and 21 are:

$$\begin{aligned} U(X,0) &= 0 && \text{no slip at wall.} \\ V(X,0) &= 0 && \text{no mass added or removed from boundary layer at wall.} \\ S(X,0) &= S_w(X) && \text{enthalpy ratio at wall depends only on local recovery temperature.} \\ \lim_{Y \rightarrow \infty} S &= 0 && \text{local stagnation temperature approaches free-stream total temperature.} \\ \lim_{Y \rightarrow \infty} U, U_e(X) &&& \text{boundary layer velocity approaches external velocity.} \end{aligned} \quad (23)$$

Some correlations between transformed and physical parameters which result from the Mager-type transformation are as follows:

$$\text{Longitudinal velocity, } U = (T_e/T_{T0})^{1/2} U_e = [C(\chi)] U_e \quad (24)$$

$$\text{Velocity potential, } \psi = \psi_e \quad (25)$$

$$\text{Boundary Layer Shape Factor, } H = \left[1 + \frac{\gamma-1}{2} M_e^2\right] H_{tr} + \frac{\gamma-1}{2} M_e^2. \quad (26)$$

$$\text{Momentum thickness, } \Theta = \Theta_{tr} (T_{T0}/T_e)^{\frac{\gamma+1}{2(\gamma-1)}}. \quad (27)$$

$$\text{Displacement thickness, } \delta^* = (\Theta_{tr} + \Delta^*) (T_{T0}/T_e)^{\frac{\gamma+1}{2(\gamma-1)}} - \Theta_{tr} (T_{T0}/T_e)^{\frac{\gamma+1}{2(\gamma-1)}}. \quad (28)$$

The combining and manipulation of equations 20 and 21 produce the equation

$$\begin{aligned} \frac{\partial}{\partial X} [U(U_e - U)] + \frac{\partial}{\partial Y} [V(U_e - U)] + \frac{\partial U_e}{\partial X} (U_e - U) \\ + U_e \frac{\partial U_e}{\partial X} S = - \nu_0 \frac{\partial^2 U}{\partial Y^2} \end{aligned} \quad (29)$$

The transformed momentum thickness Θ_{tr} , and the transformed displacement thickness, Δ^* , are defined as

$$\Theta_{tr} = \int_0^\Delta \left(\frac{U}{U_e}\right) \left(1 - \frac{U}{U_e}\right) dY \quad (30)$$

$$\Delta^* = \int_0^\Delta \left(1 - \frac{U}{U_e}\right) dY \quad (31)$$

and the transformed boundary layer shape factor follows as

$$H_{tr} = \Delta^* / \Theta_{tr} \quad (32)$$

Integrating equation 29 with respect to Y between the limits Y=0 and Y=Δ (where Δ is a distance normal to the surface sufficiently large such that the conditions S=0 and U=U_e are both satisfied), applying the chain rule and equations 30 and 31, the following equation form can be obtained:

$$\frac{d\Theta_{tr}}{dX} + \frac{1}{U_e} \frac{dU_e}{dX} \left[2\Theta_{tr} + \Delta^* + \int_0^\Delta S dY \right] = \frac{\nu_0}{U_e^2} \left(\frac{\partial U}{\partial Y} \right)_{Y=0}. \quad (33)$$

The fundamental definition of the boundary layer shear stress is expressed by

$$\tau_w = \mu_w \left(\frac{\partial u}{\partial y} \right)_{y=0} \quad (34)$$

By utilizing equations 14, 24, 32 and 34 and a reference temperature technique such that

$$(\mu/\rho)_w = \mu_0/\rho_0 (T_{r0}/T_{ref}), \quad (35)$$

equation 33 becomes

$$\frac{d\theta_{tr}}{dX} + \frac{\theta_{tr}}{U_e} \frac{dU_e}{dX} \left[2 + H_{tr} + \frac{1}{\theta_{tr}} \int_0^\Delta S dY \right] = \left(\frac{T_{r0}}{T_e} \right) \left(\frac{T_{ref}}{T_{r0}} \right) \frac{\tau_w}{\rho_e U_e^2} \quad (36)$$

which is the form of the transformed momentum integral equation presented in reference 2.

The moment-of-momentum integral equation is derived in a similar manner. The differential form the momentum equation 29 is multiplied by the parameter Y and the results inturn integrated with respect to Y from Y=0 to Δ . The resulting integral equation obtained is,

$$\begin{aligned} \frac{dH_{tr}}{dX} = & \frac{-1}{2U_e} \frac{dU_e}{dX} \left[H_{tr} (H_{tr} + 1)^2 (H_{tr} - 1) \right] \left[1 + \frac{2}{(H_{tr} + 1)\theta_{tr}} \int_0^\Delta S dY \right. \\ & - \frac{2(H_{tr} - 1)}{H_{tr}^2 (H_{tr} + 1)\theta_{tr}^2} \int_0^\Delta S Y dY \\ & + \frac{H_{tr} (H_{tr}^2 - 1)}{\theta_{tr}} \left(\frac{T_{r0}}{T_e} \right) \left(\frac{T_{ref}}{T_{r0}} \right) \frac{\tau_w}{\rho_e U_e^2} \\ & \left. - \frac{(H_{tr}^2 - 1)(H_{tr} + 1)}{\theta_{tr}} \left(\frac{T_{r0}}{T_e} \right) \left(\frac{T_{ref}}{T_{r0}} \right) \frac{\tau_w}{\rho_e U_e^2} \int_0^1 \frac{\gamma}{\gamma_w} d\left(\frac{Y}{\Delta}\right) \right] \quad (37) \end{aligned}$$

The Ludwig-Tillman skin-friction relationships for incompressible turbulent flow, both convenient and valid over a wide range of pressure gradients, is given as

$$C_f = \frac{\tau_w}{\frac{1}{2} \rho U_e^2} = 0.246 e^{-1.561 \cdot H_i} R_{e\theta}^{-0.268} \quad (38)$$

The Reynolds number based on momentum thickness is defined as

$$R_{e\theta} = U_e \theta / \nu \quad (39)$$

With the application of the reference enthalpy concept, equations 24 and 27, and the relations

$$\frac{p_{ref}}{\rho} = \frac{T}{T_{ref}} \quad (40)$$

and

$$\nu_{ref} = \nu_0 \left(\frac{\mu_{ref}}{\mu_0} \right) \left(\frac{\rho_0}{\rho_{ref}} \right) \quad (41)$$

equation 38 can be put in the form

$$\frac{C_f}{2} = \frac{\tau_w}{\rho_e U_e^2} = \frac{0.123 (T_e / T_{ref}) (\mu_{ref} / \mu_0)^{0.268}}{e^{1.561 H_i} (U_e \theta_{tr} / \nu_0)^{0.268}} \quad (42)$$

This is the expression of skin coefficient for compressible flow in terms of the transformed velocity, momentum thickness and reference temperature (and viscosity).

The integrals which appear in the transformed momentum and moment-of-momentum equations, 36 and 37, shall be reduced to a usable form. The recovery factor is defined as

$$r = \sqrt[3]{P_r} \quad (43)$$

VOUGHT AERONAUTICS COMPANY

for a turbulent boundary layer. For a Prandtl number of unity, the recovery temperature will be equal to the freestream stagnation temperature. Therefore, for adiabatic flow, the value of S in equation 22 would be zero and the integrals will be zero. To evaluate the integrals at an arbitrary surface temperature, the Crocco relation is employed together with a power law assumption for the velocity profiles, i.e.

$$\frac{h_s - h_w}{h_o - h_w} = \frac{U}{U_e} = \frac{U}{U_e} \quad (44)$$

and

$$\frac{U}{U_e} = \left(\frac{Y}{\Delta} \right)^{1/m} \quad (45)$$

Since the purpose of the Mager-type transformation is to render the boundary layer equations analogous to the incompressible form, the transformed and incompressible shape factor are near equal. Using this information, the integrals are evaluated as

$$\int_0^{\Delta} S dY = S H_i \theta_{tr} = \left(\frac{h_w}{h_o} - 1 \right) H_i \theta_{tr} \quad (46)$$

and

$$\int_0^{\Delta} S Y dY = \left(\frac{h_w}{h_o} - 1 \right) \frac{H_i^2 (H_i + 1)^2}{2(H_i - 1)(H_i + 3)} \theta_{tr}^2 \quad (47)$$

Substituting equations 22, 24, 38 and 46 into equation 36, the momentum equation becomes

$$\frac{d\theta_{tr}}{dX} = \left(\frac{T_{ref}}{T_o} \right) \left(\frac{C_f}{2} \right) - \frac{\theta_{tr}}{U_e} \frac{dU_e}{dX} \left[2 + \frac{h_w}{h_o} H_i \right] \quad (48)$$

By the same procedure, the term of equation 37 containing the integration in Y reduces as

$$\left[1 + \frac{2}{(H_i+1)\Theta_{cr}} \int_0^{\Delta} S dY - \frac{2(H_i-1)}{H_i^2(H_i+1)\Theta_{cr}^2} \int_0^{\Delta} S dY \right] \\ = 1 + \left(\frac{h_w}{h_o} - 1 \right) \frac{H_i^2 + 4H_i - 1}{(H_i+1)(H_i+3)} \quad (49)$$

The integral contained in the last term of equation 37 is not so easily simplified. An empirical relation,

$$\int_0^{\Delta} \frac{Y}{\gamma_w} d\left(\frac{Y}{\Delta}\right) = \frac{0.003075 H_i - 0.003352}{C_f/2} \quad (50)$$

was established from the data presented in reference 2 in terms of the variables H_i and C_f . Once the analytical model was complete, further empirical corrections in the last term of equation 37 found necessary to correlate with measured test data. These correlation factors take the form of

$$F1 = C_p / \left(1 + \frac{\gamma-1}{2} M_e^2 \right) \quad (51)$$

$$\left. \begin{aligned} F2 &= 1.0, \quad \text{when } \frac{dM_e}{dX} \geq 0 \\ &= 1.0 + \left(\frac{dM_e}{dX} \right)^2, \quad \text{when } \frac{dM_e}{dX} < 0 \end{aligned} \right\} \quad (52)$$

with the further restriction that

$$(F1)(F2) \leq 1.0 \quad (53)$$

VOUGHT AERONAUTICS COMPANY

By employing those methods required in establishing equation 48 and applying the empirical parameters presented, equation 37 reduces to the form

$$\begin{aligned} \frac{dH_i}{dX} = & - \frac{H_i(H_i+1)^2(H_i-1)}{2} \left[1 + \left(\frac{h_w}{h_o} - 1 \right) \frac{H_i^2 + 4H_i - 1}{(H_i+1)(H_i+3)} \right] \frac{1}{U_e} \frac{dU_e}{dX} \\ & + \frac{H_i(H_i+1)^2}{\Theta_{tr}} \left(\frac{T_{ref}}{T_o} \right) \frac{C_f}{2} \\ & - (F1)(F2) \frac{(H_i^2-1)(H_i+1)}{\Theta_{tr}} \left(\frac{T_{ref}}{T_e} \right) (.003075 H_i - .003352) \end{aligned} \quad (54)$$

In subprogram TURBLT, the two transformed boundary layer equations 48 and 54 are solved simultaneously using an iterative finite difference numerical integration procedure. Specifically, the process employed divides the surface being analyzed into small increments. For each surface increment, a value for H_i and Θ_{tr} is assumed at the downstream end of that increment and then, using the average value for all pertinent parameters over the surface increment, the two equations 48 and 54 are solved. The results are compared with the initial estimates and an iteration carried out to converge on a solution.

The program is provided with the properties of the gas stream flowing adjacent to the surface and the initial (upstream) values of momentum thickness, Θ , and incompressible shape factor H_i (these two values must be input by the program user which requires some estimate of the boundary layer conditions entering the exhaust system). With a surface increment's upstream (2) boundary layer condition, the program makes an assumption as to the downstream (1) growth. The conditions and properties values over the increment are averaged, equations 42, 51 and 53 are evaluated and, in turn, equations 48 and 54 are solved simultaneously utilizing the equations

$$\Theta_{tr1} = \Theta_{tr2} + \frac{d\Theta_{tr}}{dX} (X_1 - X_2) \quad (55)$$

and

$$H_{i1} = H_{i2} + \frac{dH_i}{dX} (X_1 - X_2) \quad (56)$$

The initial estimate is corrected, the solution process continued until the parameters converge. Inturn, the parameters for the following increments are solved in a systematic order.

From the solution obtained, local physical boundary layer parameters along the surface are computed by the program. These are

boundary layer thickness,

$$\delta = \alpha_{tr} \left(\frac{T_{ro}}{T_e} \right)^{\frac{r+1}{2(r-1)}} \left[H_{i2} + 2 + \left(\frac{H_{i2} + 1}{H_{i2} - 1} \right) + \frac{r-1}{2} M_e^2 (H_{i2} + 1) \right] \quad (57)$$

local skin friction coefficient,

$$C_f = .246 e^{-1.56 H_{i2}} \left(\frac{\sqrt{V}}{u_e \theta} \right)^{0.268} \quad (58)$$

local convection heat transfer coefficient,

$$h_c = \frac{C_f}{2} \sqrt{\frac{\gamma q}{R_g}} \left(P_r \right)^{-2/3} \cdot C_p P_{ro} (T_{ro})^{-1/2} M_e \left(1 + \frac{r-1}{2} M_e^2 \right)^{\frac{-(r-1)}{2(r+1)}} \\ \cdot e^{1.561 [H_{i2} - 1.3 - .2(3.25r - 2.25) M_e^2]} \quad (59)$$

3.3.2 Exhaust System Surface Cooling

Three method for cooling exhaust surfaces have been incorporated into the program SIGNIR. They are film, convection-film and transpiration cooling. These cooling methods were selected as the more efficient means of cooling surfaces. They give the program latitude in the types of systems which this program is applicable. The following section presents the analytical procedures employed for each of the surface cooling methods.

3.3.2.1 Film Cooling

The gaseous film cooling method incorporated by subprogram FILMCL is an empirical correlation of various investigator's data presented by reference 3. The cooling configuration utilized by the program is specifically for tangential injection of the coolant. The method proposed by reference 4 was coupled with this film cooling method to be capable of handling multiple slot configurations. The nomenclature used within this section is as follows:

A	- area, ft.^2
C_d	- flow discharge, nondimensional
C_p	- specific heat at constant pressure, $\text{Btu/lb}_m \cdot ^\circ\text{R}$
$f(v)$	- velocity mismatch factor, nondimensional
g	- gravitational acceleration, ft./hr.^2
h	- convective heat transfer coefficient, $\text{Btu/hr.ft.}^2 \cdot ^\circ\text{R}$
i	- an integer, nondimensional
K	- pressure loss coefficient, $\text{lb}_f/\text{ft.}^2$
m	- total number of cooling slots, nondimensional
M	- heat capacity ratio, $(\rho VC_p)_c/(\rho VC_p)_g$
\dot{m}	- mass flow rate, $\text{lb}_m/\text{hr.}$
n	- flow exponent, nondimensional
P	- static pressure, $\text{lb}_m/\text{ft.}^2$
P_T	- total pressure, $\text{lb}_m/\text{ft.}^2$
R	- gas constant, $\text{lb}_f.\text{ft.}/\text{lb}_m \cdot ^\circ\text{R}$
s	- slot height, ft.
St	- Stanton number $(h_g/\rho VC_p)$, nondimensional
T	- temperature or static temperature, $^\circ\text{R}$
T_r	- recovery temperature, $^\circ\text{R}$
T_T	- total temperature, $^\circ\text{R}$
UA	- overall rate of heat transfer, $\text{Btu/hr.} \cdot ^\circ\text{R}$
V	- velocity, ft./hr.
x	- distance downstream from slot, ft.
γ	- ratio of specific heats
Δ	- the change in a property, nondimensional

- η - film effectiveness
 ρ_{std} - density at standard temperature and pressure, lb_m/ft^3
 σ - ratio of density to density at standard temperature and pressure, nondimensional

Subscripts:

- c - coolant
 f - fluid film
 f' - adjacent to film
 g - mainstream gas
 s - slot
 t - total
 w - wall
 1 - coolant source
 2 - heat source

The empirical equation for film effectiveness proposed by reference 3 is

$$\eta = 1 / \left\{ 1 + 3.6 \left[\left(\frac{St_g}{M} \right) \left(\frac{x}{s} \right) \left(\frac{Tr_g}{Tr_c} \right)^{2/3} f(V) \right] \right\} \quad (60)$$

where

$$\eta = (Tr_g - T_w) / (Tr_g - Tr_c) , \quad (61)$$

$$f(V) = \left. \begin{aligned} &1 + 0.4 \arctan \left(\frac{V_g}{V_c} - 1 \right) ; \text{ when } \frac{V_g}{V_c} > 1 , \\ &= \left(\frac{V_g}{V_c} \right)^{1.5 (V_g/V_c - 1)} ; \text{ when } \frac{V_g}{V_c} \leq 1 . \end{aligned} \right\} \quad (62)$$

These equations were converted into a form where the independent variables are those available to the program. Specific terms of equation 60 were altered in form as shown.

$$\frac{St_g}{M} = \frac{h_g}{C_{p_c}} \cdot \frac{C_d A_s}{\dot{m}_c} \quad (63)$$

$$\frac{Tr_g}{Tr_c} = \frac{T_{f'}}{T_{tc}} \quad (64)$$

Equation 61 takes the form

$$T_w = T_{f1} - (T_{f1} - T_{tc}) \left(\frac{V_g}{V_c} \right)^{\frac{\gamma-1}{\gamma}} \quad (65)$$

where T_{f1} is the gas film temperature resulting from the upstream slot flow. The term

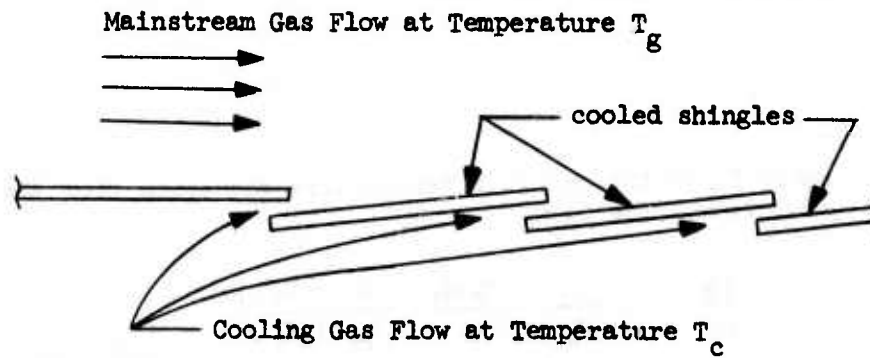
$$\frac{V_g}{V_c} = \frac{V_g}{R_c} \cdot \frac{C_d A_s}{\dot{m}} \cdot \frac{P_g}{T_{tc}} \left(\frac{P_{tc}}{P_g} \right)^{\frac{\gamma-1}{\gamma}} \quad (66)$$

from equation 62, is converted as shown which assumes isentropic flow from a common coolant plenum to the slot whose discharge static pressure adjusts to equal the mainstream gas static pressure. Combining the forgoing equations, the equation for wall temperature becomes

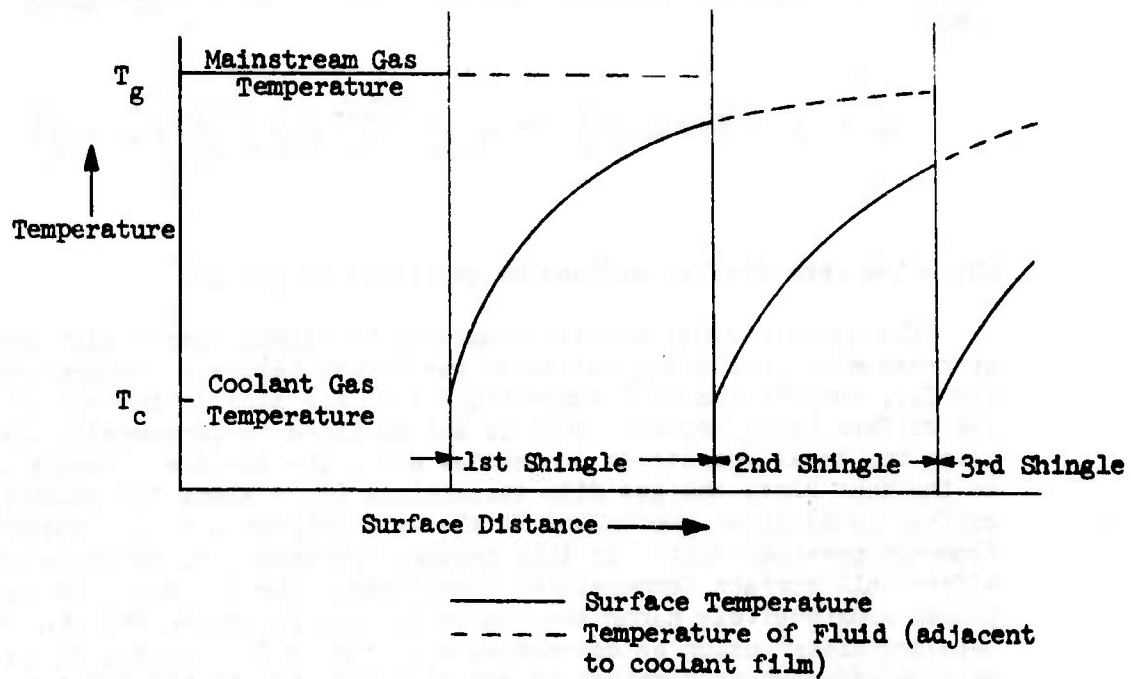
$$T_w = T_{f1} - (T_{f1} - T_{tc}) / \left\{ 1 + 3.6 \left[\frac{h_g}{C_{pc}} \left(\frac{C_d A_s}{\dot{m}_c} \right) \left(\frac{x}{S} \right) \left(\frac{T_{f1}}{T_{tc}} \right)^{\frac{2}{3}} f(v) \right] \right\} \quad (67)$$

where the term $f(v)$ is defined by equations 62 and 66.

The computational process conducted by FIIMCL starts with the upstream slot, utilizing the local gas stream recovery temperature for T_{f1} , compute the wall temperature from the slot to the end of the surface being cooled. This is accomplished in incremental steps using the local gas stream properties along the surface. Progressing to the next slot, the gas film temperature (T_{f1}) along the remaining surface is assigned the values of the wall temperature (T_w) computed from the previous slot. In this manner, upstream slot coolant films affect all surface temperatures downstream. The procedure is continued progressively along the cooled surface producing the wall temperature distribution as demonstrated in figure 2. Inturn, an area-weighted-average temperature is computed for each of the nodes assigned along this cooled surface.



(a) Multiple slot film cooled surface



(b) Multiple slot film cooled surface temperature distribution

FIGURE 2: Multiple Slot Film Cooling

VOUGHT AERONAUTICS COMPANY

A coolant flow balance is incorporated in this subprogram which provides the coolant flow properties required by the equations 66 and 67. The program user is provided the option of defining either the coolant flow rate or its source. If flow rate is defined, coolant supply temperature must also be provided. The slots are assumed to be supplied from a common plenum such that the driving total pressure to each slot is identical. The coolant flow from each coolant slot is a function of both the slot flow area and the gas stream local static pressure. The coolant total pressure and individual slot coolant flow rate is computed using an iteration process. A form of the continuity equation, using isentropic considerations, is shown in terms of the dependent variables, slot flow rate and total pressure.

$$\dot{m}_c = C_d A_s P_{Tc} \left(\frac{P_{Tc}}{P_g} \right)^{-\frac{(r+1)}{r}} \sqrt{\left(\frac{2r}{r-1} \right) \left(\frac{g}{R T_{Tc}} \right) \left[\left(\frac{P_{Tc}}{P_g} \right)^{\frac{r-1}{r}} - 1 \right]} \quad (68)$$

The selected total coolant flow rate is

$$(\dot{m}_c)_{total} = \sum_{i=1}^m \dot{m}_{c_i} \quad (69)$$

The program iterates about total pressure and flow rate to obtain a solution which provides the individual slot coolant flow rates.

If the option is selected to compute the coolant flow rate based on coolant source temperature and pressure, an extension of the forgoing process is required. This computational procedure includes the supply system pressure loss and heat transfer. The coolant supply system pressure loss is computed by the equation form

$$\sigma \Delta P_T = K (\dot{m})^n \quad (70)$$

where the system characteristics K and n are required input (see discussion in section 3.4). The program solves this equation in the form

$$(\dot{m}_c)_{total} = \left[P_{std} (P_{T1}^2 - P_{T2}^2) / K R (T_{T1} + T_{Tc}) \right]^{1/n} \quad (71)$$

The coolant plenum temperature is evaluated by the equation

$$T_{TC} = T_{T2} - (T_{T2} - T_{T1}) e^{-(UA/C_p \dot{m}_c)} \quad (72)$$

where temperature of the heat source (T_{T2}) and coolant supply overall heat transfer coefficient (UA) is required input data (see discussion in section 3.4). The combination of equations 68, 69, 71 and 72 are solved by an iteration process which provides the resulting slot flow rates and coolant plenum temperature and pressure required in determining the wall temperature.

3.3.2.2 Convection-Film Cooling

The convection-film cooling method computational procedure incorporated by subprogram CONFIM, developed by VAC, utilizes the empirical film cooling correlation presented by reference 3, the multiple slot method suggested by reference 4, and the characteristics of plate-fin heat exchanger materials as presented in references 5 and 6.

The nomenclature used within this section is as follows:

- A - area, ft.²
- C_p - specific heat at constant pressure, Btu/lb_m · °R
- d - the differential of a variable
- d_e - hydraulic diameter, ft.
- exp - exponential (e)
- f_F - Fanning friction factor, nondimensional
- f(v) - velocity mismatch factor, nondimensional
- g - acceleration of gravity, ft./hr.²
- G - gas mass flow velocity through heat exchanger core, lb_m/hr.ft.²
- h - convective heat transfer coefficient, Btu/hr.ft.² °R
- K - pressure loss coefficient, lb_f/ft.²
- L - length of convection-film cooled shingle, ft.

VOUGHT AERONAUTICS COMPANY

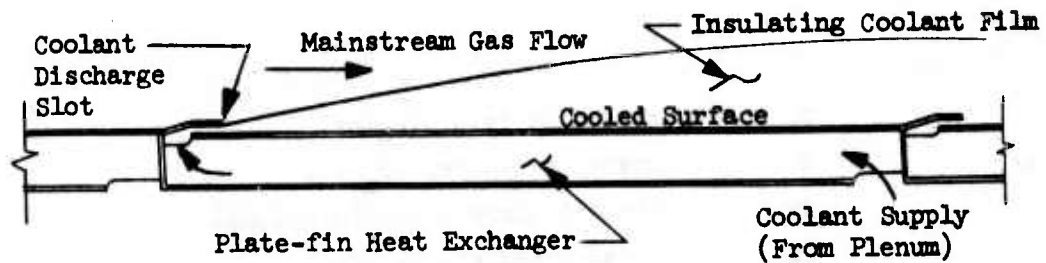
\dot{m}	- mass flow rate, $\text{lb}_m/\text{hr.}$
P	- static pressure, $\text{lb}_m/\text{ft.}^2$
Pr	- Prandtl number, nondimensional
P_T	- total pressure, $\text{lb}_m/\text{ft.}^2$
q	- heat flow rate, Btu/hr.
R	- gas constant, $\text{lb}_f\text{ft.}/\text{lb}_m \text{ } ^\circ\text{R}$
Re	- Reynolds number, nondimensional
s	- slot height, ft.
T	- temperature or static temperature, $^\circ\text{R}$
T_t	- total temperature, $^\circ\text{R}$
UA	- overall rate of heat transfer, $\text{Btu/hr. } ^\circ\text{R}$
x	- distance downstream of slot, ft.
ρ	- density, $\text{lb}_m/\text{ft.}^3$
ρ_{st}	- density at standard temperature and pressure, $\text{lb}_m/\text{ft.}^3$

SUBSCRIPTS:

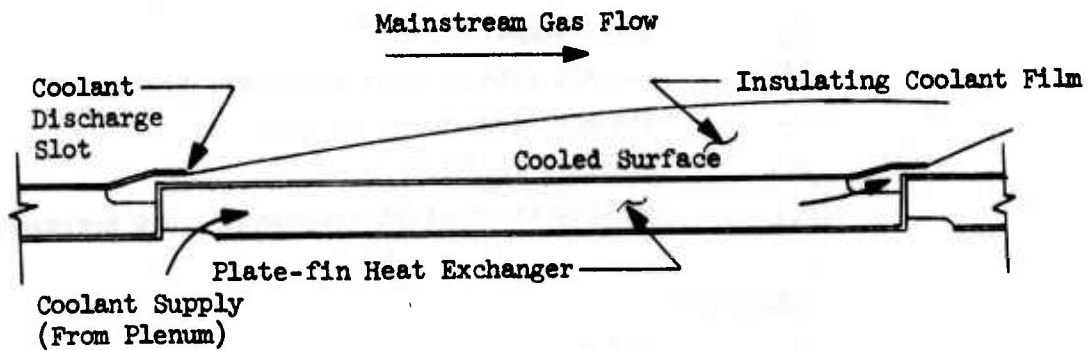
c	- coolant
cd	- coolant discharge
f	- fluid film
f'	- adjacent to film
g	- mainstream gas
hx	- heat exchanger
s	- slot
w	- wall
x	- wall location
$x+\Delta x$	- incremented wall location

Figure 3 (a) and (b) show sketches of sectioned convection/film cooling panel configurations analysis. Referring to the element shown on figure 3 (c), the heat transfer from the fluid film to the wall is equaled to that transferred from the wall to the coolant when

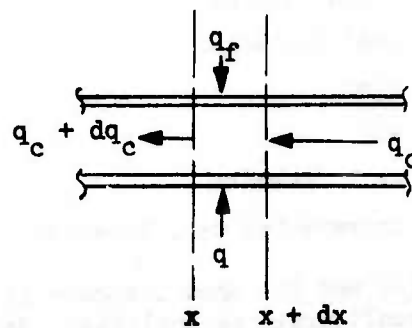
VOUGHT AERONAUTICS COMPANY



(a) Counterflow Configuration



(b) Parallel Flow Configuration



(c) Element of Cooling Panel, Energy Balance for Counterflow Scheme

FIGURE 3: Convection-Film Cooling Scheme

conduction along the wall is ignored, i.e.

$$q_f = h_f A_w (T_{tf} - T_w) = (hA)_{hx} (T_w - T_{tc}). \quad (73)$$

The wall temperature can be solved as

$$T_w = (UA) \left[T_{tf} / (hA)_{hx} + T_{tc} / (h_f A_w) \right] \quad (74)$$

where

$$(UA) = \left[1 / (hA)_{hx} + 1 / (h_f A_w) \right]^{-1}. \quad (75)$$

The heat flow from the heat exchanger to plenum coolant is considered low; small difference in temperature with a relatively low plenum side coefficient of convection. The heat gained by the heat exchanger coolant, due to the predominance of the heat flow from the film, is found to be

$$dq_c = -\dot{m}_c c_p dT_{tc} = \left(\frac{h_f A_w}{L} \right) (T_{tf} - T_w) dx. \quad (76)$$

When substituting equation 74 into this equation and rearranging, the equation becomes

$$\int_{(T_{tc})_x}^{(T_{tc})_{x+\Delta x}} \frac{dT_{tc}}{(T_{tc} - T_{tf})} = \frac{(UA)}{\dot{m}_c c_p L} \int_x^{x+\Delta x} dx. \quad (77)$$

Holding the film temperature constant over the incremental distance ΔX and integrating, the heat exchanger coolant temperature is given by

$$(T_{tc})_{x+\Delta x} = \bar{T}_{tf} - [\bar{T}_{tf} - (T_{tc})_x] \exp[(UA)\Delta x / (\dot{m}_c c_p L)] \quad (78)$$

where the average film temperature over the increment is computed by

$$\bar{T}_{tf} = [(T_{tf})_x + (T_{tf})_{x+\Delta x}] / 2 \quad (79)$$

The film temperature is evaluated by methods presented in section 3.3.2.1 where, for this case, the computed wall temperature becomes the temperature of the fluid film adjacent to the wall and the coolant temperature becomes the coolant discharge temperature. Therefore, from equation 67, the fluid film temperature is

$$T_{tf} = T_{tf'} - (T_{tf'} - T_{tcd}) \left\{ 1 + 3.6 \left[\frac{h_g (C_d A_s)}{C_{fc} (\dot{m}_c)} \right] \left(\frac{x}{S} \right) \left(\frac{T_{tf'}}{T_{tcd}} \right)^{3/2} f(v) \right\}^{-1} \quad (80)$$

where $f(v)$ is defined by equation 62. The variable $T_{tf'}$ is the fluid temperature adjacent to the cooling film as demonstrated by the temperature profiles shown on figure 2 (b).

In evaluating the variables of equation 75, the characteristics of the plate-fin material configuration selected for the heat exchanger must be known. The characteristics of several types of configurations are given in references 5 and 6. Heat transfer characteristics are presented in the form of $(h/GC_p)(Pr)^{2/3}$ versus Re . The physical characteristics, such as heat transfer and flow area, are also provided. The heat transfer data presented is for the same rate of heat transfer occurring on both walls of the heat exchanger. For the convection-film cooling method, the bulk of the heat flow occurs across only one wall. Analytically predicted, the effect of heat

VOUGHT AERONAUTICS COMPANY

flow from only one wall is a plate-fin material heat transfer area reduction of 50 percent. Predicted wall temperatures compared with empirical data shows this reduction to be more nearly 60 percent. Therefore,

$$A_{hx} = 0.4 \cdot (\text{Plate-fin material heat transfer area}). \quad (81)$$

Reference 7 shows that, under fixed mainstream conditions, the coefficient of convection along a surface can be assumed to remain constant with or without a coolant film, i.e.

$$h_f \approx h_g. \quad (82)$$

A coolant flow balance, pressure-loss analysis is conducted by subprogram CONFIM similar to that for film cooling in section 3.3.2.1. The one difference between these analyses is the pressure losses which occur between the coolant plenum and the slot exit. For any reasonable design, entrance losses should be small in comparison to the losses which occur within the coolant flow passage. Plate-fin heat exchanger characteristic data include the Fanning frictional factor (f_F) versus Re . The flow through this system, related to a series pressure loss, is

$$\dot{m}_c = \left\{ (P_{tc} - P_g) / \left[K_{cd} \rho_{st} R_c T_{cd} / P_g + f_F \left(\frac{L}{d_c} \right) / (2 g \rho_{hx} A_{flow(hx)}^2) \right] \right\}^{1/2}. \quad (83)$$

The coefficient (K_{cd}) includes all the pressure losses which occur from the downstream end of the heat exchanger passage to the coolant discharge slot.

The subprogram CONFIM can either compute the total coolant flow rate or it can be a fixed input to the program. If the total flow rate is fixed, equation 69 and 70 are solved to obtain the individual slot flow rates. Equations 69 through 72 are used to compute the overall coolant flow balance in a manner similar to that described in section 3.3.2.1. To initiate the computational procedure, initial estimates are made of the heat exchanger fluid density and the slot discharge temperature. Initial values of flow rate are computed. The gas film temperature distribution is computed utilizing equation 80. In turn, using equations 78 and 79, the temperature distribution of the heat exchanger coolant is computed based on the initial estimate of the coolant discharge temperature. The computed heat exchanger entrance coolant temperature is then compared with the coolant plenum temperature computed from equation 72. With a mismatch in temperature, an iteration is carried out, utilizing equations 78 through 80 for each surface by revising the estimate of coolant discharge temperature until the coolant entrance temperature converges. Once completed, the initial estimates of heat exchanger fluid density and slot discharge temperature are revised by the computed values and the complete computation procedure repeated, iterating until temperature values converge. The wall temperature distribution for each surface is then computed from equation 74 and an area-weighted-average surface temperature is computed for each surface node involved.

The subprogram CONFIM can also handle the parallel configuration shown on figure 3 (b). The basic equations are identical with the exception that the sign of the exponential term of equation 78 is changed. The computational procedure is carried out in a manner similar to that for the counterflow configuration but the iteration on coolant slot discharge temperature is not required.

3.3.2.3 Transpiration Cooling

The cooling of a surface utilizing a transpiring gas is computed by the subprogram TRANCL. The empirical correlation for air injected through a porous wall which was used in this program is presented in reference 8.

The nomenclature used within this section is as follows:

- A - area, ft.²
- C_p - specific heat at constant pressure, Btu/lb_m · °R
- F^p - injection mass flow ratio, $(\rho V)_w / (\rho V)_g$, dimensionless
- h - convective heat transfer coefficient, Btu/hr.ft.² · °R

VOUGHT AERONAUTICS COMPANY

i	- number of surface increments
k'	- porous wall loss factor, $\text{lb}_f/\text{ft}^2 (\text{hr} \cdot \text{ft}^2/\text{lb}_m)^{1/n}$
\dot{m}	- mass flow rate, lb_m/hr .
P	- porosity, ratio of flow area to surface area
q	- heat flow rate, Btu/hr .
R	- gas constant, $\text{lb}_f \cdot \text{ft}^2/\text{lb}_m \cdot ^\circ\text{R}$
St	- Stanton number $(h_g/\rho V C_p)$, nondimensional
T	- temperature or static temperature, $^\circ\text{R}$
T_r	- recovery temperature, $^\circ\text{R}$
T_t	- total temperature, $^\circ\text{R}$
V	- velocity, ft/hr .
z	- dimensionless parameter
ρ	- density, lb_m/ft^3
ρ_{std}	- density at standard temperature and pressure, lb_m/ft^3

SUBSCRIPTS

c	- coolant
c'	- coolant discharge
g	- mainstream gas
o	- without transpiration cooling
w	- wall

A sectioned transpiring porous wall model is shown in figure 4 and shall be used for discussion purposes.

The heat flux by convection from a gas to an uncooled wall is determined by the equation

$$q_o/A_w = h_o (T_r - T_w) \quad \dots (84)$$

At steady state conditions, heat added to the porous wall from the mainstream is removed by the coolant flow. The lateral heat transfer by conduction is assumed to be zero, i.e. no temperature gradient exists along the wall. The heat addition from the mainstream is transferred to and carried off by the coolant gas. This is presented by the

heat balance

$$\dot{q} = h A_w (T_r - T_w) = \dot{m}_c C_{pc} (T_{tc}' - T_{tc}). \quad (85)$$

For a good design, the heat transfer efficiency between the porous wall and coolant passing through the wall will permit the coolant discharge temperature (T_{tc}') to approach the wall's outer surface temperature (T_w).

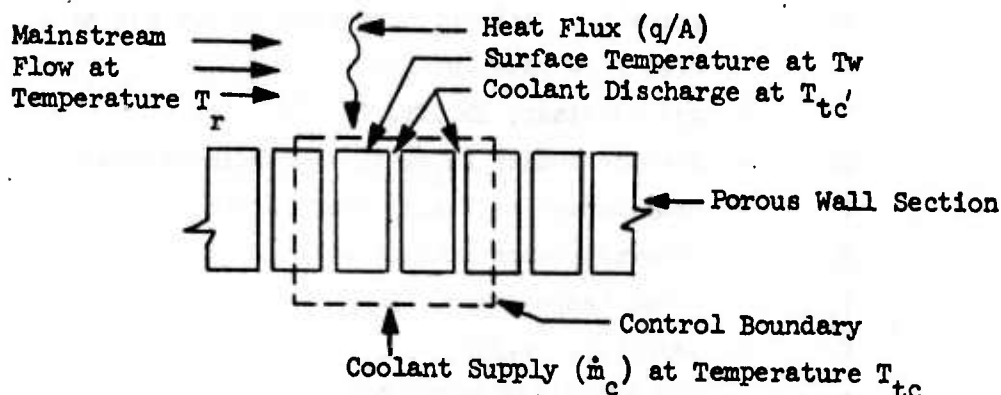


FIGURE 4: Transpiration Cooling, Sectioned Porous Wall Model

Assuming this to be the case, then equation 85 can be written as

$$h A_w (T_r - T_w) \simeq \dot{m}_c C_{pc} (T_w - T_c). \quad (86)$$

The coefficient of convection (h) on a transpiration surface is difficult to obtain. An equation derived by reference 8, compared with the empirical data presented in reference 9, relates the heat flow rate to a surface with and without transpiration cooling under the same imposed mainstream conditions. Correlation is provided by the relationship

$$\frac{\dot{q}}{\dot{q}_0} = \sqrt{\left(\frac{1}{2} \frac{F}{St_0}\right)^2 + 1} - \frac{1}{2} \frac{F}{St_0} \quad (87)$$

where

$$F = (\rho_c V_c) / (\rho_g V_g). \quad (88)$$

With the aid of the continuity equation and the definition of Stanton number,

$$St_0 = h_0 / (C_{pg} \rho_g V_g), \quad (89)$$

the ratio

$$F / St_0 = (C_{pc} \dot{m}_c) / (P A_w h_0). \quad (90)$$

VOUGHT AERONAUTICS COMPANY

From equations 84, 86, 87 and 90, an equation defining wall temperature in terms of known variables can be obtained, i.e.

$$T_w = (T_{tc} + z T_r) / (z + 1) \quad (91)$$

where

$$z = \left[\left(\frac{h_o A_w}{C_{pc} \dot{m}_c} \right) + \left(\frac{C_{pg}}{2 P C_{pc}} \right)^2 \right]^{1/2} - \frac{C_{pg}}{2 P C_{pc}} \quad (92)$$

The subprogram TRANCL solves equation 91, with equation 92, for the wall temperature distribution based on the coolant flow distribution along the transpiring surface.

The coolant flow conditions are established by this program in a manner similar to that discussed in section 3.3.2.1. The same options are available, i.e. the coolant flow rate fixed or computed based on its source conditions. The pressure loss across the wall is computed from equation 70. Since the mainstream static pressure may vary along the surface being cooled, surface increments are taken by the program which permit the coolant flow rate to vary along the surface. The flow relationship for the surface increments, assuming that the same plenum feeds the complete surface, is found to be

$$\dot{m}_{ci} = A_{ci} \left[P_g (P_{tc} - P_g) / (K' P_{st} R_c T_{tc}) \right]^{1/n} \quad (93)$$

where the total coolant flow rate is

$$\dot{m}_c = \sum_{i=1}^{ii} \dot{m}_{ci} \quad (94)$$

If the coolant flow rate is fixed by the user, equation 93 and 94 are solved to provide the flow for each surface increment. When the program is required to compute the coolant flow rate, these equations in conjunction with equation 71 and 72 are solved in a manner similar to that presented in section 3.3.2.1.

3.3.3 Exhaust System Radiation

Radiant energy is interchanged between the internal surfaces of the exhaust system and emitted from the exhaust system surfaces to a remote detector. Internal radiation is required for an internal surface heat balance which produces the surface temperature distribution within the exhaust system. The irradiation incident upon the detector provides the signature of the particular exhaust system under investigation. Two parameters offer difficulty in the computing of radiation; geometric view factors and gray body interchange factors. This section presents the methods by which SIGNIR calculates these parameters.

The nomenclature used within this section and its subsections is as follows:

A	- surface area, ft. ²
\tilde{A}	- matrix element
B	- radiosity, Btu/hr. ft. ²
dA	- differential element of area, ft. ²
E_b	- black body emissive power, Btu/hr.ft. ²
F	- geometric radiation view factor
\tilde{g}	- gray body interchange factor
H	- irradiation, Btu/hr.ft. ²
Q	- heat rate, Btu/hr.
r	- radial distance, ft.
δ_{ij}	- Kronecker delta (1, when $i=j$; 0, when $i \neq j$)
ϵ	- emissivity
θ	- An angle measured from the normal from a surface
ρ	- reflectivity

SUBSCRIPTS:

i	- surface designator (or matrix row index)
j	- surface designator (or matrix column index)
1	- surface designator
2	- surface designator

VOUGHT AERONAUTICS COMPANY

The computing of net radiation exchange occurring between two isothermal surfaces, 1 and 2, is based on the Stefan-Boltzmann law and defined by the equation

$$Q_{1-2} = \sigma A_1 \mathcal{F}_{1-2} (T_1^4 - T_2^4) . \quad (95)$$

The net amount of radiant energy entering a surface (1) is the summation of the contribution from all other surfaces, i.e.

$$Q_1 = \sum_j Q_{1-j} = \sum_j \sigma A_1 \mathcal{F}_{1-j} (T_1^4 - T_j^4) . \quad (96)$$

Calculation of the internal geometric view factors is accomplished by subprogram VIEW and the external view factors by subprogram REDII. The systems gray body interchange factors are computed by subprograms SCRPTF for internal radiation interchange and REDI for the external case.

3.3.3.1 Geometric Radiation View Factor

The view factor between a black radiating surface (1) and a black receiving surface (2) is that fraction of the radiation leaving surface 1 that is intercepted by surface 2. The defining equation for geometric view factors, purely a geometric relationship, is given by

$$F_{dA_1-dA_2} = \frac{\cos \theta_1 \cos \theta_2}{\pi r^2} dA_2 . \quad (97)$$

The relationship between the variables used and the surfaces are shown on figure 5. The view factor between surfaces is obtained by integrating over the surfaces, i.e.

$$F_{1-2} = \frac{1}{A_1} \iint_{A_2} \frac{\cos \theta_1 \cos \theta_2}{\pi r^2} dA_1 dA_2 . \quad (98)$$

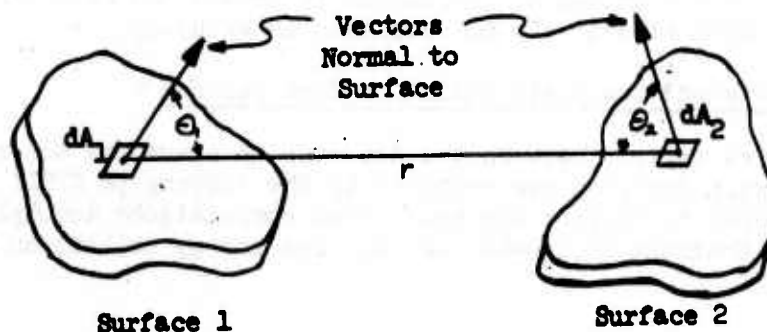


FIGURE 5: Surface Geometry For Geometric View Factors

The black body view factors are utilized for gray surfaces when they are considered to radiate in a diffused manner.

The subprogram VIEW computes the internal exhaust system geometric view factors required for the radiation calculation. This program was developed for use under NASC contract number N00019-68-C-0571 and is completely documented by reference 10. The exhaust system is sub-divided into isothermal segments (nodes) for the mathematical model. Each segment is represented by a frustum of a cone, a cylinder or a disk of common axis. The geometric considerations for these axisymmetric segments substantially reduce the integration problems confronted in the solution of equation 98. The subprogram VIEW takes advantage of the system axisymmetric characteristic and can determine the view factor between any of the models selected segments. It also has the ability to determine view factors where complete or partial shadowing by an intervening surface exists.

The symmetry of the exhaust system permits equation 97 to be placed in cylindrical coordinates which requires integration in four variables. In subprogram VIEW, one of the integrations is accomplished leaving only three variables requiring numerical integration methods. All geometric considerations and numerical integration methods utilized have been presented in reference 10.

A modification was incorporated in the interest of reducing program computational time requirements. The increment size selection for numerical integration was permitted to vary in a systematic manner. The program first defines the increment size as the node itself and a value for the view factor is computed. The node increment size is then reduced by one half by the program and a second view factor computed. Its magnitude is then compared with the first value obtained and if the percent change in magnitude is found greater than 0.1%, the program again reduces the increment size by one half. A value for the view factor is computed and a comparison made with the last value computed. This process is continued until the tolerance requirement is met or until the view factor is computed based on a maximum of 16 node increments. This modification proved to substantially reduce the required computer time with effectively no reduction in accuracy.

3.3.3.2 External Geometric Radiation View Factors

The view factors between the detector in space and the exposed exhaust system surfaces are computed by the subprogram REDII; a program developed to support the analytical computations accomplished under NASC Contract N00019-68-C-0571. The energy collection area of

VOUGHT AERONAUTICS COMPANY

the detector is considered to be an element of one square unit for calculation purposes. With this single consideration, equation 97 can be stated as

$$F_{DA_1-A_2} = \int_{A_2} \frac{\cos \theta_1 \cos \theta_2}{\pi r^2} dA_2 \quad (99)$$

The normal to the detector area is assumed to intersect the exhaust system at the point where the exit plane and system axis intersect. Each node within the exhaust system is subdivided into elements such that the summation of the detector to element view factors provide the numerical integration for the view factor from detector to node.

Subprogram REDII checks positioning of each element to determine if a view is possible ($\theta < 90^\circ$) and checks possible shadowing by any intervening surfaces. A discussion of the geometric consideration undertaken by the subprogram REDII is covered in references 11 and 12.

3.3.3.3 Gray Body Interchange Factors

Radiant energy is reflected from non-black surfaces. In an enclosure, the reflection of energy can occur numerous times. These multiple reflections of radiation are accounted for through gray body interchange factor for surfaces which reflect radiation in a diffused manner. These factors are computed within subprogram SCRPTF for the internal exhaust system and by subprogram REDII for system to detector irradiation.

The radiosity of an isothermal surface 1 is equal to the sum of the radiation emitted, reflected and transmitted. Opaque surfaces such as those used within exhaust systems transmit no radiation, therefore

$$B_i = \rho_i H_i + \epsilon_i E_{bi} \quad (100)$$

The total irradiation on surface 1 is the sum of the contributions from each of the other surfaces, i.e.

$$H_i = \sum_j F_{ij} B_j \quad (101)$$

VOUGHT AERONAUTICS COMPANY

which involves the diffuse geometric radiation view factor. Written in matrix notation (i = row index, j = column index), equations 100 and 101 become

$$\{B_i\} = \{F_{ij} H_j\} + \{\epsilon_i E_{bi}\} \quad (102)$$

and

$$\{H_i\} = [F_{ij}] \{B_j\} \quad (103)$$

Combining equations 102 and 103 and solving in terms of the radiosity, i.e.

$$\{B_i\} = [\rho_i F_{ij}] \{B_j\} + \{\epsilon_i E_{bi}\} \quad (104)$$

$$[s_{ij} - \rho_i F_{ij}] \{B_j\} = \{\epsilon_i E_{bi}\} \quad (105)$$

and

$$\{B_i\} = [s_{ij} - \rho_i F_{ij}]^{-1} \{\epsilon_i E_{bi}\} \quad (106)$$

the radiosity can be expressed as

$$\{B_i\} = [\tilde{A}_{ij} \epsilon_j] \{E_{bi}\} \quad (107)$$

where

$$[\tilde{A}_{ij}] = [\delta_{ij} - \epsilon_i F_{ij}]^{-1} . \quad (108)$$

The net rate at which radiation enters a gray surface per unit area and time is equal to the difference between the absorbed and the emitted radiation. Assuming the absorptivity of the surface equals its emissivity, this can be expressed as

$$\left\{ \frac{Q_i}{\epsilon_i A_i} \right\} = \{H_i\} - \{E_{bi}\} . \quad (109)$$

Combining equations 103, 107 with 109 gives

$$\left\{ \frac{Q_i}{\epsilon_i A_i} \right\} = [F_{ij}] [\tilde{A}_{ij} \epsilon_j] \{E_{bi}\} - \{E_{bi}\} . \quad (110)$$

This can be written as

$$\{Q_i\} = [\epsilon_i A_i (D_{ij} - \delta_{ij})] \{E_{bi}\} \quad (111)$$

where

$$D_{ij} = \sum_k F_{ik} \tilde{A}_{kj} \epsilon_j . \quad (112)$$

The gray body interchange factor from surface j to surface i is defined such that the net heat exchanged between the two surfaces is given by

$$Q_{j-i} = A_j \mathcal{Y}_{ji} (E_{bj} - E_{bi}) \quad (113)$$

or

$$Q_{j-i} = A_i \mathcal{Y}_{ij} (E_{bj} - E_{bi}) \quad (114)$$

The net amount of heat entering surface i is obtained by the summation of the contributions of each of the surfaces, i.e.

$$Q_i = \sum_j Q_{ji} = \sum_j A_i \mathcal{Y}_{ij} (E_{bj} - E_{bi}) \quad (115)$$

Transforming to matrix notation, equation 115 becomes

$$\{Q_i\} = [A_i \mathcal{Y}_{ij}] \{E_{bj}\} - \left\{ \sum_k A_i \mathcal{Y}_{ik} E_{bi} \right\} \quad (116)$$

or, can be written as

$$\{Q_i\} = [A_i \mathcal{Y}_{ij} - \delta_{ij} \sum_k A_i \mathcal{Y}_{ik}] \{E_{bi}\} \quad (117)$$

VOUGHT AERONAUTICS COMPANY

Comparing the elements of equations 111 and 117, it may be seen that for $i \neq j$,

$$A_i F_{ij} = \epsilon_i A_i D_{ij} \quad (118)$$

and for $i = j$,

$$A_i F_{ii} = \sum_k A_i F_{ik} + \epsilon_i A_i (D_{ii} - 1) \quad (119)$$

Since each of the surfaces considered is isothermal, the interchange factor of a surface from itself is not required and the diagonal, equation 119 need not be solved. Equations 118, along with 108 and 112, are solved to obtain the gray body interchange factors required for internal radiation calculations.

The interchange factors for the detector involve only the irradiation from the exhaust system, consequently the Kronecker delta terms of equations 111 and 117 are zero and again, only equation 118 is required.

3.3.4 Exhaust System Heat Balance

A thermal heat balance is conducted within the exhaust system to provide the temperature distribution along all exhaust system surfaces. Each surface has been subdivided into isothermal segments (nodes) and it is the temperature of these segments that is desired. The subprogram TASLB is employed to compute these temperatures. This subprogram is a modified version of the existing program Thermal Analysis System 1 written by the Jet Propulsion Laboratory, California Institute of Technology for NASA under contract no. NAS 7-100.

The nomenclature used within this section is as follows:

- A - surface area, ft.^2
- C - overall conductance coefficient, $\text{Btu/hr. ft.}^2 \text{ } ^\circ\text{R}$
- F - gray body radiation interchange factor, nondimensional

VOUGHT AERONAUTICS COMPANY

- R - vector
- S - square matrix
- T - temperature, °R
- σ - Stefan-Boltzmann constant, $= 0.1713 \times 10^{-8}$ Btu/ft.²
hr. (°R)⁴

For any given internal exhaust system node, a steady state energy balance can be stated as the sum of the energy addition is equal to the sum of the departing energy. The balance for a node i can be written as

$$\sum_j C_{ij} A_i (T_i - T_j) + \sum_j \sigma A_i \mathcal{F}_{ij} (T_i^4 - T_j^4) = 0 \quad (120)$$

and stated as the net energy exchange from node i is zero.

For a system of nodes, the energy balance can be written in matrix form as

$$[C_{ij} A_i] \{T_i\} + [\sigma A_i \mathcal{F}_{ij}] \{T_i^4\} = 0 \quad (121)$$

The solution used follows the Newton-Raphson iteration method for nonlinear algebraic equations utilizing the matrix form

$$[S_{ij}] \{T_i\} = \{R_i\} \quad (122)$$

The off-diagonal elements of the square matrix are

$$S_{ij} = C_{ij} A_i + 4 \sigma A_i \mathcal{F}_{ij} T_j^3 \quad (123)$$

while diagonal elements are

$$S_{ii} = S_{ii} - C_{ij} A_i - 4\sigma A_i Y_{ij} T_i^3 \quad (124)$$

The vector R has the form

$$R_i = -3\sigma A_i Y_{ij} (T_i^4 - T_j^4) \quad (125)$$

Subprogram TAS1B solves this matrix, equation 122, for the temperature (T) vector in an iterative manner revising the values of temperature in matrix S and R with each iterative step until the process converges on a final solution.

3.3.5 Exhaust System Radiation Emission

The spectral radiation passed from an engine exhaust system to a detector is dependent on the conditions of the systems exposed hot metal, the separation between the two and the media through which the energy must pass. The following section presents the theory utilized in computing the spectral emission from an exhaust system to a detector and the attenuation of infrared energy as it passes through the atmosphere.

3.3.5.1 Spectral Emission

The spectral radiation passing from the exhaust system surfaces to a remotely located infrared detector is computed by the subprogram REDI. This program was developed by VAC under NASC Contract No. N00019-68-C-0571 and reported in reference 11. The only modification incorporated by this program is a reduction in the size of the spectral wavelength band interval resolved.

VOUGHT AERONAUTICS COMPANY

The following is a list of nomenclature used throughout this section.

- A - surface area, ft.²
- B - radiosity, Btu/hr. ft.²
- C - a constant
- exp - exponential (e)
- E_b - black body emissive power, Btu/hr. ft.²
- F - geometric radiation view factor
- \mathcal{H} - gray body interchange factor
- Q - heat rate, Btu/hr.
- r - range, ft.
- R - a constant
- T - temperature, °R
- U - a constant
- $\gamma(\lambda)$ - Gauss quadrature formula coordinant
- δ_{ij} - Kronecker delta (= 1, when i = j; = 0, when i ≠ j)
- Δ - incremental change in a variable
- ϵ - emissivity
- λ - wavelength, microns
- ρ - reflectivity
- Ω - solid angle, steradians

SUBSCRIPTS:

- i - matrix row index (or surface indicator)
- j - matrix column index

The amount of radiant energy in the wavelength band from λ to $\lambda + \Delta\lambda$ which is incident on an IR detector may be written as the sum of the energy contributions from each of the individual exhaust system surface nodes. That is,

$$\left(\frac{\Phi}{A}\right)_{\lambda \text{ to } \lambda + \Delta\lambda} = \sum_i F_i B_i, \lambda \text{ to } \lambda + \Delta\lambda \quad (126)$$

The radiosity may be expressed in terms of the black body emissive power for each surface. The expression is obtained in a manner similar to that of equation 106. Written in terms of matrix notation,

$$\{B_i, \lambda \text{ to } \lambda + \Delta\lambda\} = [\delta_{ij} - \rho_i F_{ij}]^{-1} \{\epsilon_i E_{bi, \lambda \text{ to } \lambda + \Delta\lambda}\}, \quad (127)$$

where the radiosities are shown to be independent of the properties of the detector. Equation 126 and 127 are combined to form the matrix equation

$$\left\{\left(\frac{Q}{A}\right)_{\lambda \text{ to } \lambda + \Delta\lambda}\right\} = \{F_j\} [\delta_{ij} - \rho_i F_{ij}]^{-1} \{\epsilon_i E_{bi, \lambda \text{ to } \lambda + \Delta\lambda}\}. \quad (128)$$

From a development similar to that used in section 3.3.3.3, equation 128 can be written as

$$\left\{\left(\frac{Q}{A}\right)_{\lambda \text{ to } \lambda + \Delta\lambda}\right\} = \{F_j\} \{E_{bi, \lambda \text{ to } \lambda + \Delta\lambda}\} \quad (129)$$

where F_j is the gray body interchange factor from the receiver to an exhaust system surface node.

The black body emissive power of surface node 1 is obtained by integrating Planck's equation for radiation between the limits of λ to $\lambda + \Delta\lambda$ where the value of $\Delta\lambda = 0.05$ microns. That is,

$$E_{bi, \lambda \text{ to } \lambda + \Delta\lambda} = \int_{\lambda}^{\lambda + \Delta\lambda} \frac{C_1 d\lambda}{\lambda^5 [\exp(C_2 / \lambda T_i) - 1]}. \quad (130)$$

VOUGHT AERONAUTICS COMPANY

The integral is evaluated by means of numerical integration with the Gauss quadrature formula for four selected abscissas. The following equations are employed.

$$E_{b_i, \lambda \text{ to } \lambda + \Delta\lambda} = (\Delta\lambda) [R_1 \psi(\lambda_1) + R_2 \psi(\lambda_2) + R_3 \psi(\lambda_3) + R_4 \psi(\lambda_4)] \quad (131)$$

where

$$\psi(\lambda_n) = \frac{C_1}{\lambda_n^5 [\exp(C_2 / \lambda_n T_i) - 1]} \quad , \quad (132)$$

$$\lambda_n = \lambda + (U_n + 1/2)(\Delta\lambda) \quad (133)$$

and $U_1 = -0.4305682$	$R_1 = 0.1739274$	(134)
$U_2 = -0.1699905$	$R_2 = 0.3260726$	
$U_3 = 0.1699905$	$R_3 = 0.3260726$	
$U_4 = 0.4305682$	$R_4 = 0.1739274$	

The subprogram REDI computes the spectral radiation incident on the detector by solving the matrix equation 129 and utilizes equation 131 to compute the black body spectral emissive power. This radiant intensity, incident radiation per unit solid angle, is computed by multiplying the spectral radiation flux of equation 129 by the square of the range. The solid angle itself would be calculated as

$$\Omega = A / r^2 \quad . \quad (135)$$

The computed radiant intensity is therefore independent of the energy collection area of any specific detector.

3.4 SPECIAL COMPUTATION CONSIDERATIONS

Program SIGNIR is basically self contained, dependent only on the system model produced from the physical exhaust system configuration. With the latitude provided in exhaust system configurations, certain specific items concerning a system may be required to be provided by the user to complete the model and derive the desired information. The following sections are included to assist the user. They cover a method to approximate system thrust change and establish the required form for pressure loss and heat transfer parameters necessary for program input.

3.4.1 Thrust Change Resulting From Suppressing Exhaust System

A method is presented by which the exhaust system thrust change associated with the infrared suppression of a system can be approximated by the user. To be capable of obtaining this information, both suppressed and unsuppressed configurations must be run by program SIGNIR. Available as output data from each of these configurations is a computed "thrust loss factor." This factor is the summation of the internal exhaust system axial pressure-area forces, surface friction forces and the coolant momentum flux gain. The method assumes that the suppression of the system does not effect engine operating conditions and the flow condition entering the exhaust system are unchanged by the configuration change.

The nomenclature used within this section is as follows:

A	- cross sectional area, ft. ²
C_D	- coefficient of discharge
d	- differential of a quantity
F	- thrust force factor, lb.
\vec{F}	- force vector, lb.
F_{drag}	- coolant duct drag force, lb.
F_D	- coolant duct reaction force, lb.
F_f	- frictional force, lb.
F_{PA}	- pressure-area force, lb.
M	- Mach number
\dot{m}_c	- coolant mass flow, lb./sec.
\vec{n}	- unit normal vector
n	- number of coolant ducts
P	- pressure, psia
q	- dynamic pressure, psf
r	- radius, ft.
S	- projected coolant duct area normal to flow, ft. ²
\mathcal{J}	- reaction force, lb.
\vec{u}	- velocity vector, ft./sec.
u	- velocity, ft./sec.
x	- system coordinate

VOUGHT AERONAUTICS COMPANY

- γ - ratio of specific heats
- Δ - change in a parameter
- ρ - density, lb/ft.³

SUBSCRIPTS:

- amb - ambient
- cd - coolant system discharge
- ce - coolant system entrance
- cs - control surface
- ent - entrance
- ex - exit
- sup - suppressed
- tc - tailcone
- unsup - unsuppressed

Special notations:

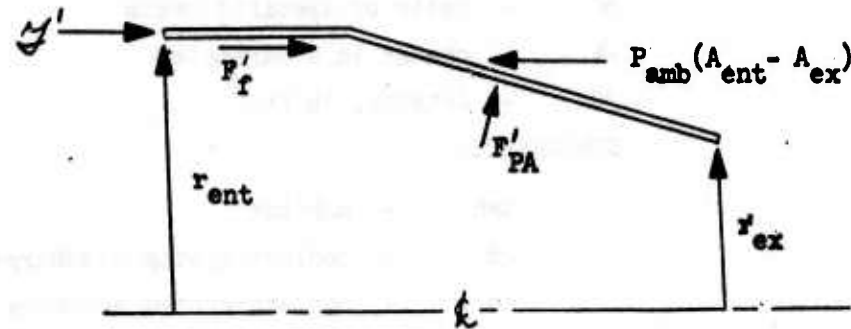
- ' - applies to tailpipe
- " - applies to centerbody
- ''' - applies to splitter

The thrust acting on a system is determined from the momentum equation for steady state flow conditions, i.e.

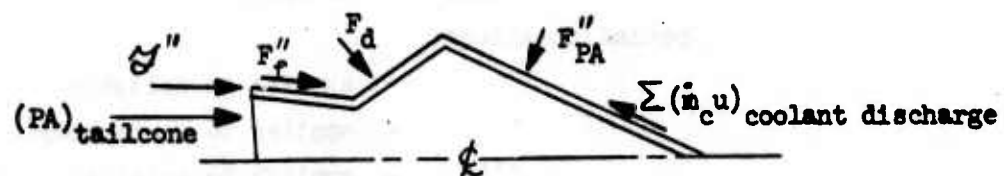
$$\int_{cs} \bar{u} (\rho \bar{u} \cdot \bar{n}) dA = \sum \bar{F} \quad (159)$$

Figure 6 shows components of an exhaust system similar to the demonstration problem presented in Appendix III. The components have been isolated such that individual force balances can be performed on each of the surfaces. A force balance conducted in the axial direction on the exhaust system tailpipe (Figure 6a) produces

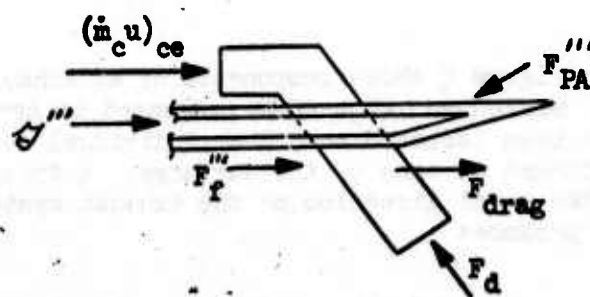
$$\mathcal{J}' + (F_f')_x + (F_{PA}')_x - P_{amb} (A_{ent} - A_{ex}) = 0 \quad (160)$$



(a) Tailpipe



(b) Centerbody



(c) Duct Splitter And Coolant Supply Duct

FIGURE 6: Exhaust System Force Diagram

VOUGHT AERONAUTICS COMPANY

where the force \mathcal{Y}' is the reaction force. A force balance conducted on the exhaust system centerbody (figure 6b) results in the equation form

$$\mathcal{Y}'' + (F_f'')_x + (F_{PA}'')_x + (F_D)_x + (PA)_{tc} = \sum (\dot{m} U_x)_{cd} \quad (161)$$

In addition to these, a force balance on the splitter with the coolant ducts (figure 6c) yields the equation

$$\begin{aligned} \mathcal{Y}''' + (F_f''')_x + (F_{PA}''')_x + (F_{drag})_{cd} - (F_D)_x \\ = - (\dot{m}_c U)_{ca} \end{aligned} \quad (162)$$

The total thrust acting on the system is equal to the sum of these individual forces (thrust components), i.e.

$$\mathcal{Y} = \mathcal{Y}' + \mathcal{Y}'' + \mathcal{Y}''' \quad (163)$$

With equations 159 through 163, the total system thrust becomes

$$\begin{aligned} \mathcal{Y} = & - \sum (F_f)_x - \sum (F_{PA})_x + P_{amb} (A_{ent} - A_{ex}) \\ & - (PA)_{tc} + \left[\sum (\dot{m}_c U)_{cd} - F_{drag} \right. \\ & \left. - (\dot{m}_c U)_{ca} \right] \end{aligned} \quad (164)$$

VOUGHT AERONAUTICS COMPANY

If the engine dimensions, ambient pressure and the pressure applied to the tailcone are assumed to remain fixed for configuration comparison, the terms P_{amb} and $(PA)_{tc}$ are the same for the two configurations. The program computes a "force factor" which is equated by the expression

$$F = -\sum (F_f)_x - \sum (F_{PA})_x + \sum (\dot{m}_c U)_{cd} \quad (165)$$

The thrust change between configuration can be written as

$$\Delta Y = Y_{unsup} - Y_{sup} \quad (166)$$

and expanded to the form

$$\begin{aligned} \Delta Y = & [F - P_{amb} A_{ex}]_{unsup} - [F - P_{amb} A_{ex}]_{sup} \\ & - [F_{drag} + (\dot{m}_c U)_{cd}]_{sup} \end{aligned} \quad (167)$$

This equation, developed from a rather specific configuration, is general in nature and should be found to apply to almost all jet configurations encountered. In cases where both configurations have the same tailpipe exit area and no cooling system exists on the suppressed configuration, equation 167 reduces to the simple form of

$$\Delta Y = (F)_{unsup} - (F)_{sup} \quad (168)$$

For this particular case, the thrust change is only dependent on the "force factors" provided by the program SIGNIR.

VOUGHT AERONAUTICS COMPANY

In general, the user will have to solve the thrust change equation form shown in equation 167. With the program input and output data, the first two terms of this equation can be evaluated. The last term involves a knowledge of the particular suppressed configuration under investigation. If coolant ducts are present and pass through the exhaust gas stream, the drag force produced is a function of the duct configuration and the gas stream properties. This force must be computed by the program user. To assist in this effort, the parasite drag caused by ducts can be evaluated by the equation.

$$F_{drag} = C_p n S q = C_p n S \frac{\gamma P M^2}{2} . \quad (169)$$

The values of pressure, Mach no. and ratio of specific heats are available from the program for the specific gas stream location required. The drag coefficient is dependent on duct profile and flow Reynolds number.

The coolant duct entrance momentum flux, $(\dot{m} u)$, must be included if coolant air is extracted from the system as shown in the sample problem. If test data is not available, this function can be estimated by assuming the entrance is a fairly well designed inlet whose flow contraction ratio is approximately 0.7. The momentum flux of the flow stream captured by the coolant system entrance, is approximated by the equation

$$(\dot{m} u)_{ce} \approx 0.7 \gamma n P A M^2 \quad (170)$$

where the value of pressure, Mach no. and ratio of specific heats are provided by the program as stream conditions at the coolant duct entrance location.

The thrust change associated with the infrared suppression of an exhaust system can be computed from equation 167. Specific information required to accomplish this task can be obtained from equations 169 and 170 and the output data from the program SIGNIR.

3.4.2 Pressure Loss Parameters

When surface cooling is employed by the exhaust system, the pressure loss characteristics must be supplied by the program user to define the particular cooling system configuration employed. Program input data requires values of the loss coefficient (K) and the flow exponent (n) for specific segments of the cooling system. If these values are not available from measured data, they must be acquired through empirical data presented in available reference material such as reference 16.

The nomenclature used within this section is as follows:

- A - flow area, ft.²
- K - loss coefficient, psf/(lb./sec.)ⁿ
- K_t - nondimensional loss coefficient
- \dot{m} - mass flow rate, lb/sec.
- n - flow exponent
- q - dynamic pressure, lb/ft.²
- u - flow velocity, ft./sec.
- ΔP_t - change in total pressure, lb/ft.²
- ρ - fluid density, lb/ft.³
- ρ_{std} - density at standard atmospheric temperature and pressure, lb/ft.³
- σ - fluid density ratio (ρ/ρ_{std})

The form of the pressure loss equation used by program SIGNIR is

$$\sigma \Delta P_t = K (\dot{m})^n \quad (171)$$

in which K is a dimensional loss parameter and $n \approx 2$. These values can be obtained directly from system test data. When flow loss estimations are required, other empirical loss data must be utilized. These are frequently presented as a dimensionless loss parameter (K_t) versus the flow Reynolds number. The pressure loss associated with this loss parameter is defined by the equation

$$\Delta P_t = K_t q \quad (172)$$

where

$$q = \frac{1}{2} \rho U^2 \quad (173)$$

Using a value of two for exponent n , these two loss parameters are related by

$$K = K_t / (2 \rho_{std} A^2) \quad (174)$$

where the area (A) is that associated with the dynamic pressure (q) used in equation 172. For pressure losses which occur in series, the loss coefficient is computed by the equation

$$K = \frac{1}{2 \rho_{std}} \sum_i \left(\frac{K_t}{A^2} \right)_i \quad (175)$$

When a parallel flow system is employed, the required loss coefficient is computed by the equation

$$K = \frac{1}{2 \rho_{std}} \left[\sum_i \left(\frac{A^2}{K_t} \right)_i \right]^{-2} \quad (176)$$

Equations 175 and 176, based on $n = 2$, provide the user a means of computing the loss coefficient for systems in which estimated values are required.

3.4.3 Heat Transfer Parameters

Special paths of heat flow for the exhaust systems mathematical model can be established by the user to supplement the basic program process. These improve the programs general heat balance by incorporating the characteristics of a specific system through defining additional heat transfer paths to heat sources or sinks. Heat transfer parameters are used to define the barrier to heat

VOUGHT AERONAUTICS COMPANY

transfer for any surface coolant supply system and to special fluid nodes (see section 4.2.6). In both cases, an overall heat transfer coefficient is required by the program to describe this barrier to heat flow if it is to be included in the heat balance.

The following is a list of nomenclature used within this section.

- A - area normal to heat flow path, ft.²
- a - Reynolds number - exponent
- b - Prandtl number - exponent
- c - convection coefficient constant
- h - convection film coefficient, BTU/hr. ft.² °R
- k - conductivity, BTU/hr. ft. °R
- L - characteristic length, ft.
- Pr - Prandtl number
- Re - Reynolds number
- t - material thickness, ft.
- U - overall heat transfer coefficient, BTU/hr. ft.² °R

SUBSCRIPTS:

- d - duct
- i - inner
- o - outer

For a surface cooling system, an overall heat transfer coefficient (UA) can be employed to establish the barrier for a heat path from a known heat source to the coolant passing through the coolant supply ducting system. If the coolant flow rate is provided as a fixed program input, a coefficient is not required. If the heat source is such that no heat transfer will occur (source and coolant temperatures identical), a UA value of one will permit proper program operation without requiring the user to compute the actual value. When a temperature difference exists between the coolant and heat source, a supply system overall heat transfer coefficient should be computed by the user for program input. The path from the heat source to coolant will normally pass through a series of barriers which are both the inside and outside gas films and duct conduction. For this series configuration, the overall heat transfer coefficient can be computed by the equation

$$UA = 1 / \left[\left(\frac{1}{hA} \right)_i + \left(\frac{t}{kA} \right)_d + \left(\frac{1}{hA} \right)_o \right] . \quad (177)$$

VOUGHT AERONAUTICS COMPANY

The value of conduction (k) for the duct is a material property and can be found in reference material such as reference 16. Convection film coefficients are functions of gas flow properties and the duct configuration. These are normally evaluated through an equation of the form

$$h = c \frac{k}{L} (Re)^a (Pr)^b \quad (178)$$

Values for the constants of a , b , and c are usually presented as a function of Reynolds number for a specific configuration and can be found in numerous references; two common references are 17 and 18.

When special fluid nodes have been incorporated in the exhaust system model, an overall heat transfer coefficient is required to define the barrier to heat transfer between the fluid node and its adjacent node in the system. These normally will follow a path from a surface to fluid node passing through a conducting wall and a convection film. The overall heat transfer coefficient is computed in manner similar to that presented, in this particular case the equation is found to be

$$UA = A / \left(\frac{L}{k} + \frac{1}{h} \right) \quad (179)$$

Again, the values of k and h must be obtained based on empirical data.

With these equations, the user can provide the overall heat transfer required as program input in most of the cases that will confront him.

VOUGHT AERONAUTICS COMPANY

4.0 REFERENCES

1. Bernstein, A., W. Heiser and C. Nevenor, "Compound Compressible Nozzle Flow", AIAA Paper No. 66-663 presented at the AIAA Second Propulsion Joint Specialist Conference held at Colorado Springs, Colorado, June 13-17, 1966.
2. Sasman, P. K., Robert J. Cresci, "Compressible Turbulent Boundary Layer With Pressure Gradient and Heat Transfer", AIAA Journal, Vol. 4, No.1, January, 1966.
3. Haering, G. W., "A Proposed Correlation Scheme for Gas-Film Cooling Data", Air Force Aero Propulsion Laboratory, TR-66-56, August, 1966.
4. Sellers, J. P. Jr., "Gaseous Film Cooling With Multiple Injection Stations", AIAA Journal, Vol. 1, No. 9, September 1963.
5. London, A.L., and R. K. Shah, "Offset Rectangular Plate-Fin Surfaces, Heat Transfer and Flow Friction Characteristics", Transaction of the ASME, Journal of Engineering for Power, July 1968.
6. Kays, W. M. and A. L. London, Compact Heat Exchangers, Second Edition, McGraw-Hill Book Co., 1964.
7. Hartnett, J. P., R. C. Birkebak and E. R. Eckert, "Velocity Distribution, Effectiveness and Heat Transfer of Air Injected Through a Tangential Slot into a Turbulent Boundary Layer", Transaction of the ASME, Journal of Heat Transfer, Vol. 83, series C, No. 3, 1961.
8. Culick, F. E. E., "The Compressible Turbulent Boundary Layer With Surface Mass Transfer", Massachusetts Institute of Technology Naval Supersonics Laboratory, TR-454, August 1960.
9. Foganioli, R. P. and A. R. Saydah, "Turbulent Heat Transfer and Skin-Friction Measurements on a Porous Cone With Air Injection at High Mach Numbers", AIAA Journal, Vol. 4, No. 6, 1966.
10. Wolfe, G. W., "Derivation and Computer Program Development (NVIEW) for the Calculation of Radiation View Factors Between Axisymmetric Sub-Divisions of a Turbine Engine Exhaust System", Vought Aeronautics Division, LTV Aerospace Corporation, Report No. 2-53900/OR-2829, August 1970.

VOUGHT AERONAUTICS COMPANY

11. Mouritsen, T. E., G. W. Wolfe, and G. F. Thomas, "Development of Infrared Suppression System for A-7 Aircraft (U), Phase I Report", Vought Aeronautics Division, LTV Aerospace Corporation, Report No. 2-53910/88-2543, October 1968. (CONF.)
12. Mouritsen, T. E., A. N. Blaser, "Development of Infrared Suppression System for A-7 Aircraft (U), Final Engineering Report", Vought Aeronautics Division, LTV Aerospace Corporation, Report No. 2-53910/OR-5534, October 1970. (CONF.)
13. Altshuler, T. L., "Infrared Transmission and Background Radiation by Clear Atmosphere", General Electric Document No. 61SD199, Dec. 1961, (AD 401923).
14. Handbook of Military Infrared Technology, Office of Naval Research, Dept. of the Navy, 1965.
15. Handbook of Geophysics and Space Environment, Air Force Cambridge Research Laboratories, Office of Aerospace Research, United States Air Force, 1965.
16. Society of Automotive Engineers, Aero-Space Applied Thermodynamics Manual, Second Edition, 1969,
17. Jakob, Max, Heat Transfer, Vol. 1, John Wiley and Son, Inc., 1959.
18. McAdams, W. H., Heat Transmission, McGraw-Hill Book Co., Inc., 1954.

5.0 PLUME SIGNATURE

The following pages are reproductions of documents which are difficult to obtain or considered essential to the definition of the plume emission/transmission calculations.

THE UNIVERSITY OF MICHIGAN
THE INFRARED AND OPTICS LABORATORY

MEMO TO: File

28 January 1970

FROM: G. Lindquist

SUBJECT: How to use FS+TAU5.

FS is a general program to computer radiances, absorptances, and apparent temperatures through a path having any desired temperature and pressure variations with distance and can be used for isothermal and nonisothermal single gases or three-gas mixtures, two of which can be absorbing. The latest band model techniques are used and the lines are allowed to be overlapping (although an option to use the non-overlapping line case is available). An option is also available which allows the radiances from a hot gas source to be first computed and then adjusted by the transmittance of an atmospheric path inserted in front of the hot gas source. This method is, of course, incorrect and is used only for comparison purposes.

The path through which the calculation is to proceed is described by 5 linear arrays XTEMP, TEMP, PRES1, PRES2, and PRES3. XTEMP describes distance from the observer. The other four arrays describe the temperature and the pressures of absorbing gas 1 and 2 and the broadening gas, 3, at the distances corresponding to the values of XTEMP (see Figure 1). Note that the observer is always at a value of XTEMP = 0. NT specifies the number of values that are in each of these arrays.

The size of the increments through which the integration over the above described path takes place is determined by the four variables NDIV, DL, PATHLN, and IPL. Two options are available determined by the value of IPL. For IPL = -1, PATHLN is taken to contain the total distance over which the integration is to take place (its value must

MEMO TO: File

-2-

28 January 1970

be \leq the last value in the array XTEMP). This path length is then divided into NDIV equal increments of length $DL(1) = \dots = DL(NDIV) = \frac{PATHLN}{NDIV}$. For $IPL = +1$, the value of PATHLN is ignored and NDIV values of the incremental length DL, must be read in. The temperatures and pressures for each segment of length DL are taken by interpolation in the functional variations of temperature and pressure described by TEMP, PRES1, PRES2, and PRES3 versus XTEMP. In this program all distances are in centimeters, all temperatures in $^{\circ}K$, and all pressures in atmospheres.

The frequency range over which the calculations are made is determined by the three variables NFREQ, NUFRST, and NUINC. NUFRST describes the first frequency to be computed, NUINC describes the amount by which the frequency is to be incremented between successive frequencies for which computations are desired and NFREQ is the number of frequencies for which computations are desired. If NUFRST is set to be less than 0, then the program expects to find the NFREQ frequencies for which calculations are desired in the array NU.

The band model parameters for the absorbing gas or gases are expected to be in an external file and are to be in the proper order. The array GAS contains the names of the absorbing gases, and if $GAS(1) = 'H2O'$ (as is set in the data statement) the first file must contain the band model parameters for H2O, etc.

The band model parameters used are the average line width to spacing ratio multiplied by $\frac{1}{2\pi}$ called β , and the average line strength to spacing ratio, called k . The following describes the order they are to be in for each gas:

28 January 1970

<u>Line #</u>	<u>Contents of Line</u>
1	Number of temperatures, NTEMP, for which β is read in, number of frequencies, NNU, for which β is read in (format = 2I5)
2	Up to 72 characters of format to be used to read the data immediately following this line (format = 18A4)
3.	Values of frequency for which β is given. There should be as many values as specified in line 1:
.	Up to 72 characters of format to be used to read the data immediately following this line (format = 18A4)
.	Values of temperature for which β is given. There should be as many values as specified in line 1.
.	Up to 72 characters of format to be used to read the data immediately following this line (format = 18A4)
.	Values of β as a function of frequency and temperature. The order of the values is as follows: values of β at the first fre- quency for the NTEMP values of temperature, the values of β at the 2nd frequency for the NTEMP values of temperature, up through the NNU frequencies.

The same series of lines is used to read in the k's as a function of temperature and frequency (starting with a line similar to line 1).

28 January 1970

Currently the band model parameters for water vapor are contained in a file named SX90:BKH20 and the corresponding parameters for CO2 are contained in SX90:BKCO2. The program values have been preset so that, unless the user reads in other values, GAS(1) is 'H2O', GAS(2) is 'CO2' and GAS(3) is 'N2'. Appropriate values for the broadening coefficients are also preset. The upper and lower frequency limits for these values are 1750 and 4300 cm^{-1} . They are valid for temperatures between 300°K and 3000°K.

The equation used for the effective half-width is:

$$\beta_e = \frac{\sum_{i=1}^n k(\nu, T_i) \times (273.15/T_i) \times \beta(\nu, T_i) \times (P_i + \alpha \times P_{B,i}) \times (DL)_i}{\sum_{i=1}^n k(\nu, T_i) \times (273.15/T_i) \times P_i \times (DL)_i}$$

The exponent (η) of the overlap factor $(\beta/\beta_e)^\eta$, can be treated in three ways:

- (1) set equal to namelist input EXPO
- (2) calculated as $f(x_e)/\sqrt{x_e} \times .6366$
- (3) calculated so that:

$$\eta = 0. \text{ for } x_L \leq 1.$$

$$\eta = (x_L - 1.)/9. \text{ for } 1. < x_L < 10.$$

$$\eta = 1. \text{ for } x_L \geq 10.$$

P_i , T_i and P_{Bi} are the pressure of the absorbing gas, the temperature and the pressure of the broadening gas respectively corresponding to the i -th value of DL. In this program GAS(3) is always treated as the broadening gas, α is the broadening coefficient.

28 January 1970

The input parameters are read from two logical IO units: the band model parameters are read from unit 3 and all other input data from unit 1. The data read from unit 1 are read in via a namelist statement whose name is IN. The program object module is currently in two files which must be concatenated to run the program. They are SX90:NFSOBJ and SX90:NTAU5OBJ. Subroutines from the file ST82:SUBPACK are also required. All printed output is written on logical IO unit 6. Punched cards for the Benson-Lehner plotter (if desired) are written on unit 2. The logical IO unit on which data for the CALCOMP plotter are written can be specified by the value of ICPLLOT. Thus a sample run statement appears as follows (assuming it is being run from project SX90). \$RUN NFSOBJ+NTAU5OBJ+ST82:SUBPACK;
1 = <Data> 2 = <Plot> 3 = BKH2O+BKCO2 6 = <Output>

where <Data> is the name of the file on which the users data for the namelist IN is stored

<Plot> is the name of the file where plotter card images for the Benson-Lehner plotter are to be written. The 2 = <Plot> is not needed if no plotter cards are required.

<Output> is the file where line images for the printer are to be written.

Following is a glossary of the parameters that can be varied via the namelist IN.

GAS	name(s) of gas(es), format A4
NT	number of input temperatures (integer) and pressures to be read in.

TEMP Input temperatures ($^{\circ}\text{K}$) (real numbers)

XTEMP Path positions for temperatures and pressures (real numbers) (cm)

PATHLN Total path length (cm) (real number) needed only if IPL < 0

NFREQ Number of wavenumbers for which the calculations are to be made (integer)

NUFRST First wavenumber for which the calculation is to made (real number). If NUFRST $\leq 0.$, the wavenumbers (NU) are to be read in.

NUINC Wavenumber increment (real number). This is read in only when NUFRST > 0. and the NU's are to be calculated.

NU Wavenumbers (real numbers); to be read in only if NUFRST $\leq 0.$

NDIV Number of increments over which the summation is to be taken:

$$\sum_{i=1}^{\text{NDIV}} N_{\nu}^*(T_i) \left(\text{TAU}(\nu, 1-i) \text{TAU}(\nu, i) \right)$$

If NDIV is negative, NDIV increments, temperatures, pressures of gases 1, 2, 3 are written. If NDIV is 1, or -1, the case is isothermal and the first values of TEMP and PRES1, PRES2, and PRES3 are used (integer).

NAG number of absorbing gases (integer)

ALPHA broadening coefficients (real numbers) e.g. .2 for $\text{H}_2\text{O}-\text{N}_2$; .769 for CO_2-N_2 . They must correspond in order to absorbing gas order.

28 January 1970

PRES1 Pressures of gas 1 (real numbers). (atmospheres)
 PRES2 Pressures of gas 2 (real numbers). (atmospheres)
 PRES3 Pressures of gas 3 (real numbers). (atmospheres)
 IPL $\left\{ \begin{array}{l} > 0, \text{DL's read in} \\ < 0, \text{the program sets } \text{DL}(i) = \text{PATHLN}/\text{NDIV} \end{array} \right\}$ integer
 DL Path increments (NDIV in number) (real numbers). If
 IPL > 0, DL's read in.
 ITYPE $\left\{ \begin{array}{l} 1, \text{overlapping lines} \\ 2, \text{nonoverlapping lines (remember: calculations for gas} \\ \text{mixtures cannot be done with ITYPE=2)} \end{array} \right\}$ integer
 EXPO $\left\{ \begin{array}{l} \geq 0., \eta = \text{EXPO} \\ = -9., \eta = 0. \text{ for } x_L \leq 1. \\ \eta = (x_L - 1.)/9. \text{ for } 1. < x_L < 10. \\ \eta = 1. \text{ for } x_L \geq 10. \\ < 0. \text{ and } \neq -9., \eta = f(x_e)/\sqrt{x_e} \cdot 0.6366 \end{array} \right\}$ real number
 IPRNT $\left\{ \begin{array}{l} > 0, \text{TAU's are printed for IPRNT wavenumbers and NDIV} \\ \text{increments} \\ \leq 0, \text{TAU's are not printed.} \end{array} \right\}$ integer
 ICPLT $\left\{ \begin{array}{l} < 1, \text{data is not stored for CALPLOT.} \\ > 1, \text{data stored for CALPLOT on logical IO unit number ICPLT.} \end{array} \right.$
 In this case, the integer value of ICPLT must be set equal to some
 file name in the \$RUN command.

28 January 1970

IPLOT	{ > 1, data punched on cards for the Benson Lehner plotter on logical IO unit 2. < 1, data not punched on cards.
LCODE	{ 6, points 0, lines for punched data (RAD, ABS, TSTAR VS NU)
LCODEA	{ 6, points 0, lines for punched data (TSTAR VS ABS)
XMAX	maximum abscissa limit (real numbers)
XMIN	minimum abscissa limit (real numbers)
TSMAX	maximum ordinate (TSTAR) limit (real numbers)
TSMIN	minimum ordinate (TSTAR) limit (real numbers)
RMAX	maximum ordinate (RAD) limit (real numbers)
RMIN	minimum ordinate (RAD) limit (real numbers)
TODAY	date program is run (format ' --/--/--') or other ID information
METHOD	= ' CORRECT' ; calculations done in the normal correct way. = ' WRONG ---' ; hot gas through atmosphere done in the incorrect way.

These quantities
all apply to the
use of the Benso.
Lehner plotter
and may be igno-
red if IPLOT < 1

THE UNIVERSITY OF MICHIGAN
THE INFRARED AND OPTICS LABORATORY

MEMO TO: File 17 April 1970
FROM: G. Lindquist *GL*
SUBJECT: Additions and Changes to FS

Since the last memo was written several changes have been made on FS+TAU5. These changes make it more flexible and update the procedure so that short flames through long paths are now correctly computed. These changes are outlined here.

1) A third option is now available for the treatment of the input path data. In the previous version (see memo of 28 January 1970) the path element parameters were always determined by interpolation in arrays describing the temperature and pressure variation along the path. These arrays are TEMP, PRES1, PRES2, and PRES3 with the array XTEMP containing the path distances corresponding the values in the other 4 arrays. The new option, used by setting IPL = 2, allows the interpolation procedure to be bypassed, and the values in the arrays TEMP, PRES1, PRES2, and PRES3 are identified directly with the corresponding values in the path element array DL. The array XTEMP is ignored when this option is used. For example with IPL = 1, the values of TEMP would be associated with the values of XTEMP as follows:

TEMP(1) = 300
TEMP(2) = 600
TEMP(3) = 900

XTEMP(1) = 0
XTEMP(2) = 10
XTEMP(3) = 20

which would describe a path with temperature that increases from 300°K to 900°K in the first 20 cm. A value of DL(1) = 10. would result in linear interpolation in the array TEMP to obtain the value of temperature for that DL. Thus the temperature

17 April 1970

obtained would be 450°K . For the same input data, if $\text{IPL} = 2$, the value of $\text{TEMP}(1)$ would be identified directly with $\text{DL}(1)$, i.e., the first element, 10 cm long, would have a temperature of 300°K .

II) A change is made in the way atmospheric paths are treated. It is now possible to insert an atmospheric path in front of the hot gas and calculate the result correctly without having to re-insert the hot gas portion of the plume along with it. To do this involves a change in the use of the variable `METHOD`. Previously setting `METHOD = 'WRONG'` set the program so that it would treat the input namelists in pairs and use the second namelist to compute attenuation values which were then applied to the results from the first namelist (using "wrong" method). Setting `METHOD = 'CORRECT'` returned the program to its original mode.

In the revised program, the specification of the variable `METHOD` either 'WRONG' or 'CORRECT' in a namelist implies that this namelist is to be used as an atmospheric path in front of the path described by the last namelist in which `METHOD` was not specified. The name to which `METHOD` is set determines the type of calculation to be done, correct or wrong.

Thus if the radiance from a given hot gas is to be calculated as seen through several paths, using both the "CORRECT" and the "WRONG" methods, the namelists would appear as follows:

hot gas

&IN (Description of hot gas) &END

Correct adjustment of
hot gas by first path:

&IN `METHOD = 'CORRECT'`, (Description of
first path) &END

17 April 1970

Correct adjustment of hot
gas by 2nd path

& IN METHOD = ' CORRECT' , (Description of 2nd
path) & END.

Wrong adjustment of
hot gas by 3rd path

& IN METHOD = ' WRONG' , (Description of 3rd
path) & END

It is emphasized that, if METHOD is not specified, the current namelist is taken as a hot gas, as opposed to an intervening atmospheric path, and subsequent namelists with METHOD specified will be treated as atmospheric paths applied to it. Note that the first namelist executed should describe a hot gas or other source ; specification of METHOD in the first namelist will lead to erroneous (and probably disastrous) results.

III) The third change made in the program is that the determination of the exponent in the overlap factor $(\beta/\beta_e)^\eta$, described on page 4 of the 28 January memo, has been changed so that certain extreme paths are treated correctly. The form that η now takes is quite complex and is described in a separate memo to be written shortly. The following paragraph explains the options available and should replace the paragraph beginning in the middle of page 4 of the memo of January 28, 1970.

The exponent η of the overlap factor $(\beta/\beta_e)^\eta$, can be treated in two ways

- 1) set equal to namelist input, EXPO
- 2) computed according to the approximation described in a later memo on this subject.

Also, the description of the use of EXPO on page 7 of the 28 January memo should be changed to read

EXPO $\left\{ \begin{array}{l} 0. \leq \text{EXPO} \leq 1., \eta = \text{EXPO} \\ > 1., \text{ or } < 0., \eta \text{ computed from approximation described in} \\ \text{later memo.} \end{array} \right.$

THE UNIVERSITY OF MICHIGAN
THE INFRARED AND OPTICS LABORATORY

MEMO TO: 3211 File

22 July 1970

FROM: G. Lindquist *GL*

SUBJECT: How to use the program PLUMES

PLUMES is a program designed to compute the radiant intensity from a cloud of hot gas. This is done by dividing the projected area of the cloud into elements, and computing the temperature and pressure distribution along a line of sight through the cloud at the center of each element. A band model calculation for the temperature and pressure distribution along a particular line of sight done in a manner identical to that performed by the program FS (Ref. 1) - yields the radiance along that line of sight. The summation of the product of such radiances times the projected area of the element associated with that line of sight yields the radiant intensity of the total gas cloud as viewed at a distance. In the current formulation the program was designed to handle rocket and jet engine exhaust plumes so that its use is limited to axisymmetric sources. Sufficient generality is included so the gas cloud can be viewed from any aspect. Also an atmospheric path can optionally be inserted between the gas cloud and the observer. Two absorbing gases and a broadening gas can be included. Normally these are H_2O , CO_2 and N_2 .

The number of input parameters is large and they can best be described in groups corresponding to their function in the program. All the parameters described here are read in by means of a namelist statement from input unit 1. The name of the namelist is IN.

Plume Specification

The gas cloud is assumed to be axisymmetric so that it is entirely specified by specifying the conditions on one side of a plane containing the plume axis. The plume is so specified by specifying the temperature and total pressure distributions in such a plane using polar coordinates with origin at the center of the nozzle exit plane (all of the plume is taken to lie downstream of the nozzle exit plane).

This specification can be handled in two ways, controlled by the variable SETUP3. If SETUP3 is negative the plume parameters are read from input unit 3 according to a format described in Appendix A. In this mode, the composition of the plume is fixed in the following way. The inputs from unit 3 are only temperature and total pressure. The partial pressures of the three gases used are then determined by the parameters PARP1, PARP2, and PARP3 which are the mole fractions of gases 1, 2, and 3 respectively. Options are also available to allow the input parameters read in on unit 3 to be dimensionless temperatures, pressures, and distances. These options are contained in the variables PZERO, TZZRO, and RRATIO. The values read in on unit 3 for temperature are multiplied by TZZRO, for pressure by PZERO and for distance by RRATIO. If any of these options are not to be used, the particular parameter should be set equal to 1.

If SETUP3 is set positive it is assumed that the plume specifications have already been read from unit 3 in a previous calculation.

If SETUP3 is zero, the plume parameters are calculated using an idealized gas dynamic plume model (see Ref. 2) characterized by an initial region, in which mixing occurs adjacent to a potential core, and a main region in which mixing

with the ambient determines the physical parameters. Figure 1 shows a diagram of such a plume. The boundary of this plume model also determines the extent of the area over which the plume integration takes place. Thus, it is necessary to include the quantities which describe this boundary even though SETUP3 is negative, i.e. plume pressures and temperatures are to be read in rather than calculated.

The parameters which describe the gas dynamic plume model are as follows:

RO	the radius of the nozzle exit (cm)
ZC	the length of the mixing region of the plume (cm)
PANGD	the angle between the plume axis and the outer boundary of the plume in the mixing region (degrees)
ZMAX	the total length of the plume (cm)
ZCC	the length of the potential core of the plume (cm)

If SETUP3 is zero, parameters are needed which describe the physical properties of the gas dynamic model. These are described as follows:

TPL1	temperature in the potential core
TPL2	ambient temperature (temperature of gas surrounding plume)
P11	pressure of gas 1 in the potential core
P12	ambient pressure of gas 1
P21	pressure of gas 2 in the potential core
P22	ambient pressure of gas 2
P31	pressure of gas 3 in the potential core
P32	ambient pressure of gas 3

To repeat, RO, ZC, PANGD and ZMAX must be included as input even if SETUP3 is not zero to define the region over which integration takes place. The remainder of the parameters describing the gas dynamic plume model are needed only if SETUP3 = 0.

Atmospheric Path Specification

In order to include an atmospheric path in front of the plume it is only necessary to specify the altitude of the plume and of the observer in cm (ALTPLM and ALTOBS respectively), the range between the plume and the observer in cm (RANGE) and the number of elements into which the atmospheric path is to be broken (NA). The proper temperatures and pressures are obtained from a model atmosphere contained in the program. If no atmospheric path is to be inserted set RANGE = 0.

Frequency Range

It is possible to include two groups of frequencies in any one calculation. The first group is specified by the variables NFREQ, NUFRST, and NUINC. NUFRST describes the first frequency to be computed, NUINC describes the spacing between frequencies and NFREQ describes the number of frequencies in the first group of frequencies. The second group of frequencies is described by the variables NFREQ1, NUFRS1, and NUINC1 which correspond exactly in usage to NFREQ, NUFRST and NUINC. Thus, for example in one calculation the frequency ranges from 2100 to 3000 and from 3500 to 4000 cm^{-1} can both be covered. If only one group of frequencies is to be covered, NFREQ1, NUFRS1, and NUINC1 can be ignored. Alternatively, NUFRST can be set negative and the program then expects to find NFREQ values of frequency read in as the array NU.

Bandmodel Parameters

The bandmodel parameters for the absorbing gases are expected to be in external files in the expected order. The order is the same as was given for use in the program FS (see Ref. 1). The band model parameters for the first absorbing gas (usually H_2O) are read from input unit 4, and the band model parameters for the 2nd absorbing gas (usually CO_2) are read from unit 5. The array GAS contains the names of the gases to be considered, usually 'H2O', 'CO2', and 'N2' in that order.

Fineness of the Plume Integration

Integration takes place in three dimensions in this program. The plume is projected into a plane which is perpendicular to the line of sight from the plume to the observer and passes through the center of the nozzle exit. Two dimensions of the integration occur as integration over the area of the plume as projected into this plane. The origin of the coordinate system used in this plane is at the center of the nozzle exit. Polar coordinates are used. The third dimension is perpendicular to the above mentioned plane and occurs as integration along each of the lines of sight through the plume. To obtain a line of sight radiance as the result of this integration, this integration is carried out over the transmittance along the line of sight.

The fineness of the transmittance integration is controlled by a variable NMAX. The maximum and minimum expected temperatures are read in as TMAX and TMIN and this range is divided into NMAX temperature increments. In calculating through a line of sight, each time the boundary of one of these temperature

increments is crossed, a transmittance element is established. Thus, a line of sight which traverses the full range of TMAX to TMIN will be divided into NMAX elements. Lines of sight with alternately increasing and decreasing temperatures will be divided into more elements, and lines of sight having only small temperature variations will be divided into correspondingly fewer elements. The temperature is divided into increments according to the inverse 2nd power of the temperature so that higher temperatures yield smaller increments. This procedure is useful without modification for plumes having only a limited temperature range. If the temperature range is large, or if the temperatures are clustered around two or more values, such a breakup is not very advantageous. For such occurrences, provisions have been made to allow the temperatures defining the temperature increments to be read in directly. This is done by setting ICHOOZ=1 and reading in NMAX+3 values for the temperature increment boundaries using the array TLIM, e.g. by including in the namelist IN a line such as ICHOOZ=1, TLIM = t_1 , t_2 , --- t_{NMAX+3} ; where t_1 --- t_{NMAX+3} are the temperature increment boundaries. If the values of TLIM are read in TMAX and TMIN can be ignored.

The fineness of the integration over the radial dimension in the plane of projection is also controlled by NMAX (the controlling of integration fineness in two dimensions by one variable resulted in some loss of flexibility but was done to reduce the number of input variables that needed to be considered). The value of the radial increment is chosen so that, with a blob of gas which has equal extent in all directions, the number of radial increments will approximately equal the average number of line of sight transmittance increments. In the edge regions of the plume the radial incre-

ment size is allowed to increase with decreasing average temperature. The reason for this is to reduce the computing time by computing fewer radiance values for regions where the radiance will be very small compared to the peak radiance values.

The fineness of the integration over the angular dimension in the projected plane is not variable. This angular dimension is called PHI in the program. This angle for a given line of sight lies in the plane of projection. It is the angle between the projection of the plume axis into the above mentioned plane and the line from the center of the nozzle exit to the intersection of the given line of sight with the same plane (all lines of sight through the plume are taken to be parallel to the line of sight from the observer to the plume so that all lines of sight are perpendicular to the above mentioned plane). The values of PHI currently used in the integration are: 0° , 6° , 18° , 36° , 60° , 90° , 120° , 144° , 162° , 174° , 180° . Integration over $180^\circ < \text{PHI} < 360^\circ$ is accounted for by multiplying the result for $0 < \text{PHI} < 180^\circ$ by two.

Modifications to the above integration procedure can be made by simple modifications to the program itself.

Other Features

Three auxiliary temperatures are available for use. If TBACK is set non-zero, a black background at temperature TBACK will be placed behind the plume. If TBACKC is set non-zero, radiance values equal to a black body at TBACKC will be subtracted from all radiance values as a background compensation. If TNOZ is non-zero, in case where the line of sight looks up the nozzle a black background at TNOZ will be used to represent the inside of the nozzle. In addition if OBSCUR is set non-zero, an opaque disc of radius OBSCUR in cm will be placed at the nozzle exit and any lines of sight

from the front
which intersect this disc will be ignored.

Following is a glossary of all variables which can be set via namelist IN. Not all are mentioned in the text since they are merely control parameters. Also a group of parameters controls the scales used in making plotter cards for the Benson-Lehner plotter. The details of the transmittance calculation are exactly as described in Ref. 1.

The program can be run by the use of the following statement (assuming it is run from SX90) \$RUN PO+SX27:SO +ST82:SUBPACK+NTAU5OBJ; 1=<data> 3=<plume data> 4=BKH2O 5=BKCO2 9=<plotter cards>

The execution time of this program is long and it occupies a great deal of computer memory so that it is economically feasible to run it only in batch mode. In the above statement words enclosed in "< >" e.g. <data> indicate file names where that particular information either is stored on input, or to be stored on output. Printed output comes from unit ~~7~~ and unit 8.

GLOSSARY OF INPUT PARAMETERS

Data is read in by means of namelist IN, the elements of which are:

SETUP3	<p>> -0, plume conditions are not read in</p> <p>= 0., the plume conditions are calculated from certain required input data (TPL1, TPL2, P11, P12, P21, P22, P31, P32)</p> <p>< -1., plume conditions read in by means of 3=FDNAME in \$RUN instructions. FDNAME is the file in which the information is stored.</p>	
SETUP1	<p>> 1., k, β for absorbing gas 1 not read in.</p> <p>< 1., k, β for absorbing gas 1 read in by means of 4=FDNAME in \$RUN instructions. FDNAME is the file where the data is stored.</p>	<p>These variables can almost always be ignored since the program sets them automatically.</p>
SETUP2	<p>> 1., k, β for absorbing gas 2 not read in.</p> <p>< 1., k, β for absorbing gas 2 read in by means of 5=FDNAME in \$RUN instructions. FDNAME is the file where data is stored.</p>	
NUFRST	<p>first wavenumber in first group of wavenumbers for which calculations are to be made (real number).</p> <p>=0., wavenumbers are not to be calculated but to be read in via NU</p>	
NFREQ	<p>number of wavenumbers in first group of wavenumbers for which the calculations are to be made.</p> <p>(integer)</p>	
NUINC	<p>wavenumber increment (in wavenumbers) in first group of wavenumbers (If NUFRST=0., NUINC can be ignored)</p>	
NU	<p>wavenumbers (real numbers) (If NUFRST=0., the wavenumbers are read in; if not, NU can be ignored)</p>	
NUFRS1	<p>first wavenumber in 2nd group of wavenumbers.</p>	
NFREQ1	<p>number of wavenumbers in 2nd group of wavenumbers (integer)</p>	
NUINC1	<p>wavenumber increment in 2nd group of wavenumbers.</p>	
NA	<p>number of increments for the atmospheric path (integer ≤ 20)</p>	
ALTOBS	<p>altitude of the observer or observing instrument (real number, in cm)</p>	

ALTPLM	altitude of the exhaust plume (real number, in cm)
RANGE	distance from observer to plume (real number, in cm)
ALPHA	broadening coefficients for absorbing gases 1 and 2. (.2 for H ₂ O-N ₂ , and .769 for CO ₂ -N ₂) Can be ignored if the gases are 'H ₂ O', 'CO ₂ ' and 'N ₂ '.
GAS	names of the two absorbing gases and the broadening gas. Can be ignored if the gases are to be 'H ₂ O', 'CO ₂ ' and 'N ₂ '.
IATMO	> 0, atmospheric path information is printed. < 0, atmospheric path information is not printed.
RO	radius of plume at nozzle exit (real number, in cm)
PANGD	plume angle (real number, in degrees)
ZC	length of plume after which plume diameter remains constant. (real number, in cm)
ZCC	length of potential core of plume (real number, cm).
OBSCUR	obscuration of line of sight at $z=0$. (Radius of circular obscuration at nozzle exit centered about plume axis) (real number, in cm).
ZMAX	maximum length of plume
TMAX	maximum temperature of plume ($^{\circ}$ K)
TMIN	minimum temperature of plume ($^{\circ}$ K)
ASPDEG	aspect angle in degrees (real number)
NMAX	approximate number of increments into which two of the three dimensions is divided. The total number of cubes into which the plume will be divided $\approx (NMAX)^2 \cdot 11$
TBACK	temperature of background behind plume ($^{\circ}$ K)
TBACKC	temperature of background radiance which is to be subtracted from radiance values ($^{\circ}$ K)
TNO2	temperature of inside of nozzle (used if line of sight looks up the nozzle) $^{\circ}$ K.

TODAY	date program is run (format real *A8)	
ITYPE	1, overlapping lines 2, nonoverlapping lines	
EXPO	≤ 0 or > 1 , η determined by special interpolation procedure (Ref. 3) $0 \leq EXPO \leq 1$, $\eta = EXPO$	
INPRNT	> 0 , path information printed < 0 , path information not printed	
IPLOT	< 0 , results not punched on cards for Benson Lehner plotter > 0 , results punched on cards for IPLOT plots.	
IDE	label for punched data (format 3A4)	
XMAX	array giving maximum abscissa value for each of the IPLOT plots (wavenumbers) (real number) (should have IPLOT values)	These variables control the output for the Benson Lehner plotter.
XMIN	array giving minimum abscissa value for each of the IPLOT plots (wavenumbers) (real number) (should have IPLOT values).	
ISCALE	< 0 , automatic scaling off, maximum ordinate value for plots taken from RMAX > 0 , automatic scaling on.	these variables control the output for the Benson Lehner plotter.
RMAX	array giving maximum ordinate value (radiant intensity) (real numbers) for each of the IPLOT plots (should have IPLOT values if ISCALE < 0).	
LCODE	6, points 0, lines	
ITAU	< 0 , transmittances are not printed > 0 , transmittances are printed for ITAU wavenumbers.	
IL	< 0 , line of sight radiances are not printed > 0 , line of sight radiances are printed for IL wavenumbers	

If data for plume is to be calculated (SETUP3=0. in namelist), the following elements must be in namelist; otherwise they can be ignored.

TPL1	temperature in core (real number, $^{\circ}\text{K}$)
TPL2	temperature at edge (real number, $^{\circ}\text{K}$)

P11	pressure of GAS(1) in core (real number, atm)
P12	pressure of GAS(1) at edge (real number, atm)
P21	pressure of GAS(2) in core (real number, atm)
P22	pressure of GAS(2) at edge (real number, atm)
P31	pressure of GAS(3) in core (real number, atm)
P32	pressure of GAS(3) at edge (real number, atm)

Some of the namelist elements are preset by means of DATA statements:

SETUP3= -10.	EXPO = -9.
SETUP1=-10.	ITAU = -1
SETUP2= -10.	IPRNT = -1
NUFRST = 0.	IL = -1
NA = 10	ITYPE = 1
ALPHA(1) = .2	TNOZ = 900. (⁰ K)
ALPHA(2) = .769	TBACK = 0.
IATMO = -1	TBACKC = 0.
IPLOT = -1	GAS = 'H2O' , 'CO2' , 'N2'
IDE = 'RAD VS NU'	ISCALE = 1
LCODE = 6	

REFERENCES

1. G. Lindquist, How to Use FS+TAU5, Memo to File, 28 January 1970.
Also G. Lindquist, Additions and Changes to FS, Memo to File,
17 April 1970.
2. F. Simmons, Gas Dynamic Model for Jet Engine Exhaust Plumes,
Memo to Project 2043 File, 18 June 1970.

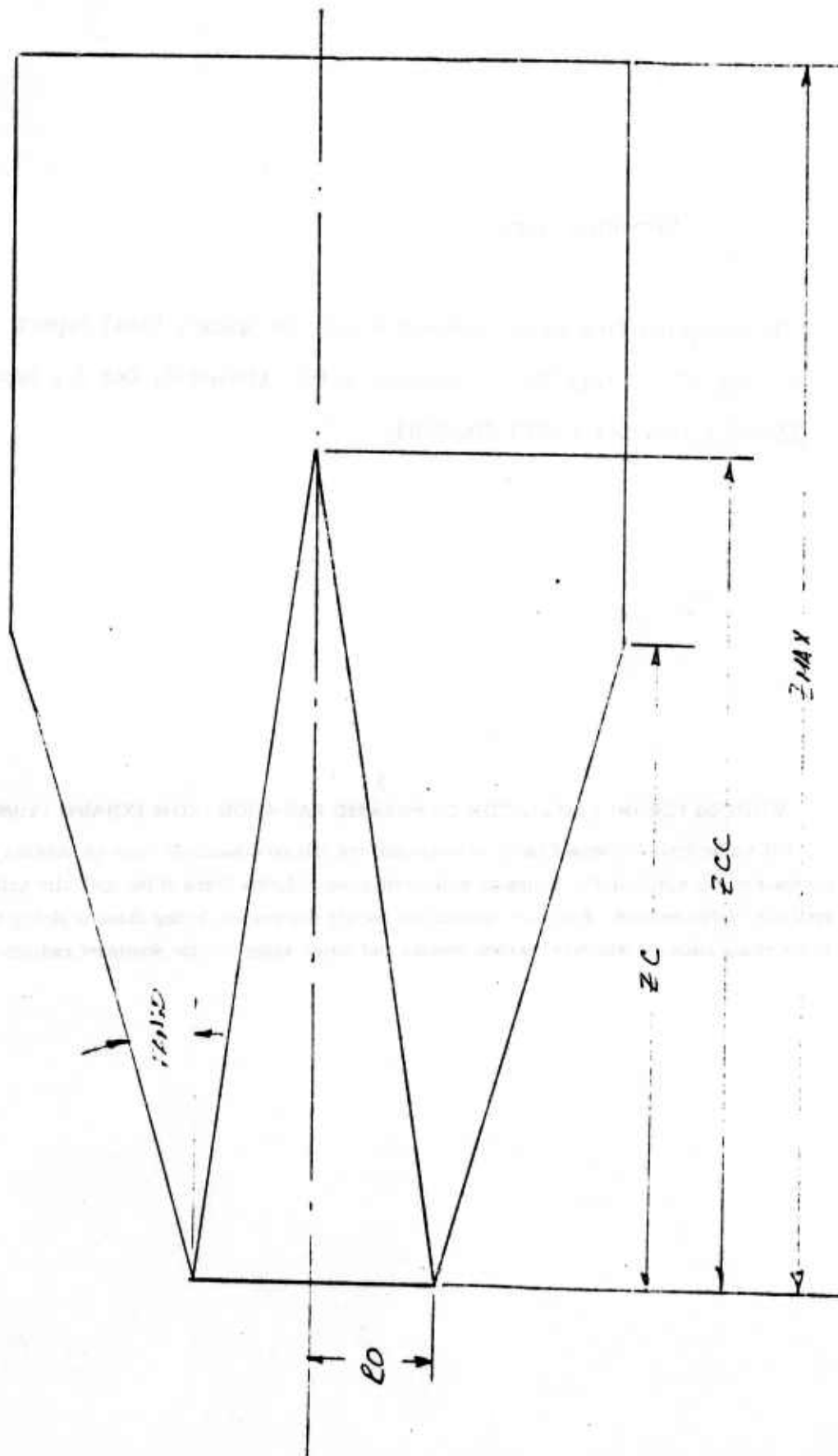


FIGURE 1. DIAGRAM OF PLUME BOUNDARY, A CONTINUAL CONCENTRATION PLUMES.

Extracted From:

"IR Radiation From Rocket Exhaust Plumes in Space", Final Report
17 July 67 - 7 July 70. F. Simmons and G. Lindquist, Oct 70, Report
3211-1-F contract F04701-70C-0004.

3

METHODS FOR THE CALCULATION OF INFRARED RADIATION FROM EXHAUST PLUMES

(U) Aside from condensed particle emission, the infrared radiation from an exhaust plume consists of the spectral-line emission in the vibration-rotation bands of the optically active products of combustion. For most operational rocket engines, excluding those utilizing fluorine or its compounds as oxidizers, carbon dioxide and water vapor are the dominant radiators. For

these well-known molecules, modern quantum-mechanical methods can easily provide the line positions corresponding to the differences in the vibrational and rotational energy levels associated with emission or absorption of photons. However, at higher temperatures, many vibrational and rotational levels become populated, and the number of spectral lines contributing to the radiation increases enormously. There is not presently, nor will there be in the foreseeable future, sufficient data on the line strengths and widths to perform exact calculations of radiative transfer for such hot gases. Moreover, even if these data were available, their application in a line by line calculation of the spectral-radiance distribution and radiant intensity in a complex flow field would be quite impractical, even with modern high-speed computers.

(U) Consequently, approximate methods must be invoked to handle the treatment of radiation from highly nonuniform and nonisothermal gases such as exhaust jets. The most sophisticated of these approximate methods for treating infrared radiative transfer is the use of a molecular band model to obviate the requirement of considering the variation in absorption and emission in two dimensions: spatial—along the nonisothermal path through the radiating region; and spectral—over the contour of each spectral line. In essence, a molecular band model is a simple mathematical representation for the location and distribution in strengths of the rotational lines: the most generally useful model is one which assumes a random location of lines (an assumption which is quite realistic for polyatomic molecules in which many vibrational and rotational energy levels become populated in several vibrational degrees of freedom). By this means, the consideration of the variation in emission and absorption over the contours of individual spectral lines can be obviated, and radiative transfer expressions developed which require only consideration of variations along the optical path. Thus, spectral radiances can be calculated over the projected area of a radiating body of gas (e.g., an exhaust plume) and integrated to yield spectral radiant intensities.

(U) Band models are generally formulated in terms of two parameters which are combinations of the average values of three basic variables: the line strengths, widths, and separations. These parameters are functions of both wavelength and temperature for band models applied to gases which emit as well as absorb, and are determined experimentally in the laboratory from measurements of absorption in isothermal samples of gas. Their use in calculations of radiant emission for nonisothermal paths then involves the above radiative-transfer relations.

(U) Molecular band models were originally developed some years ago for the treatment of atmospheric absorption in meteorological applications; a review of the state of the art in this area has been published as a Willow Run report [10]. The extension of band models to handle the case of inhomogeneous hot gases has been the subject of recent research at The University of Michigan [11-18], UCLA [19], General Dynamics/Convair [20,22], and Warner and Swasey [21]. For the most part the motivation for these studies was the calculation of radiation from rocket exhaust plumes; this subject was reviewed at a recent NASA-sponsored symposium [17]. The inhomogeneous gas band-model expressions developed at The University of Michigan represent a further advance beyond the nonisothermal band-model formulations developed elsewhere

and based on the Curtis-Godson approximation.* The University of Michigan band models involve application of the "nearly-weak" line and "nearly-strong" line approximations [12, 14], each of which reduces to the Curtis-Godson approximation and, thus each provides an identical value when applied to the calculation of transmission through an inhomogeneous gas. However, when applied to the calculation of emission, these two approximations provide significantly different results, especially for the case of optical paths exhibiting a large variation in temperature. Accordingly, each has an appropriate range of optical depths, and, for the intermediate region, an interpolation between the two can be made.

(U) The resultant formulation for this band model in terms of the average spectral radiance (specific intensity) \bar{I}_ν , the Planck function $I_\nu^*(T)$ of the local temperature, and average spectral absorptance $\bar{\alpha}(\nu)$ in the frequency interval $\delta\nu$ is [12, 18]:

$$\bar{I}_\nu = \beta_e \int_0^{f(x_L)} I_\nu^*(\bar{f}) \exp(-\beta_e \bar{f}) d\bar{f} \quad (1)$$

and

$$\bar{\alpha}(\nu) = 1 - \exp \left[-\beta_e f(\bar{x}_L) \right] \quad (2)$$

The function \bar{f} is the Ladenburg-Reiche function (or a simple algebraic approximation thereof) of the dimensionless optical depth \bar{x} , in accordance with the following definitions:

$$\bar{f} \equiv f(\bar{x}) = \bar{x} e^{-\bar{x}} \left[J_0(i\bar{x}) - iJ_1(i\bar{x}) \right] \approx \bar{x} / (1 + \pi \bar{x} / 2)^{1/2} \quad (3)$$

$$\bar{x} = \beta_e^{-1} \int_0^X \bar{k}(X') \left(\frac{\beta}{\beta_e} \right)^\eta dX' \quad (4)$$

The quantity $\bar{k} = \bar{k}(\nu, T)$ is the first band-model parameter: the average absorption coefficient which can be identified with the ratio of average line strength to spacing. The quantity $\beta = \beta(\nu, T)$ is the second band-model parameter: the line overlap factor which is proportional to the ratio of line width to spacing. The effective value, β_e , is the weighted average along the entire path of length L :

$$\beta_e = \frac{\int_0^{X_L} \beta \bar{k} dX}{\int_0^{X_L} \bar{k} dX} \quad (5)$$

where X is the optical depth in centimeter-atmospheres normalized to standard conditions. The exponent η provides for the interpolation between the nearly weak and nearly strong line approximations by means of the empirically derived specifications: $\bar{x}_L < 1$, $\eta = 0$; $1 \leq \bar{x}_L \leq 10$, $\eta =$

* (U) The Curtis-Godson approximation, in essence, provides the means for representing an inhomogeneous path by an equivalent homogeneous one: it was originally developed to facilitate calculations of absorption along nonuniform paths in the atmosphere.

$[(\bar{x}_L - 1)/9]; \bar{x}_L > 10, \eta = 1$. The validity of this band model for calculations of radiation from inhomogeneous bodies of hot gases is indicated in Figs. 2 and 3; these figures show predicted and observed spectra for samples of H_2O and CO_2 at a pressure of 1 atm in a 60 cm path with a symmetrical triangular profile in temperature with values of $1250^\circ K$ at the center and $400^\circ K$ at the ends [18].

(U) The preceding examples illustrate the capability of this band model to provide reliable values of infrared radiances, both in magnitude and spectral distribution, for moderate optical depths of water vapor and carbon dioxide in which temperatures vary by a factor of 3 or so. A more severe test of the model is an application to a region in which the temperature varies by an order of magnitude. To test the model for this case, a number of measurements was recently made at the Willow Run Laboratory (under a NASA-supported study of infrared spectroscopy as a diagnostic tool [54] of the infrared emission from 2.5-cm methane-oxygen flame. The results are shown in Fig. 4. The upper spectrum is that of the flame viewed directly; the smoother line represents the results of the band-model calculation based on the flame model, shown in Fig. 5, which takes into account variations in H_2O and CO_2 concentrations due to both recombination and dilution in the mixing region. The temperature in the flame varied from the adiabatic flame value of $3000^\circ K$ at the center to the ambient value of $300^\circ K$ at the boundary; this close agreement speaks well for the band model. However, a limitation of this model appeared in applications involving a small, hot source imbedded in a large, cool, absorbing region. The lower spectrum in Fig. 4 represents such a case; the 2.5-cm flame viewed through a 10-m path of ambient air. Here the band model, in the form specified above, exhibited poor agreement and anomalous behavior, and, hence, required some modification. The modified band model then yielded predictions in close agreement with the observations, as indicated in Fig. 4. The modification consists of an improved method of interpolation between the nearly weak and nearly strong line approximations, i.e., the evaluation of η , which was derived from a comparison with calculations using the exact equation of transfer. This subject will be discussed in detail in another publication. For purposes of the present study, the differences in the predictions of the band model between the original and modified form are negligible.

4

THE PLUME-RADIATION COMPUTER CODE

(U) A computer code has been compiled for the calculation of spectral-radiance distributions and spectral-radiant intensities of exhaust plumes viewed from long ranges at various aspects. The main part of the code consists of a program designated PLUMES, in which plume properties (i.e., temperatures and species partial pressures) are put in as functions of radial and axial distances; therefore, at the moment, the code is limited to axisymmetric sources. The aspect angle is specified, and, through a transformation of coordinates, the plume properties are determined along the various parallel lines of sight through the plume over the entire

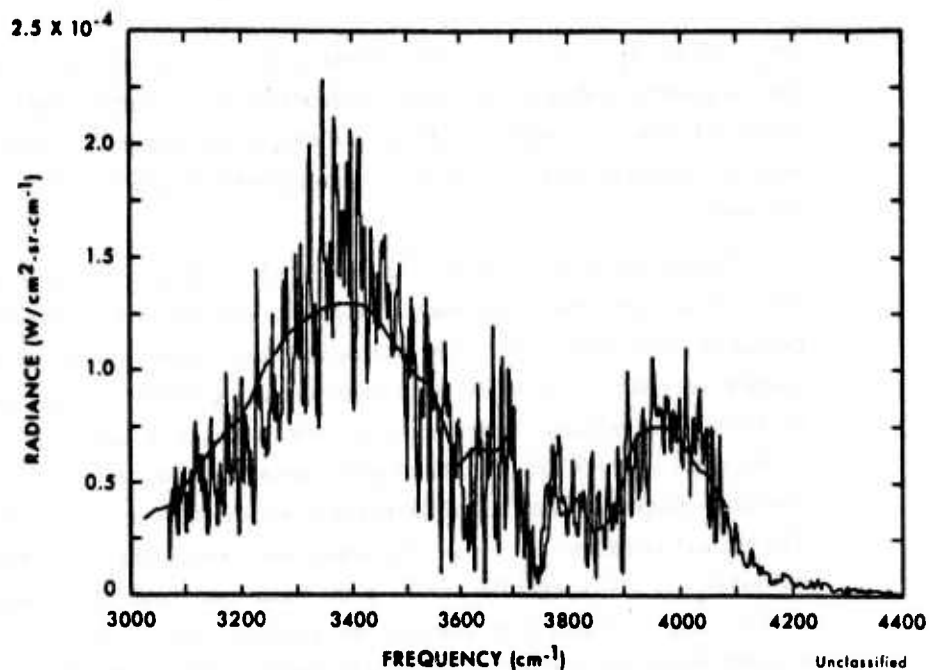


FIGURE 2. COMPARISON OF NONISOTHERMAL H_2O SPECTRA WITH BAND-MODEL CALCULATIONS. Run 10216811.

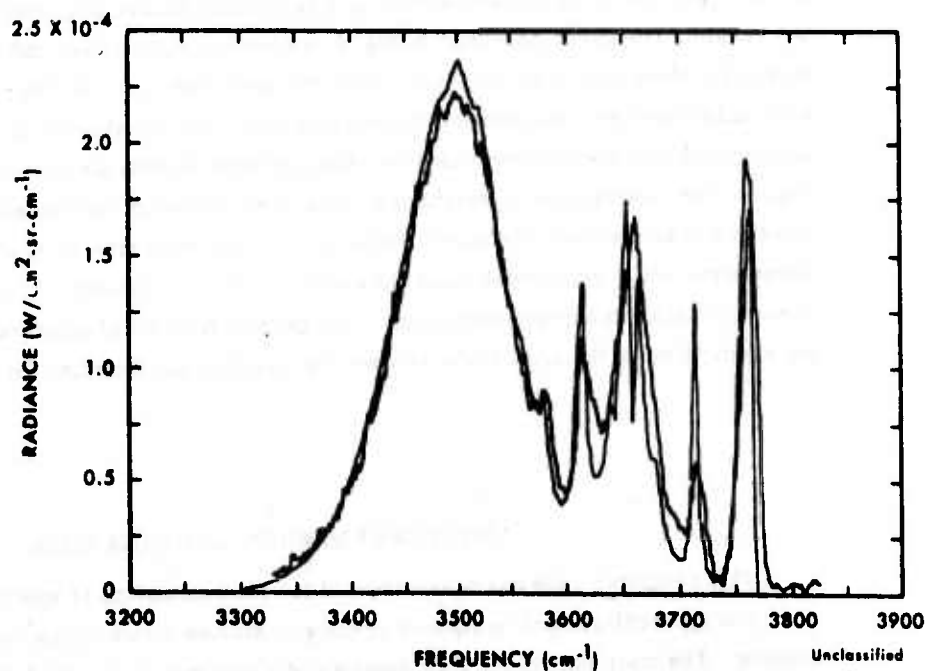


FIGURE 3. COMPARISON OF NONISOTHERMAL CO_2 SPECTRA WITH BAND-MODEL CALCULATIONS. Run 10216812.

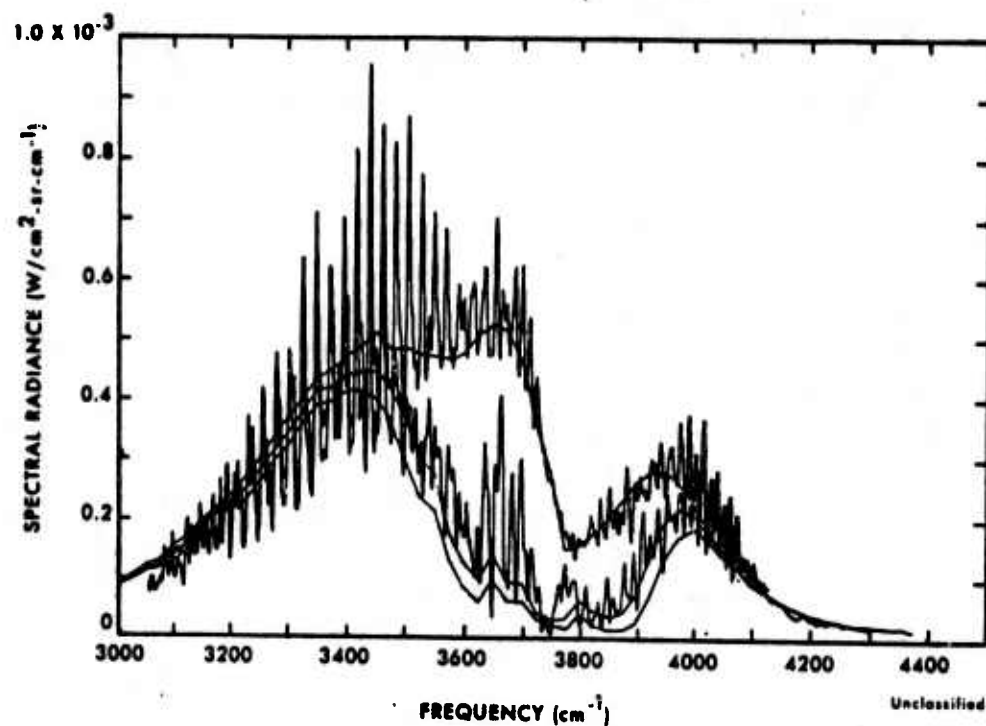


FIGURE 4. OBSERVED AND PREDICTED SPECTRA FOR 1-in. DIAMETER CH_4/O_2 FLAME

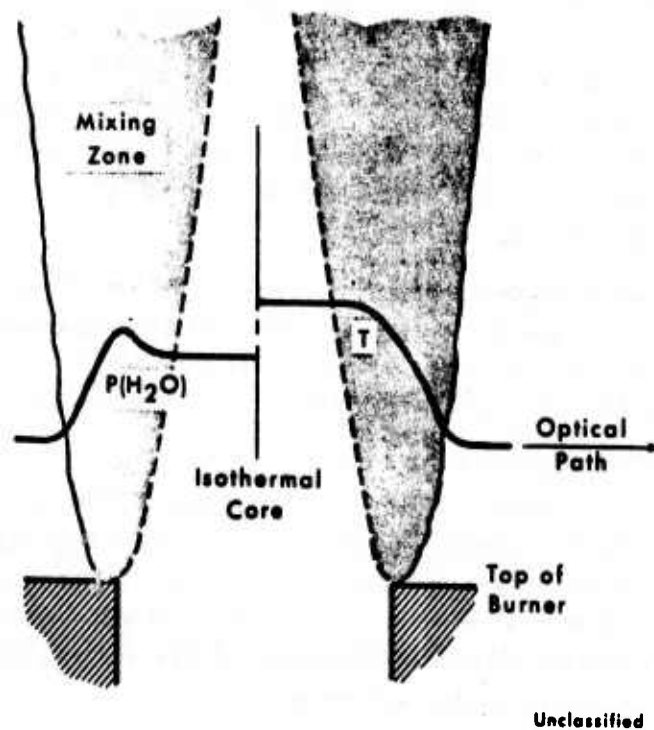
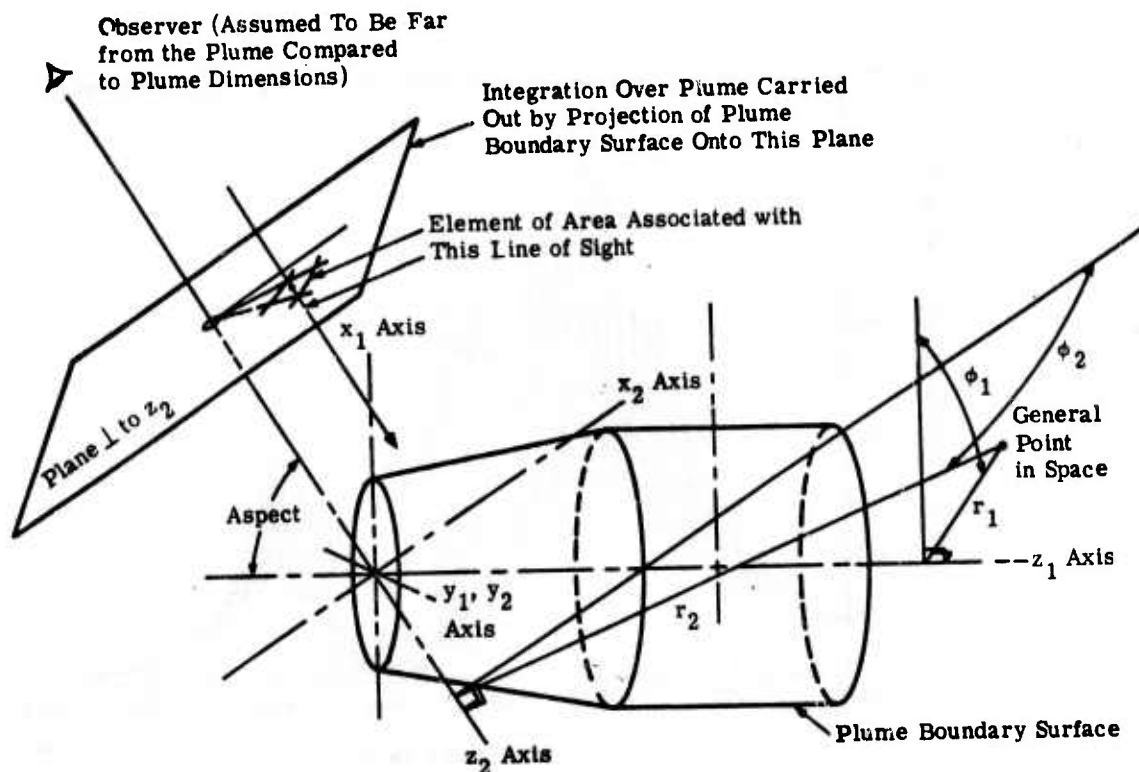


FIGURE 5. REPRESENTATION OF FLAME STRUCTURE



Unclassified

FIGURE 6. DIAGRAM OF THE TWO COORDINATE SYSTEMS USED IN INTEGRATING OVER THE PLUME

projected area in the line of sight, as indicated in Fig. 6. Provisions are made for varying the incremental sizes, both of the elements in the plume projection and the linear segments of the optical path through the gas, with the finer resolution being near the nozzle exit where the steepest gradients occur. These values then become input to the band-model subroutine, which has been designated XTAU.

(U) The band model, as specified in Eqs. (1) through (5), has been programmed by means of the trapezoidal approximation. The band-model parameters, extracted from the extensive tabulations of the GD/Convair group [20], are contained in two-dimensional files as functions of temperature and frequency. An initial, final, and increment of frequency are specified.

(U) The calculation then proceeds as follows. The PLUMES program starts at the first increment of area on the projection of the plume and specifies the conditions along the path through the gas. The XTAU subroutine then starts at the first frequency, calculates the net spectral radiance at the boundary, proceeds through successive frequencies until the last, and returns the values of spectral radiance vs. frequency to PLUMES for storage. PLUMES then submits the path conditions for the second incremental area, and the process is repeated until the entire area of the plume projection is covered.

The spectral radiances at the specified frequencies are then summed to yield spectral-radiant intensities. The program then proceeds to the next aspect angle and repeats the process. In addition to the primary output of spectral-radiant intensities as functions of frequency and aspect angle, spectral-radiance maps at specified frequencies and angles can be called for.

(U) A few details of the spectral-radiance calculations are as follows. The nonisothermal path through the plume is described by a number of isothermal-path elements of varying length. At a particular frequency, the radiance is computed by evaluating the radiative-transfer equation in the following form

$$I_{\nu} = - \int_1^{\bar{\tau}_L} I_{\nu}^* d\bar{\tau} \quad (6)$$

which is simply an alternative form of Eq. (1). Thus, it is necessary to determine both I_{ν}^* (the blackbody function) and $\bar{\tau}$ as a function of position along the path. The routine XTAU computes the transmittance from the beginning of the path to each of the boundaries between path elements. These values, in conjunction with the blackbody function, are used in evaluating Eq. (6) by the trapezoidal rule.

(U) Upon the choice of a frequency and a set of elemental path lengths, temperatures, and pressures, the routine XTAU first computes β_e by evaluating Eq. (5). Then, \bar{x} , given by Eq. (4), is computed from the beginning of the path to each of boundaries between path elements. The revised interpolation technique mentioned earlier is used to determine η . In this revised procedure, η is itself a function of \bar{x} (as well as of β/β_e). Thus, the exact determination of \bar{x} involves a trial and error procedure in which a value of η is estimated, a value of \bar{x} then calculated, and, η , in turn, recalculated until convergence of \bar{x} and η occurs. In the present program, only one iteration in this procedure is used, but the error introduced by this simplification is very small. Once the values of \bar{x} are known from the beginning of the path to the various elemental boundaries, the various transmittances are simply calculated from $\bar{\tau}(\nu) = 1 - \bar{\alpha}(\nu)$ using Eq. (2). From the temperatures of the various path elements, I_{ν}^* can be evaluated, and the integration of Eq. (6) performed.

(U) This program requires a large amount of storage, and its execution time is long, so that efforts have been directed toward breaking the plume into elements in as efficient a manner as possible. In some regions of the plume, this effort has led to a coarser incrementation of the plume than is desirable. From experience, it has been determined that in such areas the contributions to the spectral-radiant intensity are somewhat underestimated. Further work is needed to completely eliminate this bias.

(U) Further details of the operation of this program are given in Appendix IV.

Appendix IV DETAILS OF THE PLUME-RADIATION COMPUTER CODE

(U) This program computes the radiant intensity of the plume from a rocket or jet engine exhaust as observed through an arbitrary atmospheric path. The elements of the atmospheric path are computed first and then appended in front of the elements through each line of sight through the plume. The band-model calculation for every line of sight is thus a nonisothermal band-model calculation including the path and that line of sight.

(U) The primary coordinate system used for the plume calculation is a cylindrical coordinate system with the origin at the center of the nozzle exit. This coordinate system is shown in Fig. 6 along with a generalized plume boundary surface. The program is written such that the plume boundary must be a conical section immediately downstream of the nozzle exit, followed by an optional cylindrical section. This surface serves only to define the region over which integration takes place; the plume parameters can be arbitrarily set within the volume enclosed by this surface. This primary coordinate system is denoted by subscript 1 in the figure. The axis of this system, z_1 , is coincident with the plume axis, and the $\phi_1 = 0$ direction is the projection in the $z_1 = 0$ plane of the line of sight directed from the center of the nozzle exit to the observer.

(U) The second coordinate system used in the calculation is shown in Fig. 6 with subscript 2. The z_2 axis is directed along the line of sight from the observer to the plume. Its origin coincides with that of the primary coordinate system. The $\phi_2 = 0$ direction is the projection in the $z_2 = 0$ plane of the plume axis directed downstream from the nozzle exit. The integration of the plume radiance over the whole plume is carried out by projecting the plume boundary surface into a plane perpendicular to the z_2 axis.

(U) The calculation proceeds as follows:

- (1) The band-model parameters are read in.
- (2) The specifications of the plume boundary (cone angle, nozzle exit, radius, length of conical section and length of cylindrical section) are read in.

- (3) The observing aspect (in degrees from nose-on direction) and the parameters describing the atmospheric path between the plume and the observer (path length, altitudes of both the observer and the plume) are read in. Also, the required atmospheric properties are read in at this point.
- (4) The frequencies for which calculations are desired are either read in or computed from an initial value and increment.
- (5) The properties of the plume flow field (temperatures, and the partial pressures of the three gases, H_2O , CO_2 and N_2) are read in (in spherical coordinates corresponding to the primary coordinate system). An option is also available in which, from ambient and core values read in, the plume properties are computed according to an internally specified functional relationship within the plume boundary. If this option is used, only core and ambient values for temperature and the three partial pressures are required.
- (6) Various control parameters are read in which specify various functions, such as the fineness of the integration over the plume (NMAX), the number of elements into which the atmospheric path is divided (NA), the type of plume data read in (SETUP3), and others controlling printing and plotting.
- (7) The temperature range over which the plume data extend is read in and then divided into a number of segments (equal to NMAX) according to the 2nd power of the temperature. The higher the temperature, the smaller the temperature segment. The boundaries of the segments are used to divide the individual lines of sight into elements.
- (8) Subroutine ATMO is used to divide the atmospheric path into NA elements. At this point, the length, temperature and partial pressures of H_2O , CO_2 and N_2 for each atmospheric path element are stored.
- (9) Integration over the plume proceeds as follows. A polar element in the plane perpendicular to the z_2 axis is constructed. The initial size of this element is determined by one of the central parameters, NMAX. A line of sight through the center of this element is constructed and its intersections with the plume boundary surface determined in the z_2 , r_2 , and ϕ_2 coordinate system. If there is only one or zero points of intersection, the current line of sight is at or outside the plume boundary. The program then determines where this line of sight lies with respect to the plume boundary and either chooses a new element or terminates the computation, whichever is required. If two intersections are formed, the program proceeds to divide the path between these two intersections into elements. The temperature profile along this line of sight is examined and an element defined whenever the temperature profile crosses one of the boundaries of the temperature segments defined earlier. The length of each of these elements is stored along with its corresponding mean temperature and partial pressures.

- (10) The elements of the atmospheric path determined earlier are appended in front of the element for the line of sight currently being considered. The band-model transmittance routine TAU5 is now used to compute elemental transmittances for the combination of the atmospheric path and the current line of sight. Radiance values at the observer are now calculated and, when multiplied by the area of the current element projected into a plane perpendicular to the z_2 axis, are stored in a running sum which will be the plume radiant intensity when the calculation is complete. This paragraph is repeated for all frequencies desired.
- (11) An average temperature for the current line of sight is computed. This is used to modify the radial size of the next element in the integration. The next element is now constructed in the same ϕ_2 direction but incremented radially. The radial size of this element is based on the average temperature of the previous element compared to the average temperature of the first element in the current ϕ_2 direction. The first two elements in any ϕ_2 direction have the same radial dimension, but the smaller the average temperature of succeeding elements, the larger the radial size of the increment and vice versa. The value of ϕ_2 remains constant and r_2 is incremented until a line of sight passes outside the plume. At this point ϕ_2 is incremented and elements are again constructed starting at $r_2 = 0$. When a new element has been defined, the calculation returns to the point of paragraph 9 and repeats the line-of-sight and radiance calculations. When ϕ_2 has been incremented over its full range (90° in the case of 90° aspect, 180° in the case of all others) the calculation is complete.
- (U) The running sum of radiance times elemental area for each frequency is multiplied by 2 to account for the fact that integration took place over only one half of the plume, and the results are printed as the radiant intensity.

REFERENCES

Unclassified

1. Near Infrared Phenomenology Workshop (U), Aerospace Corporation, El Segundo, Calif., April 1968 (SECRET).
2. Rocket Plume Phenomena Specialists' Meeting (U), Aerospace Corporation, San Bernardino, Calif., July 1968 (SECRET).
3. Arnold Engineering Development Center, Rocket Plume Technology Conference (U), Tullahoma, Tennessee, October 1968 (SECRET).
4. Launch Phase Summary (U), Vols. I, II, Reports No. 4613-119-X(I) and 4613-119-X(II), Willow Run Laboratories of the Institute of Science and Technology, The University of Michigan, Ann Arbor, 1966 (SECRET).
5. H. G. Wolfhard and S. Tuttle, Assessment of Presently Available Knowledge of the High-Altitude Rocket Exhaust Radiation for Ballistic Missile Defense (U), IDA Report P-350, September 1967 (SECRET).
6. R. Kuiper, Summary of Rocket Exhaust Plume Radiation (U), Aerospace Corporation, Report TOR-0200(4413)-4, February 1969 (SECRET).
7. R. Zirkind, Text on Rocket Plume Phenomenology (in preparation).
8. H. W. Liepmann and A. Roshko, Elements of Gasdynamics, Sec. 4.14, John Wiley and Sons, Inc., New York, 1957.
9. H. G. Wolfhard and R. C. Mollander, Launch-Phase Detection: Considerations for an Improved System (U), IDA Study S-344, May 1969 (SECRET).
10. D. Anding, Band-Model Methods for Computing Atmospheric Slant-Path Absorption, Report No. 7142-21-T, NAVSO P-2499-1, Willow Run Laboratories of the Institute of Science and Technology, The University of Michigan, Ann Arbor, 1967.
11. F. S. Simmons, C. B. Arnold, D. H. Smith, and N. F. Kent, Studies of Infrared Radiative Transfer in Hot Gases, Vol. I: Spectral Absorptance Measurements in the $2.7\text{-}\mu$ H_2O Bands, Report No. 4613-91-T, August 1965, Vol. II: Formulation of Band Models for Nonisothermal Paths, Report No. 4613-92-T, June 1965, Vol. III: Nonisothermal Radiance Measurements in the $2.7\text{-}\mu$ H_2O Bands, Report No. 4613-93-T, December 1965, Willow Run Laboratories of the Institute of Science and Technology, The University of Michigan, Ann Arbor.
12. F. S. Simmons, "Band Models for Nonisothermal Radiating Gases," Appl. Opt., Vol. 5, 1966, p. 1801, Appl. Opt., Vol. 6, 1967, p. 1423.
13. F. S. Simmons and H. Y. Yamada, Relations for Molecular Radiative Transfer Based on a Random-Line Band Model, Report No. 4613-150-T, Willow Run Laboratories of the Institute of Science and Technology, The University of Michigan, Ann Arbor, February 1967.
14. F. S. Simmons, "Radiances and Equivalent Widths of Lorentz Lines for Nonisothermal Paths," J. Quant. Spectr. and Radiative Transfer, Vol. 7, 1967, p. 111.
15. H. Y. Yamada, "Total Radiances and Equivalent Widths of Doppler Lines for Nonisothermal Paths," J. Quant. Spectr. and Radiative Transfer, Vol. 7, 1967, p. 997.
16. H. Y. Yamada, "Total Radiances and Equivalent Widths of Isolated Lines with Combined Doppler Collision Broadened Profiles," J. Quant. Spectr. and Radiative Transfer, Vol. 8, 1968, p. 1463.
17. F. S. Simmons, Application of Band Models to Inhomogeneous Gases, Specialist Conference on Molecular Radiation, NASA TM X-53711, October 1967.

18. F. S. Simmons, H. Y. Yamada, and C. B. Arnold, **Measurement of Temperature Profiles in Hot Gases by Emission-Absorption Spectroscopy**, Report No. 8962-18-F, NASA CR-72491, Willow Run Laboratories of the Institute of Science and Technology, The University of Michigan, Ann Arbor, April 1969.
19. D. K. Edwards et al., **Radiation Heat Transfer in Nonisothermal Nongray Gases**, ASME Paper No. 66-WA/HT-25, 1966.
20. C. B. Ludwig et al., **Study on Exhaust Plume Radiation Predictions**, NASA CR-61233, General Dynamics Corporation, 1968.
21. B. Krakow et al., **Use of the Curtis-Godson Approximation in Calculations of Radiant Heating by Inhomogeneous Gases**, NASA TM X-53411, Warner-Swasey Company, 1966.
22. J. A. L. Thomson, **Radiation Model for Nonscattering Rocket Exhaust Gases**, Specialist Conference on Molecular Radiation, NASA TM X-53711, 1967.
23. *A. G. DeBell, F. S. Simmons, and B. P. Levin, **Spectral Radiances and Emissivities of Rocket Exhaust Plumes (U)**, Rocketdyne Report No. R-3216, 1961 (SECRET).
24. K. N. C. Bray, **"Atomic Recombination in a Hypersonic Wind Tunnel Nozzle,"** J. Fluid Mech., Vol. 6, 1959, p. 1.
25. *F. S. Harshbarger, **Compilation of Atlas, Titan I, Titan II, and Minuteman Rocket Engine Parameters (U)**, Report No. AE62-0967, General Dynamics/Astronautics, 1962 (CONFIDENTIAL).
26. F. C. Boynton, Wayne State University, Private Communication, 1969.
27. E. M. Landsbaum, Aerospace Corporation, Private Communication, 1970.
28. *E. R. Bartle et al., **Some Spectral Radiance Measurements of a Statically Fired Titan II Second Stage Rocket Engine (U)**, Report No. AE 62-0968, General Dynamics/Astronautics, 1962 (CONFIDENTIAL).
29. *R. P. Parrish, **Spectral Radiation Measurements at Simulated Altitude of the Exhaust Plume from a Full-Scale XLR-91-AJ-5 Titan II Rocket Engine (U)**, AEDC-TDR-63-152, 1963 (CONFIDENTIAL).
30. S. A. Golden, Aerojet-General Corporation, Private Communication, 1969.
31. *F. Harshbarger, **An Evaluation of Spectral Radiance Measurements at the Nozzle Exit of a Titan II Second Stage (U)**, Report No. DBE 64-007, General Dynamics/Astronautics, 1964 (SECRET).
32. *W. J. Wagner, **Close-Proximity Spectral Radiance Measurements of Missile-Sized Rocket Engine Exhaust Plumes (U)**, Rocketdyne Report R-5843, 1964 (SECRET).
33. A. G. DeBell, Rocketdyne, Private Communication, 1967.
34. A. Sutor, Rocketdyne, Private Communication, 29 April 1970.
35. J. E. Reardon and R. M. Huffaker, **Radiative Heat-Transfer Calculations for Saturn Exhaust Plumes**, Specialist Conference on Molecular Radiation, NASA TM X-53711, 1967.
36. R. Phinney, **"Criterion for Vibrational Freezing in a Nozzle Expansion,"** J. Am. Inst. Aeronautics and Astronautics, Vol. 1, 1963, p. 496.
37. K. F. Herzfeld, **Relaxation Phenomena in Gases**, Thermodynamics and Physics of Matter, Princeton University Press, 1955.
38. F. Boynton, Wayne State University, Private Communication.
39. F. Boynton, **The Multitude Supersonic Flow Computer Code**, Report No. DBE 67-003, General Dynamics/Convair, 1967.

40. P. W. Huber and A. Kantrowitz, "Heat-Capacity Lag Measurements in Various Gases," *J. Chem. Phys.*, Vol. 15, 1947, p. 275.
41. E. H. Kennard, *Kinetic Theory of Gases*, McGraw-Hill, 1938.
42. W. Griffith et al., "Structure of Shock Waves in Polyatomic Gases," *Phys. Review*, Vol. 102, 1956, p. 1209.
43. N. H. Johannesen et al., "Experimental and Theoretical Analysis of Vibrational Relaxation Regions in Carbon Dioxide," *J. Fluid Mech.*, Vol. 13, 1962, p. 213.
44. D. Weaver et al., "Vibrational Relaxation Times in Carbon Dioxide," *J. Chem. Phys.*, Vol. 47, 1967, p. 3096.
45. D. D. Eden, R. B. Lindsay, and H. Zink, "Acoustic Attenuation and Relaxation Phenomena in Steam at High Temperature and Pressure," *Transactions of the ASME, J. Eng. Power*, January 1961.
46. Y. Fujii, R. B. Lindsay, and K. Urushihara, "Ultrasonic Absorption and Relaxation Times in Nitrogen, Oxygen, and Water Vapor," *J. Acoust. Soc. Am.*, Vol. 35, 1963, p. 961.
47. H. Roesler and K.-F. Sahm, "Vibrational and Rotational Relaxation of Water Vapor," *J. Acoust. Soc. Am.*, Vol. 37, 1965, p. 383.
48. K. Yamada and Y. Fujii, "Ultrasonic Attenuation and Relaxation Times in Water Vapor and Heavy-Water Vapor," *J. Acoust. Soc. Am.*, Vol. 39, 1966, p. 250.
49. R. Mariott, "Molecular Collision Cross-sections and the Effect of Hydrogen on Vibrational Relaxation in Water Vapor," *Proc. Phys. Soc.*, Vol. 88, 1966, p. 617.
50. S. S. Penner, *Quantitative Molecular Spectroscopy and Gas Emissivities*, Addison-Wesley, 1959.
51. W. S. Benedict and E. K. Plyler, *High Resolution Spectra of Hydrocarbon Flames in the Infrared, Energy Transfer in Hot Gases*, NBS Circular 523, 1954.
52. *D. J. Carlson and A. J. Laderman, *Analytical Determination of the Spatial Distribution of Radiation Emanating from Ballistic Missiles in Flight (U)*, Report No. AFAL-TR-68-333, Philco-Ford Company, 1968 (SECRET).
53. C. J. Wang, J. B. Peterson, and R. Anderson, *Gas Flow Tables*, Report No. GM-TR-154, Ramo-Wooldridge Corp., 1957.
54. F. Simmons and C. Arnold, *Measurement of Temperature Profiles in Flames by Infrared Spectroscopy*, NASA Contractor Report, In Preparation.
55. F. S. Simmons, H. Y. Yamada, and C. B. Arnold, *Measurement of Temperature Profiles in Hot Gases by Emission-Absorption Spectroscopy*, Report No. 8962-18-F, NASA CR-72491, Willow Run Laboratories of the Institute of Science and Technology, The University of Michigan, Ann Arbor, April 1969.
56. A. G. Gaydon and H. G. Wolfhard, *Flames, Their Structure, Radiation, and Temperature*, Chapman and Hall, London, 1960.
57. S. S. Penner, *Quantitative Molecular Spectroscopy and Gas Emissivities*, Addison-Wesley, Reading, Mass., 1959.
58. H. D. Baker, E. A. Ryder, and N. H. Baker, *Temperature Measurement in Engineering*, John Wiley and Sons, Inc., New York, 1961.
59. *Temperature, Its Measurement and Control in Science and Industry*, Reinhold Publishing Corp., New York, Vol. I, 1941; Vol. II, 1954, Vol. III, 1962.
60. P. J. Dickerman (Ed.), *Optical Spectrometric Measurements of High Temperature*, University of Chicago Press, 1961.

61. R. W. Ladenburg et al. (Eds.), *Physical Measurements in Gas Dynamics and Combustion*, Princeton University Press, 1954.
62. F. Simmons, *Spectroscopic Pyrometry of Gases, Flames, and Plasmas*, ISA Trans., Vol. 2, 1963, p. 168.
63. G. Hornbeck and L. Olsen, *Emission and Absorption Studies of Jet Engine Hydrocarbon Combustion Products*, WADC Technical Report No. 57-516, AD 203 791, 1958.
64. W. Herget, *Temperature and Concentration Measurements in Model Exhaust Plumes Using Inversion Techniques*, Specialist Conference on Molecular Radiation, NASA TM X-53711, 1967.
65. R. Zirkind (Ed.), *Proceedings of the Symposium on Electromagnetic Sensing of the Earth from Satellites*, Brooklyn Polytechnic Press, 1967.
66. R. J. Prozan, *Development of a Method of Characteristics Solution for Supersonic Flow of an Ideal, Frozen, or Equilibrium Reacting Gas Mixture*, Lockheed Report No. LMSC/HREC A 782535, 1966.
67. J. A. Nicholls, *Stability of Gaseous Detonation Waves with Emphasis on the Ignition Delay Zone*, PhD Thesis, The University of Michigan, Ann Arbor, 1960.
68. T. C. Adamson, Jr., *The Structure of the Rocket Exhaust Plume without Reaction at Various Altitudes: Supersonic Flow, Chemical Processes, and Radiative Transfer*, Pergamon Press, 1964.
69. R. Kuiper, Aerospace Corporation, Private Communication, 1970.
70. C. D. Hodgman (Ed.), *Handbook of Chemistry and Physics*, Chemical Rubber Publishing Co., 40th Edition, 1958-59.

A BAND MODEL FORMULATION
FOR VERY NONUNIFORM PATHS * +

G. H. LINDQUIST

F. S. SIMMONS**

WILLOW RUN LABORATORIES
INSTITUTE OF SCIENCE AND TECHNOLOGY
THE UNIVERSITY OF MICHIGAN
ANN ARBOR, MICHIGAN

ABSTRACT

Anomalous behavior has been observed when molecular band-models incorporating the Curtis-Godson or similar approximations are applied to problems characterized by a large variation in temperature along the optical path. The nature of this misbehavior has been examined, and a procedure has been developed for its suppression in the band model previously formulated at this laboratory. This procedure is based on the use of a less restrictive assumption in the derivation of the band model from the basic equation of transfer.

* This work was supported in part by NASA under Contract NAS3-13037.

** Present Address: The Aerospace Corp., El Segundo, California

+ Published In: J. Quant. Spectrosc. Radiat. Transfer, Vol. 12, pp. 807-820.
Pergamon Press 1972. Printed in Great Britain

LIST OF SYMBOLS

A, B, C, D, E	Constants used in analytic form for η
d	average line spacing
F	function providing interpolation between nearly weak and nearly strong approximations
$f(x)$	Ladenburg-Reiche function
$g(\nu'-\nu)$	spectrometer slit function
k	absorption coefficient
\bar{k}	averaged absorption coefficient for band model
L_ν	spectral radiance $W/(\text{cm}^2 - \text{sr} - \text{cm}^{-1})$
L_ν^*	black body spectral radiance $W/(\text{cm}^2 - \text{sr} - \text{cm}^{-1})$
$L_{\nu,i}^*$	black body spectral radiance of i^{th} path element
\bar{L}_ν	spectral radiance computed using a band model
N	number of path elements in sum
S	line strength
S_e	equivalent line strength
W	equivalent width, cm^{-1}
X	optical depth coordinate, gm cm^{-2}
X_L	total optical depth of path of interest, gm cm^{-2}
X_i	optical depth coordinate of i^{th} path element, gm cm^{-2}
x	dimensionless optical depth for Curtis-Godson approximation
\bar{x}	dimensionless optical depth for nearly weak - nearly strong approximation
β	line overlap parameter, $\frac{2\pi\gamma}{d}$
$\beta_e(x)$	line overlap parameter averaged over the path extending from the observer to optical depth X

β_{eL}	line overlap parameter averaged over the whole optical depth of interest
γ	line width, cm ⁻¹
$\gamma_e(x)$	line width averaged over the path extending from the observer to optical depth X
γ_{eL}	line width averaged over the whole optical depth of interest
η	interpolation parameter between nearly weak - nearly strong approximation
ν	wavenumber, cm ⁻¹
ν_0	wavenumber of line center, cm ⁻¹
$\Delta\nu$	$\nu - \nu_0$, cm ⁻¹
τ	transmittance
$\bar{\tau}$	averaged transmittance computed using a band model
$\bar{\tau}_n$	averaged transmittance of equivalent non-overlapping lines

Introduction

A recent note ⁽¹⁾ was concerned with the application of a molecular band model for inhomogeneous radiating gases ^(2,3) to cases in which a large variation in temperature is encountered along the optical path. The specific problem considered was the calculation of thermal radiation from a relatively small combustion-product source viewed through a long atmospheric path. The particular band-model used in that study, one previously developed at this laboratory ^(2,3), was originally formulated in terms of two options, a "nearly-weak" and a "nearly-strong" line approximation, with a simple procedure for interpolation between the two for intermediate optical depths. Application of this band model in its original form yielded anomalous results; indeed, at some frequencies, the calculated values of apparent radiance with atmospheric absorption would exceed those for the hot source alone. The reasons for this misbehavior of the band model were determined, and means for its suppression were developed. In the aforementioned note, some preliminary results of the use of the modified band model were presented, and the requirements for a more complex interpolation procedure was stated. The purpose of this communication is to present the details of the revised formulation of the model, which in essence represents a closer approximation to the exact equation of transfer than the original model, or comparable ones based on the "Curtis-Godson" approximation.

The rationale in the development to follow can be illustrated by considering the growth of a single, collision broadened spectral line along a non-isothermal path. Once the formulation for such a single line is developed, it is carried over essentially unchanged to the case of a random band of overlapping lines.

The solution of the equation of transfer describing the radiance of a single isolated spectral line from a general non-isothermal source under the conditions of local thermodynamic equilibrium, negligible scattering, and no significant source of radiation behind the gas, is given by:

$$L_{\nu}(\nu) = \int_0^{X_L} L_{\nu}^*(\nu, X) k(\nu - \nu_0, X) \exp\left(-\int_0^X k(\nu - \nu_0, X') dX'\right) dX \quad (1)$$

X is the optical depth (mass per unit cross sectional area) coordinate along the line of sight through the gas and $L_{\nu}^*(\nu, X)$ is the blackbody spectral radiance. The latter is a function of frequency, or equivalently wave-number, ν , and temperature, $T = T(X)$, in turn a function of the position along the line of sight through the gas. The spectral absorption coefficient of the single line being considered, $k(\nu - \nu_0, X)$ is a function of the spectral distance from the line center $\nu - \nu_0$, and the optical depth coordinate along the path X . $L_{\nu}(\nu)$ is the spectral radiance of the gaseous source at wave-number ν due to the single spectral line. X_L is the total optical depth of the gaseous source. The total radiance due to the line is obtained by integrating over all frequencies, thus

$$L = \int_{-\infty}^{\infty} \int_0^{X_L} L_{\nu}^*(\nu, X) k(\nu - \nu_0, X) \exp\left(-\int_0^X k(\nu - \nu_0, X') dX'\right) dX d(\nu - \nu_0) \quad (2)$$

By introducing the transmittance defined as,

$$\tau(v-v_0, X) \equiv \exp \left[- \int_0^X k(v-v_0, X') dX' \right] \quad (3)$$

interchanging the order of integration and assuming that $L^*_{\nu}(v, X)$ does not vary significantly over the frequency region involved, the equation for L can be written:

$$L = - \int_0^{X_L} L^*_{\nu}(v_0, X) \frac{d}{dX} \left[\int_{-\infty}^{\infty} \tau(v-v_0, X) d(v-v_0) \right] dX \quad (2a)$$

The equivalent width, W , is defined as

$$W(X) = 1 - \int_{-\infty}^{\infty} \tau(v-v_0, X) d(v-v_0) \quad (4)$$

so that the expression for L becomes

$$L = \int_0^{X_L} L^*_{\nu}(v_0, X) \frac{dW}{dX} dX \quad (2b)$$

Since W is only a function of X , the above equation can be written

$$L = \int_0^{W(X_L)} L^*_{\nu}(v_0, X) dW(X) \quad (5)$$

By dividing up the path into N approximately isothermal elements, the expression for L can be written:

$$L \approx \sum_{i=1}^N L^*_{\nu,i} [W(X_i) - W(X_{i-1})] \quad (6)$$

where X_i is the optical path from the observer to the far boundary of the i^{th} isothermal element. $W(X_i)$ is the equivalent width corresponding to that path.

In calculating the values of $W(X_1)$ it is seen that, in general, for non-isothermal paths, the integrals over X and $\nu - \nu_0$ are not separable. To allow such separation, an approximation is usually made concerning the variation of the line shape along the path. The Curtis-Godson (4,5,6) approximation is most commonly used for this purpose. Another, that is used by these authors (1,3), is the "nearly-weak, nearly-strong" line approximation, hereafter referred to as the NW-NS approximation. Both approximations have as their purpose the separation of the integrals over X and $\nu - \nu_0$ and the replacement of the non-isothermal path with an equivalent isothermal path. Both yield satisfactory values of $W(X)$ for many cases, especially where the temperature and concentration variations are not too large.

However, in the evaluation of eq.(6), the accuracy of the integration depends not so much on the accuracy of the values of $W(X)$, but on the accuracy of differences between values of $W(X)$, i.e., on the derivative of W with respect to X . Differentiations of approximations are risky and indeed this is the point at which the anomaly mentioned earlier appears. An expression which is a reasonable approximation for W will not always yield a reasonable approximation to dW/dX . To illustrate this, let us compute the derivative of W with respect to X using each of the two approximations mentioned earlier; the Curtis-Godson approximation, and the NW-NS approximation.

Before this can be accomplished it will be necessary to obtain an expression for the equivalent width of a collision broadened line in an isothermal path. The absorption coefficient in this case is:

$$k(\nu - \nu_0, X') = \frac{S(X')}{\pi} \frac{\gamma(X')}{\gamma^2(X') + (\nu - \nu_0)^2} \quad (7)$$

where S is the line strength and γ its half width. Upon substitution into eq. (3) specialized to an isothermal path, and with the use of eq. (4), after some reduction, the following expression for W is obtained (7)

$$W(X) = 2\pi\gamma f(x) \quad (7a)$$

where f is the Ladenburg-Reiche function

$$f(x) \equiv x e^{-x} [J_0(1 x) - i J_1(1 x)] \quad (7b)$$

and $x = \frac{SX}{2\pi\gamma}$ is the dimensionless optical depth. J_0 and J_1 are Bessel functions of the first kind, of order 0 and 1 respectively. Tables of $f(x)$ are found in the literature (8,9).

Curtis-Godson Approximation

The Curtis-Godson approximation has been defined in several ways. The form described by GOODY⁽⁴⁾ is used here. It is a method whereby the equivalent width of an absorption line as viewed through a non-isothermal path can be approximated by the equivalent width through some corresponding isothermal path. The approximation is made by defining an equivalent average half width and line strength for the path extending from the observer to some point X in the path.

$$S_e(X) = \left[\int_0^X S(X') dX' \right] / X$$

$$\text{and} \quad \gamma_e(X) = \frac{\int_0^X \gamma(X') S(X') dX'}{\int_0^X S(X') dX'} \quad (8)$$

This is tantamount to saying that the denominator in the non-isothermal absorption coefficient, eq. (7), can be taken to be independent of X' and

to have the form, $\gamma_e^2(X) + (v-v_0)^2$, so that

$$\int_0^X k(v-v_0, X') dX' = \frac{\gamma_e(X) S_e(X) X}{\pi[\gamma_e^2(X) + (v-v_0)^2]} \quad (9)$$

From this, it follows that

$$W(X) = 2\pi\gamma_e(X) f(x) \quad (10)$$

where x , the dimensionless optical depth, is now defined

$$x(X) \equiv \frac{\int_0^X S(x') dX'}{2\pi\gamma_e(X)} \quad (11)$$

Eq. (10) can now be used to investigate the behavior of dW/dX in a non-isothermal gas. Differentiating (10) and making use of (8) yields after some rearrangement:

$$\frac{dW}{dX} = S(X) \left\{ \frac{df(x)}{dx} \left(2 - \frac{\gamma(X)}{\gamma_e(X)} \right) + \frac{f(x)}{x} \left(\frac{\gamma(X)}{\gamma_e(X)} - 1 \right) \right\} \quad (12)$$

By mapping the variation with optical depth X into a variation with dimensionless optical depth, x , this can be rewritten

$$\frac{1}{S(X)} \frac{dW}{dX} = \left\{ \frac{df(x)}{dx} \left(2 - \frac{\gamma}{\gamma_e}(x) \right) + \frac{f(x)}{x} \left(\frac{\gamma}{\gamma_e}(x) - 1 \right) \right\} \quad (13)$$

We can now place physical limitations on $[1/S(X)](dW/dX)$. First of all, at $X = 0$, the quantity $[1/S(X)](dW/dX)$ must be unity corresponding to the region of linear growth for small optical depths. Secondly, it must be less than one at larger optical depths as the square root region is approached. Thirdly, it must remain non-negative for all x so that the equivalent width continues

to grow with increasing x . The variation of $[1/S(X)](dW/dX)$ as given by eq. (7) is shown in Figure 1 as a function of x with γ/γ_e as a parameter. Note that γ/γ_e is the ratio of the half width at x to its average value taken over all the path before it. For $\gamma/\gamma_e < 2$ the function is well behaved, but it exhibits anomalous behavior for $\gamma/\gamma_e > 2$. In the latter case the function becomes larger than 1 for intermediate values of x , thus indicating a rate of increase of equivalent width greater than that in the linear region. This behavior is a manifestation of the errors involved in the Curtis-Godson approximation.

These errors are mentioned by GOODY⁽⁴⁾; and are treated in detail by DRAYSON⁽⁵⁾. However their analyses dealt only with the absorption (or equivalent width). More related to this study is the work of WALSHAW and RODGERS⁽¹⁰⁾ who analyzed the effect of the Curtis-Godson approximation on the derivative of transmittance with optical depth, for several band models.

Let us now examine the behavior of the NW-NS approximation in a similar fashion.

Nearly-Weak Nearly-Strong Line Approximation

This approximation is similar to the Curtis-Godson approximation in that an average for the line half width is defined. However this average is fixed for the path in question and is defined as the average over the total path X_L . Thus

$$\gamma_e = \frac{\int_0^{X_L} \gamma_e(X') S(X') dX'}{\int_0^{X_L} S(X') dX'} \quad (14)$$

Then the dimensionless optical depth is defined as:

$$\bar{x}(X) = \frac{1}{2\pi\gamma_{eL}} \int_0^X S(X') F(X') dX' \quad (15)$$

$F(X')$ is a function which must be unity in the nearly-weak approximation and γ/γ_{eL} in the nearly-strong approximation⁽¹¹⁾. A form must be chosen for the variation of $F(X')$ so that it produces a reasonable transition between the two approximations for intermediate optical depths. The equivalent width is given again as

$$W(X) = 2\pi\gamma_{eL} f(\bar{x}) \quad (16)$$

Taking the derivative of eq. (16) we obtain, for the nearly weak approximation

$$\frac{dW}{dX} = S(X) \frac{df(\bar{x})}{d\bar{x}} \quad (17)$$

and for the nearly strong approximation

$$\frac{dW}{dX} = S(X) \frac{\gamma(X)}{\gamma_{eL}} \frac{df(\bar{x})}{d\bar{x}} \quad (18)$$

$[1/S(X)](dW/dX)$ according to eqs. (17) and (18) is shown in Figure 2. It can be seen that the nearly-weak approximation never becomes physically unrealistic, i.e., $[1/S(X)](dW/dX) \leq 1$; however, for the nearly-strong approximation, the quantity $[1/S(X)](dW/dX)$ becomes greater than one at smaller values of \bar{x} for $\frac{\gamma(X)}{\gamma_{eL}} > 1$. This difficulty is accounted for in practice by the proper choice of $F(X')$. However, we are left with no information upon which to base $F(X')$ at this stage.

It appears that neither the NW-NS approximation (unless $F(X)$ is correctly and accurately specified) nor the Curtis-Godson approximation give sufficiently accurate values for dW/dX over the full range of optical depths and for all possible values of γ/γ_e . The treatment of the previous paragraphs serves to point out those regions where the approximations are not only inaccurate but yield physically meaningless results as well. On the other hand, it should be noted that the anomalies and errors in the curves for $(1/S)(dW/dX)$ as given by the Curtis-Godson approximation are not serious as long as γ/γ_e never exceeds a value of about 2. This condition has been shown to be satisfied (4,5,10) for most atmospheric paths and only becomes seriously violated for highly non-homogeneous paths. However, as an example of the latter taken from our studies (1,3), hot products of combustion viewed through long atmospheric paths yield values of γ/γ_e as large as 20.

To obtain a more acceptable expression for dW/dX , consider the growth of an isolated spectral line. The equivalent width is given exactly by

$$W(X) = 1 - \int_{-\infty}^{\infty} \exp \left[- \int_0^X k(\Delta\nu, X') dX' \right] d(\Delta\nu) \quad (19)$$

and its derivative, in terms of a Lorentz profile, by

$$\frac{dW}{dX} = \frac{1}{\pi} \int_{-\infty}^{\infty} \frac{S(X)\gamma(X)}{\gamma^2(X) + (\Delta\nu)^2} \exp \left[- \frac{1}{\pi} \int_0^X \frac{S(X')\gamma(X')}{\gamma^2(X') + (\Delta\nu)^2} dX' \right] d(\Delta\nu) \quad (20)$$

where $\Delta\nu = \nu - \nu_0$. In the original treatment of the Curtis-Godson and the NW-NS approximations, the separation of frequency-dependent and path-dependent variables was accomplished by substitution of an effective value, γ_e , in both parts of the integrand. At this point we will use such an approximation only in the exponential term. This is the key step in this derivation and is the only point of difference from previous treatments.

Thus, in terms of $\gamma_e = \gamma_e(X)$ defined by equation 8 and x by eq. (11), eq. (20) becomes

$$\frac{dW}{dX} = \frac{1}{\pi} \int_{-\infty}^{\infty} \frac{S(x)\gamma(X)}{\gamma^2(X) + (\Delta\nu)^2} \exp \left[-2x \gamma_e(X) \frac{\gamma_e(X)}{\gamma_e^2(X) + (\Delta\nu)^2} \right] d(\Delta\nu) \quad (21)$$

Note that this is equivalent to making a Curtis-Godson substitution in the expression for the derivative of W rather than in the expression for W itself. Thus the process of taking a derivative after making an approximation has been replaced by one in which the derivative is taken first and then the approximation made. Hence this treatment should be inherently better for calculating radiances than the techniques described earlier. Another way of comparing this approximation to the previous two is by considering dW/dX as the limiting value of the contribution to W from a small element of path, ΔX , viewed through the path ahead of it, X . In the previous two approximations the line shape of the element ΔX and the path in front of it are both given by the line shape for the equivalent homogeneous path. In the current approximation the element ΔX is taken to have its true line shape while the path X in front of it is taken to have an equivalent homogeneous shape. Eq. (21) has been checked against the exact relation, eq. (20), for a two layer non-isothermal path and found to be very accurate. This is reasonable based on the physical interpretation given above. Further investigation of its accuracy is to be the subject of future work. It would be possible to go on from here and fully develop a procedure for treating isolated Lorentz lines, but since our interest is ultimately in a band model, which treats the average of many lines, let us turn our attention at this point to a random band model,

treating it in a manner analogous to that used above for the isolated line.

Band Model Considerations

The calculation of an average spectral radiance at the boundary of a radiating body of gas, in a frequency interval encompassing a number of rotational lines, is represented by the relation

$$\bar{L}_\nu = \int_0^\infty g(\nu' - \nu) L_\nu(\nu') d\nu' \quad (22)$$

where $g(\nu, \nu')$ is an averaging function, e.g. the slit function of a spectrometer of moderate resolution, such as those which produce original absorption spectra from which band-model parameters are extracted. The exact spectral radiance L_ν is given by the equation of transfer, eq. (1) and (3), so that eq. (22) can be written

$$\bar{L}_\nu = \int_0^\infty g(\nu' - \nu) \int_1^{\tau(X_L)} L_\nu^*(\nu, \tau') d\tau' d\nu' \quad (23)$$

where τ is the perfectly resolved transmittance, and the primes denote variables of integration.

The order of integration in eq. (23) can be inverted, and for frequency intervals small enough that the Planck function $L_\nu^*(T)$ is essentially constant, the result is the band-model expression:

$$\bar{L}_\nu(\nu) = \int_1^{\tau(X_L)} L_\nu^*(\nu, \bar{\tau}') d\bar{\tau}' \quad (24)$$

where

$$\bar{\tau}(\nu) \equiv \int_0^{\infty} g(\nu' - \nu) \tau(\nu') d\nu' \quad (25)$$

Thus $\bar{\tau}$ is seen to be the "spectral" transmittance measured by a conventional instrument or calculated by a band-model.

The evaluation of eq. (25) to obtain the average spectral radiance \bar{L}_ν is done by first computing $\bar{\tau}$ at a number of points along the path. The blackbody radiance L_ν^* is then represented as a function of $\bar{\tau}$, and integrated numerically over $\bar{\tau}$, using, for instance, a simple summation. The various band-models in current use, including those based on the Curtis-Godson approximation and the present model in its original form, do yield values for the transmittance with an accuracy sufficient for most engineering applications. However, as in the case of isolated lines, the use of eq. (25) in essence involves a differentiation of the expression for $\bar{\tau}$ with respect to the optical path. Differentiation of course accentuates errors and uncertainties; in the isolated line case presented above, it was the derivative of the equivalent width that exhibited the misbehavior. Therefore, analogously to the case for isolated lines, an expression which yields reasonable values for $\bar{\tau}$ will not necessarily yield reasonable values for $d\bar{\tau}$ and hence \bar{L}_ν . What is needed is an expression for $\bar{\tau}$ having a derivative which will yield more realistic values of the difference in transmittance with a specified incremental increase in physical path. Such an expression can be developed as follows.

The transmittance for a band of spectral lines with some overlapping can be expressed as (4)

$$\bar{\tau} = \frac{1}{\bar{\tau}_n} \exp(\bar{\tau}_n - 1) \quad (26)$$

where $\bar{\tau}_n$ is the transmittance for an equivalent band of well-isolated non-overlapping lines. Differentiating eq. (26) with respect to the optical depth X yields

$$\frac{d\bar{\tau}}{dX} = -\bar{\tau} \frac{d\bar{\tau}_n}{dX} \quad (27)$$

which indicates that, with a reasonably accurate value for $\bar{\tau}$, the accuracy of $d\bar{\tau}/dX$ depends directly on that of $d\bar{\tau}_n/dX$. Accordingly, an improved relation for the latter will be sought.

In our current work we have used the NW-NS approximation exclusively and our consideration will be limited at this point to this model, seeking a specification of the function $F(X')$ which will yield accurate values of a transmittance derivative. The Curtis-Godson approximation contains no unspecified parameter which can be so chosen, so it will not be considered further. For the NW-NS approximation (11)

$$\bar{\tau}_n = \beta_{eL} f(\bar{x}) \quad (28)$$

where the argument of the Ladenburg Reiche function is in this case

$$\bar{x}(X) = \frac{1}{\beta_{eL}} \int_0^X \bar{k}(X') \left[\frac{\beta(X')}{\beta_{eL}} \right]^{n(X')} dX' \quad (29)$$

in which $\bar{k} = \bar{k}(\nu, T)$ is the first band-model parameter, the average absorption coefficient, identifiable as the average line strength to spacing ratio, and

$\beta = \beta(v, T)$ is the second band-model parameter, the line overlap factor, identifiable as 2π times the average line width to spacing ratio. The effective value β_{eL} is defined analogously to γ_{eL} for the single case:

$$\beta_{eL} = \frac{\int_0^{X_L} \bar{k}(X') \beta(X') dX'}{\int_0^{X_L} \bar{k}(X') dX'} \quad (30)$$

$F(X')$ has here been replaced by $\frac{\beta(X')}{\beta_{eL}} \eta(X')$, a suitable functional form for $F(X')$. Here η is an interpolation parameter between the nearly weak and nearly strong approximations, varying from 0 for the nearly weak to 1 for the nearly strong.

In an earlier study ⁽¹¹⁾, an investigation of the form for η is described. As a result of that study several empirical forms for η were determined which appeared to be reasonably useful. However, the information used to make these determinations was not greatly sensitive to values of η and hence accurate information about its form could not be extracted. One of these empirical forms is:

$$\begin{aligned} \eta &= 0 \text{ for } \bar{x} < 1 \\ \eta &= (\bar{x} - 1)/9 \text{ for } 1 \leq \bar{x} \leq 10 \\ \eta &= 1 \text{ for } \bar{x} > 10 \end{aligned}$$

This appears to make η a function of \bar{x} rather than X' , and the determination of \bar{x} an iterative procedure. However, in practice the integral for \bar{x} is evaluated by a summation and a value for η for a particular term is determined from the value for \bar{x} calculated from the sum of the preceding terms. Thus η is uniquely defined for each X' .

Differentiating eq. (28) and utilizing eq. (30) yields

$$\frac{d\bar{\tau}_n}{dX} = \frac{df}{d\bar{x}} \left[\frac{\beta(X)}{\beta_{eL}} \right]^{\eta(X)} \bar{k}(x) \quad (31)$$

which shows that the derivative of $d\bar{\tau}_n/dX$ varies with the absorption coefficient, as would be expected; the derivative of the function $f(\bar{x})$, and the local values of $\beta(X)$ and $\eta(X)$. The physical significance of eq. (31) can be seen in Figure 3, a normalized plot of $-(1/\bar{k}) d\bar{\tau}_n/dX$ vs x with β/β_{eL} as a parameter. In the limit, as $x \rightarrow 0$, the band model reduces, as it should, to a linear growth law, so that $-(1/\bar{k}) d\bar{\tau}_n/dX$ approaches unity. However, this function must be less than unity for all values of X greater than zero, in accordance with the physical requirement that the transmittance decrease monotonically with optical depth. In Figure 3, the empirical specifications for η lead to a violation of this constraint for certain values of β/β_{eL} and \bar{x} . This misbehavior is analogous to that shown earlier for isolated line growth. We now search for a better approximation to $d\bar{\tau}_n/dx$. This quantity is given by

$$\frac{d\bar{\tau}_n}{dx} = -\frac{1}{d} \frac{d\bar{W}}{dx} \quad (32)$$

where \bar{W} is an average equivalent width and d is an average line spacing in the spectral interval under consideration. For lines of equal strength and width, after some rearrangement, eqs. (32) and (21) yield:

$$\frac{d\bar{\tau}_n}{dx} = -\frac{1}{\pi} \int_{-\infty}^{\infty} \frac{\bar{k}(X)\beta(X)}{\beta^2(X) + (2\pi\Delta\nu/d)^2} \exp \left[-2x \beta_e(X) \frac{\beta_e(X)}{\beta_e^2(X) + (2\pi\Delta\nu/d)^2} \right] d\left(\frac{2\pi\Delta\nu}{d}\right) \quad (33)$$

where x denotes the dimensionless optical depth defined analogously to x as defined in eq. (11) and used in eq. (21). Rewritten in terms of the two bandmodel parameters, it becomes

$$x = \frac{\int_0^X \bar{k}(X') dX'}{\beta_e(X)} \quad (34)$$

where $\beta_e(X)$ is the average value of the second band model parameter over the path from the observer to the point X , analogous to the definition of $\gamma_e(X)$ in eq. (8)

$$\beta_e(X) = \frac{\int_0^X \bar{k}(X') \beta(X') dX'}{\int_0^X \bar{k}(X') dX'} \quad (35)$$

The distinction between β_{eL} (a constant, since it is determined over the whole path), defined in eq. (30) and $\beta_e(X)$ (a function of X , the optical depth coordinate) should be noted.

The change of variables $\tan \theta/2 = 2\pi \Delta\nu/\beta_e d$ and a trigonometric substitution yields after some manipulation

$$-\frac{1}{\bar{k}(X)} \frac{d\bar{\tau}_n}{dx} = \frac{2}{\pi} \frac{\beta}{\beta_e} \int_0^\pi \frac{\exp[-x(1+\cos\theta)]}{\left[\frac{\beta^2}{\beta_e^2}(X) + 1\right] + \left[\frac{\beta^2}{\beta_e^2}(X) - 1\right] \cos\theta} d\theta \quad (36)$$

Eq. (36) has been integrated numerically; the results are plotted in Figure 4, again as $-(1/\bar{k}) d\bar{\tau}_n/dX$ vs x with $\beta(X)/\beta_e(X)$ as a parameter. The resulting curves are well behaved and exhibit none of the anomalies seen in Figure 3. Notice that the curve for $\beta/\beta_e = 1$ is identical in both figures.

The interpolation parameter η can now be evaluated by equating eqs. (36) and (31). These two equations involve different sets of variables, i.e. eq. (36) is

in terms of x and $\beta_e(X)$, and eq. (31) is in terms of \bar{x} and β_{eL} . The relationship between \bar{x} and x is complex, depending on $\eta, \beta_e(X)$ and β_{eL} in an integral form. Furthermore, whereas x is a unique function of the optical path extending from 0 to X , \bar{x} is not a unique function in the same sense, depending, through β_{eL} , on the path between X and X_L as well. Such dependence is not physically realistic but appears as an integral part of the NW-NS approximation. In determining a form for η this non-uniqueness must be adequately accounted for so that the computed value of $(1/\bar{k}) (d\tau_n/dX)$ is unique despite the non-unique character of \bar{x} . It is very difficult to insure the existence of the latter condition except for certain types of paths. In particular if β differs significantly from its average value, β_{eL} , only in a very small portion of the optical path then the contribution from that portion of the path to the integral defining \bar{x} is negligible compared to the contributions from the remainder of the path. In this case the following approximate relation holds:

$$\int_0^X \bar{k}(X') \left[\frac{\beta(X')}{\beta_{eL}} \right]^{\eta(X')} dX' \approx \int_0^X \bar{k}(X') dX'$$

The above restriction also implies that

$$\beta_e(X) \approx \text{constant} = \beta_{eL}$$

and hence that

$$x \approx \bar{x}$$

Thus, by restricting ourselves to cases where $\beta_e(X)$ is not a strong function of X and allowing large variations in $\beta(X)$ only in very small fractions of the optical path, values for η can be found in terms of \bar{x} and β/β_{eL} (except for $\beta/\beta_{eL} = 1$,

where η is indeterminate). The resultant values of η so obtained, as a function of \bar{x} and β/β_{eL} are shown in Figure 5; using these values in eq. (31) will insure that the derivative $d\bar{\tau}/dX$ will equal that given by eq. (36). It should be noted that \bar{x} is computed by a sum so that the value of η valid for a given term of the sum is determined from the sum of the preceding terms. For convenience in application, simple analytical approximations were made to the curves of Fig. 5 by fitting them with functions of the form

$$\eta(\bar{x}, \beta/\beta_e) = \frac{\bar{x} + A (\beta/\beta_e)}{\bar{x} + B (\beta/\beta_e)} \quad (37)$$

$$\eta(\bar{x}, \beta/\beta_e) = \frac{\bar{x} C (\beta/\beta_e)}{E (\beta/\beta_e) + \bar{x} D (\beta/\beta_e)} \quad (38)$$

For any particular instance, the choice between eq. (37) and (38) is made on the basis of the quantity

$$E(\beta/\beta_e) = 1 + 0.185 \beta/\beta_e \quad (39)$$

If $\bar{x} > E$, eq. (37) is used; otherwise eq. (38) is used. Values for A, B, C, and D are tabulated in Table I. Values of $d\bar{\tau}_n/dX$ obtained by use of Table I in place of the values shown for η in Figure 5 are sufficiently accurate for most applications of this band-model.

The limitation on the variation of $\beta(X)$ and $\beta_e(X)$ mentioned earlier is not as severe as it might first appear, being satisfied in many cases of interest. For instance, in cases where a relatively small hot gaseous source is to be viewed through a long cool path, the condition is approximately met. In such a case, the value of β is almost invariant over the whole atmospheric path

which contains the largest part of the optical path. β varies substantially only in the relatively small portion of the path comprising the hot gaseous source. Hence the condition is approximately satisfied.

It should be noted that the introduction of an interpolation parameter is somewhat of an ad hoc procedure having little physical basis and is not the only way eq. (36) could be introduced into a computational procedure. An alternative way to use the above results would be the direct application of eq. (36) into a band-model computer code. The resultant values of $d\bar{\tau}_n/dX$ could then be used in eq. (27), with $\bar{\tau}_n$ in eq. (26) now evaluated in terms of x and $\beta_e(X)$. Such a procedure would obviate the need for a distinction between the nearly-weak and nearly-strong approximations and hence an interpolation procedure. Unfortunately, in the use of eq. (36), an analytic form for the solution of the integral is not easily obtained. Although a solution has been obtained in the form of an infinite series, this represents little improvement over a table of numerical values. Whether there would be a net gain in computational efficiency remains to be seen. However, it might be expected to be somewhat more satisfactory in that the restriction on the variation of $\beta_e(X)$ compared to β_{eL} required in the evaluation of η would not be needed. This alternative mode of the band-model formulation is one of the subjects of a continuing investigation.

In summary, we have shown how both the Curtis-Godson approximation and the nearly-weak, nearly-strong approximation can introduce anomalies into the radiance computed over a highly non-isothermal path for an isolated spectral line. We have then applied a Curtis Godson type approximation to the expression for the equivalent width gradient along the path, producing a formulation which yields greatly improved radiance values, exhibiting no anomalies. Generalizing

to a random band model, the expression concerning the equivalent width gradient has been used to obtain an interpolation between the nearly weak and nearly strong approximations valid for that band model.

The most important result presented herein is the form of the transmittance gradient given in eq. (36). It is the basis of a computational procedure for computing the radiance from highly non-isothermal gaseous sources which yields significant improvements over previously used techniques. It has been shown to be a better approximation than the more commonly used approximations, and yields physically realistic results for all values of the path and band model parameters.

REFERENCES

1. F. S. Simmons, C. B. Arnold, G. H. Lindquist, and F. G. Smith, *Applied Optics*, 9, 2792 (1970).
2. F. S. Simmons, *Applied Optics*, 5, 1801 (1966); 6, 1423 (1967).
3. F. S. Simmons, C. B. Arnold, and H. Y. Yamada, "Measurement of Temperature Profiles in Hot Gases by Emission-Absorption Spectroscopy," NASA CR-72491, April 1969.
4. R. M. Goody, "Atmospheric Radiation. I: Theoretical Basis," Oxford Calendar Press, 1964.
5. S. R. Drayson, *Applied Optics*, 5, 385 (1966).
6. A. C. Codgley, *JQSRT*, 10, p. 1065 (1970).
7. R. Ladenburg and F. Reiche, *Annln. Phys.*, 42, 181 (1913).
8. W. M. Elsasser, "Heat Transfer by Infrared Radiation in the Atmosphere," Harvard Meteorological Studies, Report No. 6, Harvard University, 1942.
9. L. D. Kaplan and D. F. Eggers, *J. Chem. Phys.*, 25, p. 875 (1956).
10. C. D. Walshaw and C. D. Rodgers, *Royal Met. Soc. Quart. Journal*, 89, p. 122 (1963).
11. F. S. Simmons, *JQSRT*, 7, 111 (1967).

TABLE I

COEFFICIENTS TO BE USED IN EQUATIONS (37) & (38)

<u>β/β_e</u>	<u>A</u>	<u>B</u>	<u>C</u>	<u>D</u>
0	-0.68	-0.35	0.55	0.07
2	-0.37	0.62	0.71	0.43
5	0.60	3.15	0.90	0.79
10	3.19	9.25	1.15	1.30
20	9.10	22.8	1.63	2.26
50	29.1	67.1	2.78	4.56
100	105.	209.	4.05	7.09

FIGURE
CAPTIONS

1. Equivalent width derivative in the Curtis-Godson approximation.
2. Equivalent width derivative in the nearly-weak and nearly-strong line approximations.
3. Transmittance derivative in the original band-model.
4. Transmittance derivative in the modified band-model.
5. Interpolation parameter as a function of optical depth and line overlap factor.

FIGURE 1

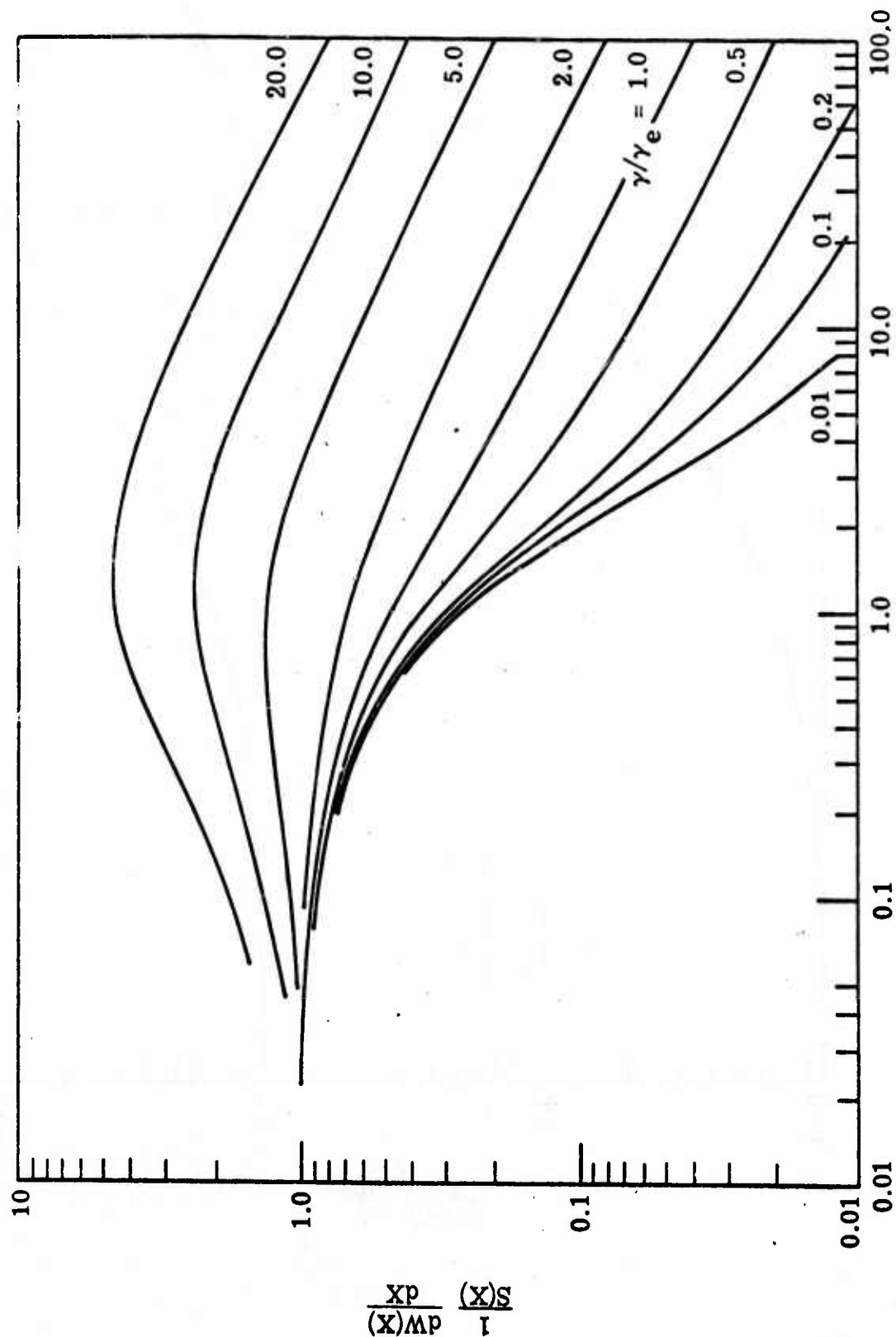


Fig. 1 DIMENSIONLESS OPTICAL DEPTH, $x(x)$

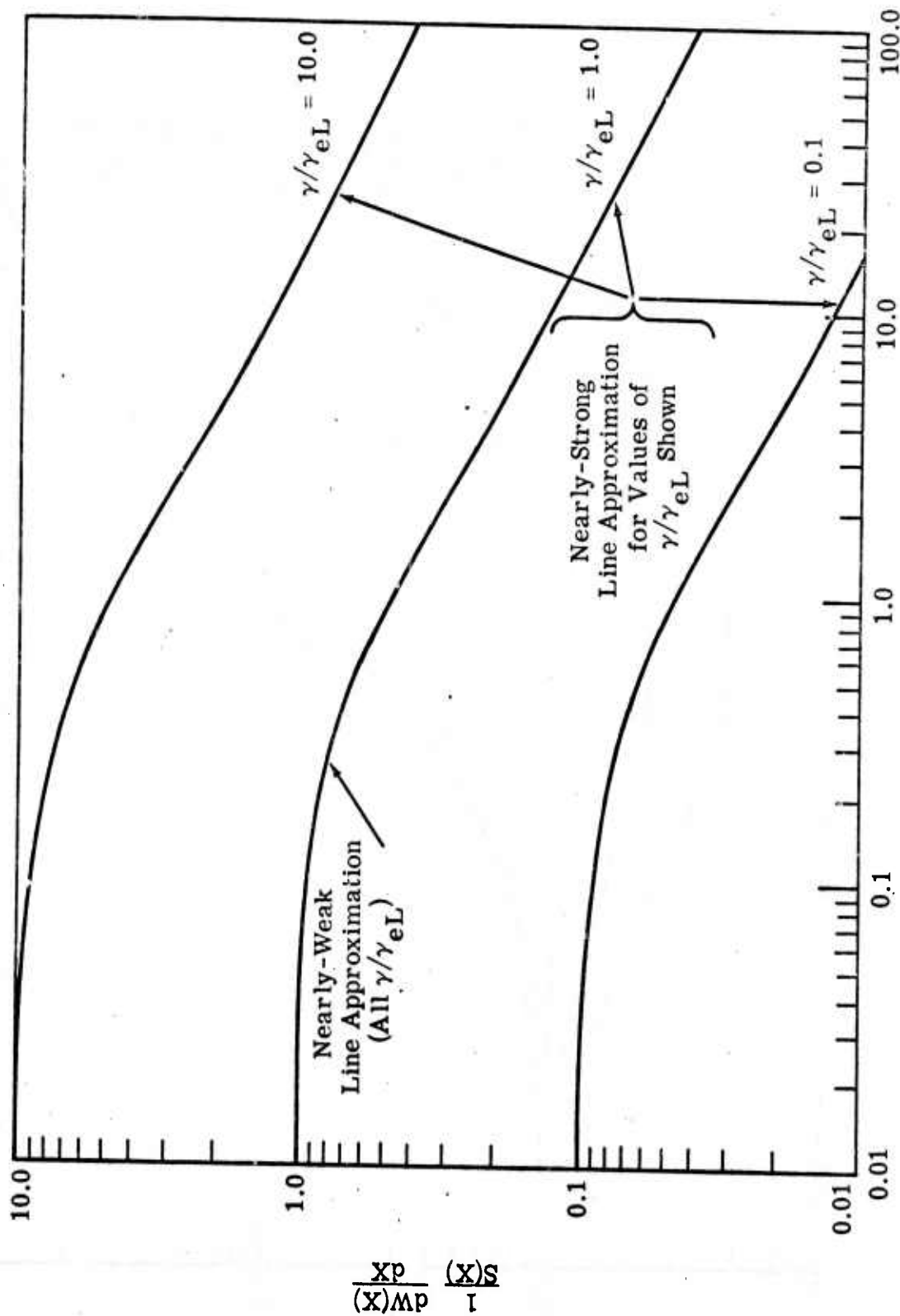


Fig. 2 DIMENSIONLESS OPTICAL DEPTH, $x(X)$

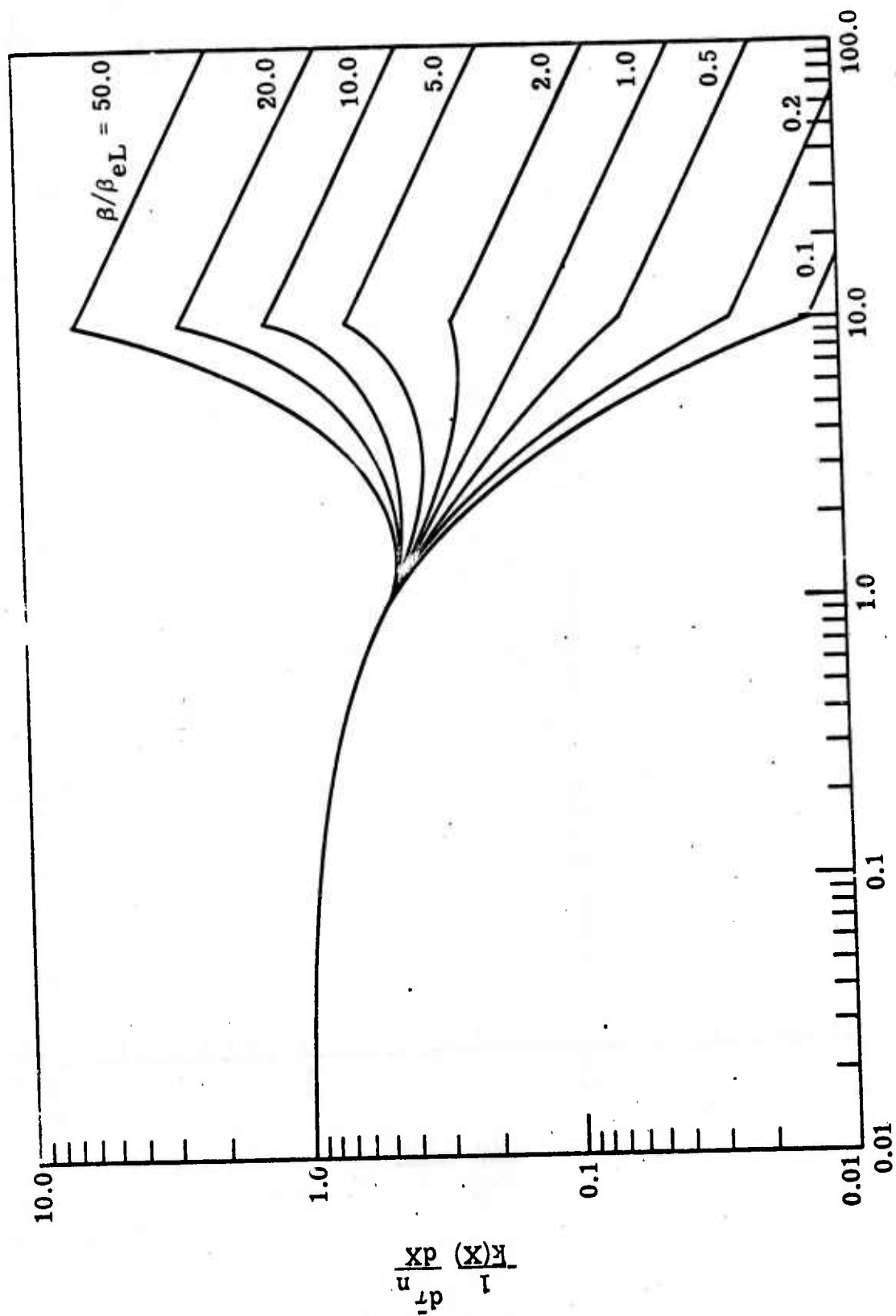


FIG. 3 DIMENSIONLESS OPTICAL DEPTH, $\bar{x}(x)$

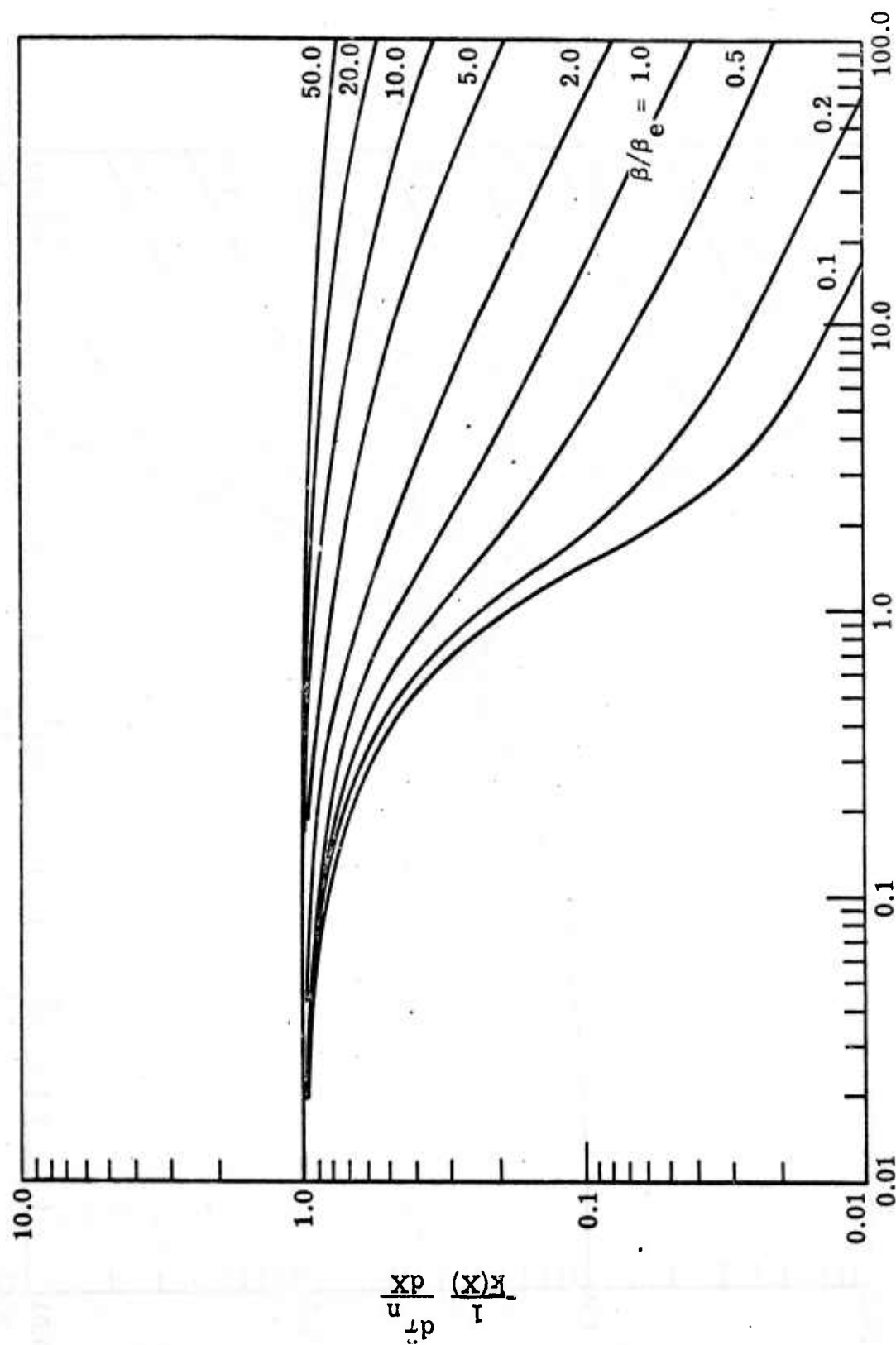


FIG. 4 DIMENSIONLESS OPTICAL DEPTH, $x(x)$

FIGURE 5

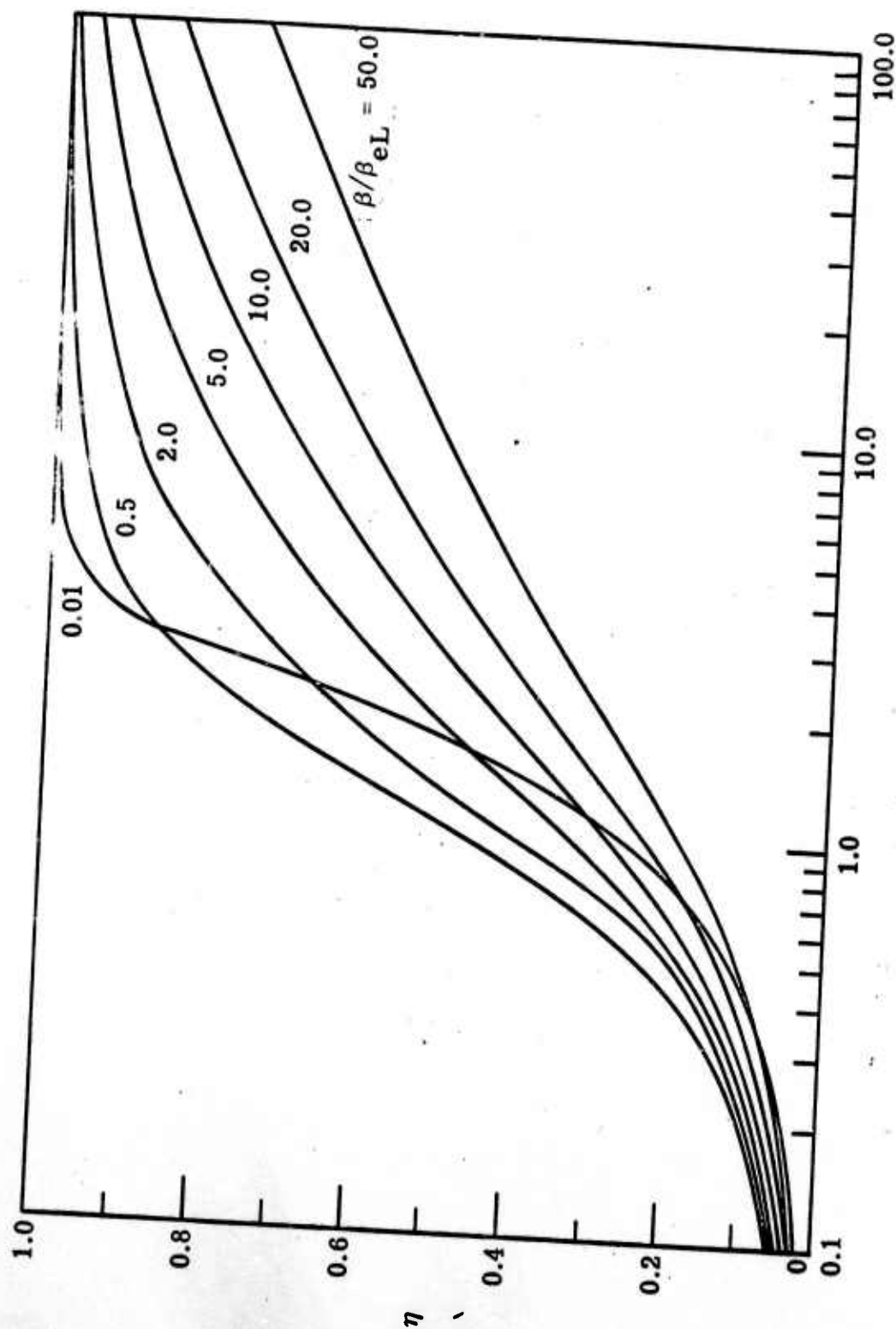


Fig. 5 DIMENSIONLESS OPTICAL DEPTH, $\bar{x}(x) \approx x(x)$